UNIVERSIDADE TÉCNICA DE LISBOA
INSTITUTO SUPERIOR TÉCNICO

Capacity Increase in Converging Mobile Communication Systems Through the Use of MIMO

Pedro Marín Fernandes
(*Licenciado*)

Dissertation submitted for obtaining the degree of
Master in Electrical and Computer Engineering

Supervisor: Doctor Luís Manuel de Jesus Sousa Correia

Jury
President: Doctor Luís Manuel de Jesus Sousa Correia
Members: Doctor Henrique José Almeida da Silva
                Doctor António José Castelo Branco Rodrigues

February 2005

To Cristina, my parents, and my sister.

Acknowledgements

First of all I wish to thank Prof. Luís Correia for having supervised this thesis. His ability to provide me with a 360º view of the problem in hands has helped me to clear out the important issues when I was buried in technical details. His astonishing balance between rigour and tolerance, discipline and flexibility, is a lesson that I shall never forget.

I am also grateful to *Instituto de Telecomunicações*, for having provided me with high-quality logistics, that have made working during many weekends and nights a less painful experience. I would also like to emphasize how important the contribution from the IST-FLOWS project was, not only for having sponsored this thesis, but also for providing me with an outlook of the convergence of standards that I would never obtain by myself.

Many thanks to João Gil and Martijn Kuipers for their thoughts on channel modelling, to Catarina Brites for her last-minute help with the symbols, and to Jorge Aguiar for his patience answering my questions on the phone from Munich. Thanks to Lúcio, Gonçalo, Carla, Cristina Reis, André, Paulo Marques, José Nascimento, and Gabriela for making the workroom so cosy and cheerful at the same time, and also for letting me run my never-ending simulations in their computers.

The completion of this work would never be possible in such a timeframe without the help of my parents, my sister and Cristina. My parents and sister have freed me from all the everyday tasks, enabling me to completely focus on the thesis. Cristina not only has supported me in her subtle way, but has also saved me many hours by helping in the edition of the present document.

Abstract

This work analyses the performance of a wireless mobile multi-antenna, multi-technology communication system relatively to its single antenna version. Three radio access technologies were considered, GSM/GPRS, UMTS, and HIPERLAN/2. Four performance indicators were used: mean bitrate, percentage of PS discarded packets/frames, percentage of CS blocked calls, and percentage of sessions routed the through the first option of access technology and target bitrate.

The underlying assumption is the consideration of the channel capacity increase to be the capacity increase of the whole system. The developed software consists of a physical layer of a convergence model. A MIMO channel model was achieved extending a SISO one.

Two antenna array sizes were considered and six applications were measured: voice call, video call, video-on-demand, web-browsing, email, and FTP. The results are shown for a scenario with all technologies and variable number of users, and with a fixed number of users accessing different sets of access technologies.

The capacity increase is shown to be dependent on the priorities of access technologies defined for each application, and on the performance of SISO. For example, 2×2 antenna configuration increases the system's mean bitrate in about 30 % relatively to SISO, when the channel capacities indicated an increase of 54 %.

Keywords

Mobile and wireless systems, MIMO, Channel modelling, Capacity, Systems convergence.

Resumo

Este trabalho analisa o desempenho de um sistema de comunicações móveis sem fios multi-tecnológico e multi-antena, relativamente à sua versão de antena única. Três tecnologias de acesso rádio foram consideradas, GSM/GPRS, UMTS e HIPERLAN/2. Quatro indicadores de desempenho foram usados: ritmo binário médio, percentagem de pacotes/tramas descartados, percentagem de chamadas bloqueadas e percentagem de sessões encaminhadas para a primeira opção de tecnologia e ritmo binário.

A hipótese subjacente foi a consideração do aumento de capacidade do canal como sendo o aumento da capacidade do sistema convergente em si. O *software* desenvolvido consiste numa camada física dum modelo de convergência. O modelo de canal MIMO foi desenvolvido a partir de um modelo SISO.

Dois agregados de antenas foram considerados e seis aplicações foram analisadas: chamada de voz, chamada de vídeo, vídeo-a-pedido, navegação na Internet, correio electrónico e FTP. Os resultados são mostrados para um cenário todas as tecnologias e número variável de utilizadores e com um número fixo de utilizadores com acesso a diferentes combinações de tecnologias.

O aumento de capacidade mostrou ser dependente das prioridades definidas para cada aplicação em termos de tecnologia de acesso e do desempenho do SISO. Por exemplo, uma configuração 2×2 incrementa o ritmo binário médio em cerca de 30 % quando a capacidade do canal indica um aumento de 54 %.

Palavras-Chave

Sistemas móveis sem fios, MIMO, Modelação de canal, Capacidade, Convergência de sistemas.

Table of Contents

List of Figures

List of Tables

List of Acronyms

2D	Two-dimensional
3D	Three-dimensional
3G	Third Generation of mobile communication
3GPP	Third Generation Partnership Project
ACF	Association Control Function
ACH	Access feedback CHannel
AoA	Angle of Arrival
AoD	Angle of Departure
AoI	Angle of Incidence
AP	Access Point
ARQ	Automatic Repeat reQuest
AS	Angle Spread
ATM	Asynchronous Transfer Mode
ATTPM	Access Technology Traffic Processing Module
BCH	Broadcast CHannel
BER	Bit Error Rate
BH	Busy Hour
BHCA	Busy Hour Call Attempt
BLER	BLock Error Rate
BN	Backbone Network
BoD	Bandwidth on Demand
BPSK	Binary Phase Shift Keying
BRAN	Broadband Radio Access Networks
BS	Base Station
CDF	Cumulative Distribution Function
CIR	Channel Impulse Response
CL	Convergence Layer

CM	Convergence Manager
CMM	Convergence Manager Module
CN	Core Network
COST	Cooperation in Scientific and Technical Research
CPCH	Common Packet Channel
C-PDU	Control Packet Data Unit
CRC	Cyclic Redundancy Check
CS	Circuit Switch(ed)
CSI	Channel State Information
DAB	Digital Audio Broadcasting
DCC	Data Link Control layer Connection Control
DCH	Dedicated CHannel
DDCM	Double Directional Channel Model
DECT	Digital Enhanced Cordless Telephone
DFS	Dynamic Frequency Selection
DL	Downlink
DLC	Data Link Control layer
DoA	Direction of Arrival
DoD	Direction of Departure
DPCCH	Dedicated Physical Control Channel
DPDCH	Dedicated Physical Data Channel
DS-CDMA	Direct Sequence-Code Division Multiple Access
DSCH	DL Shared CHannel
DVB	Digital Video Broadcasting
EC	Error Control
EIRP	Effective Isotropic Radiated Power
ESM	Elliptical Sub-region Model
ETSI	European Telecommunications Standards Institute
FACH	Forward Access CHannel
FCH	Frame Channel
FDD	Frequency Division Duplex
FEC	Forward Error Correction
FER	Frame Error Rate

FTP	File Transfer Protocol
GBAR	Gamma Beta Auto-Regressive
GBSB	Geometrically Based Single Bounce
GBSBCM	Geometrically Based Single Bounce Circular Model
GBSBEM	Geometrically Based Single Bounce Elliptical Model
GBSM	Geometrically-Based Stochastic Model
GGSN	Gateway GPRS support Node
GMSC	Gateway Mobile services Switching Centre
GOP	Group of Pictures
GPRS	General Packet Radio Service
GPS	Global Positioning System
GSM	Global System for Mobile Communications
GWSSUS	Gaussian Wide-Sense Stationary Uncorrelated Scattering
HIPERLAN/2	HIgh-PErformance Radio Local-Area Network type 2
HL/2	HIPERLAN/2
HLR	Home Location Register
IEEE	Institute of Electrical and Electronics Engineers
IMT-2000	International Mobile Telephony-2000
IP	Internet Protocol
IS-95	Interim Standard 95 (cdmaOne)
ISDN	Integrated Services Digital Network
ISI	Inter-Symbol Interference
IST	Instituto Superior Técnico
IST-FLOWS	Information Society Technology – FLexible cOnvergence of Wireless Standards and services
ITU	International Telecommunications Union
LA	Link Adaptation
LAN	Local Area Network
LCH	Long Channel
LF	Load Factor
LoS	Line of Sight
LP	Local Parameter

MAC	Medium Access Control
ME	Mobile Equipment
MIMO	Multiple-Input Multiple-Output
MPEG	Moving Picture Expert Group
MSC	Mobile Services Switching Centre
MSVM	Mobile Systems Voice Model
MSS	Maritime Satellite Service
MT	Mobile Terminal
NE	Network Element
NLoS	Non-LoS
OFDM	Orthogonal Division Frequency Multiplexing
OVFS	Orthogonal Variable Spreading Factor
PAS	Power Azimuth Spectrum
PC	Power Control
PCH	Paging Channel
PCS	Personal Communication System
PDA	Personal Digital Assistant
PDER	PDU-Error Rate
PDF	Probability Density Function
PDP	Power Delay Profile
PDS	Power Delay Spectrum
PDU	Packet Data Unit
PG	Processing Gain
PHS	Personal Handy phone System
PHY	PHYsical layer
PLMN	Public Land Mobile Network
PS	Packet Switch(ed)
PSM	Parametric Stochastic Model
PT	Priority Table
QoS	Quality of Service
QPSK	Quadrature Phase Shift Keying
RACH	Random Access CHannel in UMTS
RCH	Random access CHannel in HIPERLAN/2

RE	Radio Environment
RF	Radio Frequency
RIR	Recorded Impulse Responses
RLC	Radio Link Control
RNC	Radio Network Controller
RNG	Random Number Generator
RNS	Radio Network Subsystem
RR	Resource Request
RRC	Radio Resource Control
RRM	Radio Resource Management
RTT	Ray Tracing Technique
Rx	Receiver
SCH	Short CHannel
SDMA	Space Division Multiple Access
SDU	Service Data Unit
SF	Spreading Factor
SGSN	Serving GPRS Support Node
SIR	Signal to Interference Ratio
SISO	Single-Input Single-Output
STS	Scatterer-to-Scatterer
TBR	Target Bitrate
TDD	Time Division Duplex
TDMA	Time Division Multiple Access
ToA	Time of Arrival
TPE	Traffic Processing Engine
TR	Technology Router
TS	Time Slot
TSM	Traffic Source Model
TSMIM	Traffic Source Model Implementation Module
TUL	Technical University of Lisbon
Tx	Transmitter
UE	User Equipment
UL	Uplink

ULA	Uniform Linear Array
UMTS	Universal Mobile Telecommunication System
U-PDU	User PDU
U-SAP	User Service Access Point
USIM	UMTS Subscriber Identity Module
UTGM	User Traffic Generation Module
UTRA	UMTS Terrestrial Radio Access
UTRAN	UTRA Network
UTV	User Traffic Vector
VLR	Visitor Location Register
VoIP	Voice over IP
VRM	Virtual Ray Model
WCDMA	Wideband Code Division Multiple Access
WDCM	Wideband Directional Channel Model
WDDCM	Wideband Double Directional Channel Model
WLAN	Wireless LAN
WSI	Wireless Strategic Initiative
WWW	World Wide Web

List of Symbols

a	Amplitude of each tap
$\mathbf{a}$	Vector of independent fading samples
$\mathbf{A}^k$	Matrix of independent, circularly symmetric complex Gaussian variables of the kth tap
$\mathbf{A}_r$	Diagonal matrix representing the fading caused by the scatterers around the receiver
$\mathbf{A}_t$	Diagonal matrix representing the fading caused by the scatterers around the transmitter
c	speed of light
C	Channel capacity
$\mathbf{C}$	Shaping matrix
d	BS-MT distance
$\mathbf{d}$	Distance vector
$\mathbf{D}$	Diagonal matrix whose complex elements characterise the ToAs
d_a	Inter-antenna distance
E_b	Signal energy per bit
E_x	Energy sent by each transmit antenna
f	Carrier frequency
f_{Dmax}	Maximum Doppler frequency
g	Average gains of the h_{mn}
$G_{M/S}$	Relative gain of MIMO over SISO
$G_{M \times N / M' \times N'}$	Relative gain of a *M×N MIMO* configuration over a *M'×N'* one in terms of channel capacity
G_{R_b}	Relative gain of the mean bitrate
$G_{R_{CB}}$	Relative gain of the call blocking rate
G_{η_D}	Relative gain of the discarded packets/frames rate
$G_{\eta_{1PD}}$	Relative gain of the number of sessions routed through the 1st priority of access technology and quality/bitrate
h_{mn}	Channel transfer function between antenna m and n

$h_{mn\text{-}ideal}$	h_{mn} of the totally uncorrelated channel
$h_{mn\text{-}worst\ case}$	h_{mn} of the totally correlated channel
$\mathbf{H}$	MIMO channel transfer matrix
$\mathbf{H_{ideal}}$	MIMO channel transfer matrix of the ideal channel
$\mathbf{H_{worst\text{-}case}}$	MIMO channel transfer matrix of the worst-case channel
$\mathbf{H_{LoS}}$	Product of the coherent wave component by a steering matrix
$\mathbf{H_{stochastic}}$	Channel transfer matrix derived from stochastic model
i	Inter-cell to intra-cell interference ratio seen by the BS receiver
$\bar{i}$	Inter-cell to intra-cell BS power ratio received by user
$I_{M \times N}$	Total available spreading codes in UMTS and LCHs in HIPERLAN/2 in the MIMO-enabled convergent network
I_{inter}	Received wideband interference power at the BS due to inter-cell users
I_{intra}	Received wideband interference power at the BS due to intra-cell users
I_{Total}	Received wideband interference power (at the BS)
$\mathbf{I}$	Identity matrix
j	Imaginary unit
k	Wave number
$\boldsymbol{k}$	Wave vector
K	Rice factor
N_p	Number of multipath components or signal replicas (taps)
L_{pj}	Average attenuation between the BS and user j
m	Receive antenna index
M	Number of receive antennas
n	Transmit antenna index
$\mathbf{n}(t)$	Zero-mean Gaussian noise with independent real and imaginary parts
N	Number of transmit antennas
N_{DL}	Number of connections per cell
$N_{i\text{-}DL}$	Noise rise over thermal noise due to interference in the DL
$N_{i\text{-}UL}$	Noise rise over thermal noise due to interference in the UL
N_{UL}	Number of users per cell
N_0	Noise spectral density including thermal noise and interference
p	User scenario
P_N	Background and receiver noise power

P_{Total}	Total DL transmission power
P_{max}	Maximum Node B transmission power
P	Vector with the power distribution over the transmit antennas
R	Radius of the circular scattering region.
R_{bj}	Bitrate of user j
R_c	WCDMA chip rate
R	Channel correlation matrix
$\mathbf{R}_{Rx}^{k}$	Spatial correlation matrix of the propagation paths, that arrive at the kth tap, between the receive antennas and the scatterers that directly illuminate the receiver.
$\mathbf{R}_s$	Correlation matrix that describes the correlation of the propagation paths between the scatterers surrounding the ends of the connection
$\mathbf{R}_{Tx}^{k}$	Spatial correlation matrix of the propagation paths, that arrive at the kth tap, between the transmit antennas and the scatterers that directly illuminated by the transmitter.
S	Total number of scatterers
S_r	Number of scatterers that directly illuminate the receiver
S_t	Number of scatterers that are directly illuminated by the transmitter
t	Time variable
T_c	Coherence time of the channel
T	Non-normalised MIMO channel transfer matrix
u	Unitary vector
$\mathbf{U}_{Rx}$	Spatial eigenbases at the receive side
$\mathbf{U}_{Tx}$	Spatial eigenbases at the transmit side
v_j	Activity factor of user j at physical layer
v_r	Scalar speed of the receiver
v_t	Scalar speed of the transmitter
$\mathbf{x}(t)$	Transmitted signal
X	min(N,M)
$\mathbf{y}(t)$	Received signal
α	Channel (complex) gain
$\bar{\alpha}$	Average orthogonality factor in the cell
γ	Phase of the scatterers' reflection coefficient
Γ	Scatterers' reflection coefficient

Γ_d	Scatterers' reflection coefficient with extra randomness
$\mathbf{\Delta_{Rx}}$	Diagonal matrix whose real elements are the powers that arrive to the receive antennas from the scatterers
$\mathbf{\Delta_{scat}}$	Diagonal matrix whose real elements are the powers that arrive to the scatterers from the transmit antennas
$\delta(\cdot)$	Dirac Delta function
ζ	Elevation Angle
$\eta_{P\text{-}UL}$	Uplink load factor based on power
$\eta_{P\text{-}DL}$	Downlink load factor based on power
$\eta_{T\text{-}UL}$	Uplink load factor based on throughput
$\eta_{T\text{-}DL}$	Downlink load factor based on throughput
θ	Phase of each tap
$\mathbf{\Theta}$	Diagonal matrix whose complex elements characterise the reflection coefficients
λ	Wavelength of the carrier frequency
$\mathbf{\xi}$	Matrix whose elements are the complex gains of the orthogonal polarisations and the cross-coupling between polarisations
ρ	Signal to noise ratio at (each) receive antenna
σ^2	Noise power at the receive antenna
τ	ToA or delay
τ_{ijm}	delay of each tap
τ_{max}	maximum delay and angle spread
ϑ	Azimuthal angle
φ	Angle between the array axis and the direction of the propagation of the signal (AoA or AoD)
$\mathbf{\varphi}$	Matrix whose complex elements characterise the AoDs
φ_o	Angle from the BS-MT vector to a reference axis
$\Delta\Phi$	Phase rotation of the signals received in different antennas
$\mathbf{\Phi}$	Matrix whose complex elements characterise the AoAs
ψ	scalar product between a wave vector and a distance vector
ω	Extra randomness in the scatterers' reflection coefficient
Ω	Eigenmode coupling matrix
$*$	Convolution
$\otimes$	Kronecker product

$\odot$	Hadamard product
$\mathbb{C}$	Complex domain
$\Re$	Real domain
$(\cdot)^{\mathrm{T}}$	Transpose
$(\cdot)^{\mathrm{H}}$	Hermitian

$\odot$ Hadamard product

1

Introduction

This introductory chapter brings up the motivation of the thesis, its scope, targets and original contributions. The structure of the document is also presented.

During August 2004, the total number of mobile phones reached the 1.5 billion mark worldwide [CELL04]. This unprecedented growth was mainly launched by the Second Generation (2G) of mobile communications. Unlike the first one, the Global System for Mobile communications (GSM) uses digital technology, and has broken the umbilical link between mobile operators and phone manufacturers. The Subscriber Identity Module (SIM) card allowed users to choose their service provider and phone brand independently. Technological developments in the field of wireless and radio technology helped to miniaturise the Mobile Terminals (MTs), supplying them with a variety of non-foreseen services, such as text messaging, access to data networks, and location based services.

The recently arisen Third Generation (3G) systems are designed for multimedia applications: with them, person-to-person communication can be enhanced with high quality video and images, and access to public and private information has been improved due to higher bitrates. In the standardisation fora, Wideband Code Division Multiple Access (WCDMA) technology has emerged as the most widely adopted 3G air interface. Its specification has been performed within the Third Generation Partnership Project (3GPP) [3GPP04], which is the joint standardisation bodies from Europe, Japan, Korea, the USA and China. Within 3GPP, WCDMA is called Universal Terrestrial Radio Access (UTRA) Frequency Division Duplex (FDD) or Time Division Duplex (TDD), the name WCDMA being used to cover both FDD and TDD operations. Among its main objectives, the convergence to a common world standard, and the simplification of international roaming were claimed. These goals were only partially achieved, as a consensus between the main economical regions was not possible due to mismatching spectrum allocations, Figure 1.1, among other reasons.
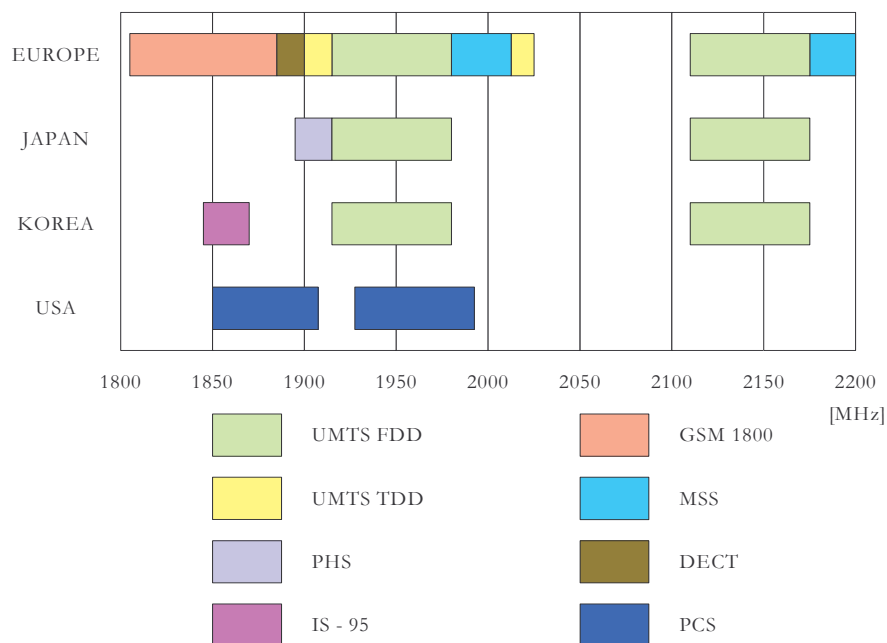
Figure 1.1: Spectrum Allocation in Europe, Japan, Korea, and USA (extracted from [Agui03]).

In Figure 1.1, PHS stands for Personal Handy phone System, MSS for Maritime Satellite Service, DECT for Digital Enhanced Cordless Telephone, PCS for Personal Communication System, and IS-95 is for the CdmaOne system.

In parallel, the enormous success of the Internet, offering ever-increasing data rates, accustomed many wired users to a number of new services, such as large file downloads, video streaming, File Transfer Protocol (FTP) and browsing in the World Wide Web (WWW). The demand to have those services on the move came naturally, with obvious benefits for the users, manufacturers, and service providers. Partial solutions to this problem progressively arose, as new standards for wireless communications, designed from scratch, proliferated: Digital Audio Broadcasting (DAB), Digital Video Broadcasting (DVB), Bluetooth, Wireless Local Area Networks (WLANs) such as IEEE 802.11 and HIPERLAN/2, etc.. They differ in the extension of covered areas, data rates, reliability, etc., which makes them more or less specific for a kind of usage. Highlighting the ones with the largest acceptance in the business and entertainment industry, WLANs have been seen as a competitive technology to the 3G cellular network one. However, due to rather small cell areas, it seems utopian to implement a nationwide coverage and, nowadays, they are seen as complementary technologies. Extending this complementarity concept to other radio access technologies, the concept of convergence of wireless standards arises as a strong proposal for the 4th Generation of mobile communications (4G) [4GMF04]. The concept of convergence or simultaneous use of standards has been systematised in [FSCS04]. 4G systems will then provide interconnection and interoperability between technologies to (seamlessly) ensure handovers between standards. This will require higher intelligence in the terminals to make the best use of the different applications locally available. At the price of an increased complexity, the vision brought up by the Wireless Strategic Initiative (WSI) [WSI04] is progressively becoming real. It aims at bridging all access technologies from fixed to satellite and from person to person to broadcast, Figure 1.2.

In parallel to the efforts that are being made to define what would a convergence of standards be like, the research community keeps on enhancing the existing technologies. In particular, it is anticipated that some future physical layer standard releases will contain enhancements related to multi-antenna transmission techniques.

Since the revolutionary publications by Telatar [Tela95], and Foschini and Gans [FoGa98], the idea of Multiple Input Multiple Output (MIMO) antenna systems has been the topic of extensive research activity worldwide. Since it exploits an additional dimension to carry information (the spatial dimension), the increase in capacity of MIMO systems over the Single Input Single Output (SISO) ones is a remedy for the increasing demands of higher data rates in wireless systems. In a fading environment, under the assumption of independent fades

and noises at different antennas, the capacity gain of multiple-antenna systems over single antenna ones can be very large. For example, if the number of receiving antennas equals the transmitting one, the capacity grows linearly with this number when it is sufficiently large.
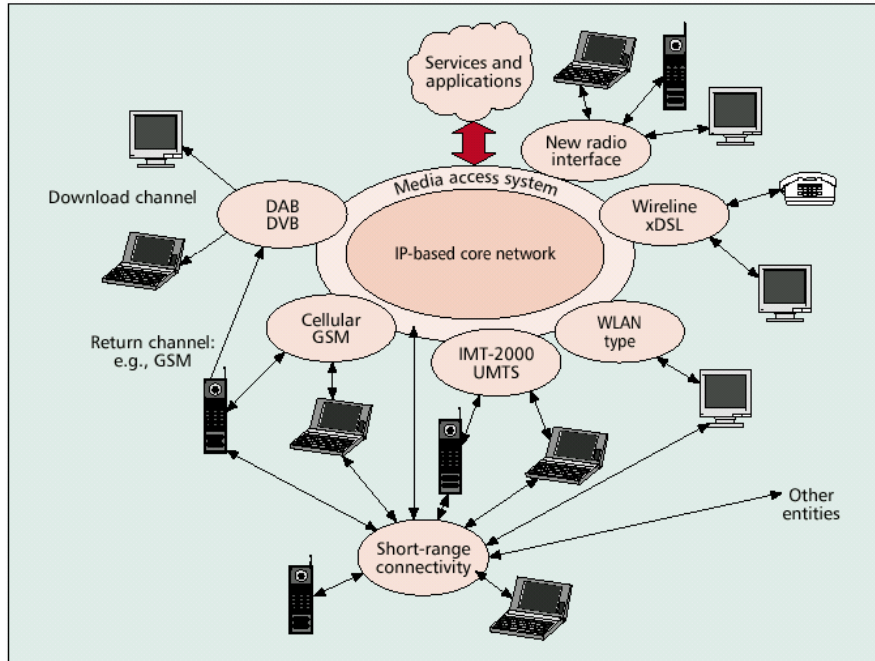
Figure 1.2: The Multi-technology Access Network (extracted from [VLLX02]).

The continued interest on MIMO has boosted channel modelling worldwide, because, until some years ago, most of the modelling activities had focused on the time-domain aspects, which are not of much help for this purpose. Along the past years, a large set of time-based models, which can be sorted according to the outdoor vs. indoor dichotomy, has been set. Usually, in outdoor scenarios, the fixed Base Station (BSs) is located much higher than the MT, around which most of the scatterers are supposed to stand. On the other hand, in indoor scenarios, the environment surrounding MT and BS is similar, which introduces symmetry to the connection. The model proposed by [Fail89] is among the most widely accepted for the outdoor environments accounting for the time dispersion and the time variation of the mobile channel, while the model proposed in [SaVa87] focuses on indoor environments.

These time-domain models have been applied successfully until recently, when the growing demand for ubiquitous high-speed connections pushed researchers to investigate new means to increase the capacity of wireless channels. The use of so-called "smart antennas" for antenna/space diversity, beamforming or even Space Division Multiple Access (SDMA), has been regarded as a powerful improvement [MFGH99]. However, the existing non-directional radio channel models were of no immediate help, as they do not appropriately model the propagation phenomena in the space domain. Some people suggested an upgraded version of pure time-domain models, such as [KlMo96] for outdoor and [SJJS00] for indoor environments. Others proposed brand new models, based either on a geometric description of

the scattering process which enables to derive the Power Delay Spectrum (PDS) and the Power Azimuth Spectrum (PAS) of the waves according to propagation laws, or based on empirical models fitting measurement results. References [MFGH99], [KlMo96], [SJJS00], and [ECSR98] present comprehensive surveys on these efforts.

Even though appropriate models were derived to embrace the spatial properties of the propagation phenomena in transmission schemes where multiple antenna elements were used at one end of the connection, the recent use of MIMO has raised again the discussion on spatial propagation when using multiple parallel paths.

MIMO being one of the probable musts for the techniques based on the physical layers of the future mobile communications, and the convergence of standards being one of the strongest proposals for 4G, it is of interest to characterise qualitatively and quantitatively the impact of the mentioned technique onto a convergent wireless scenario.

In general, the availability of MIMO spatial modes and wireless standards are two forms of diversity that can be exploited dynamically in one step or in two. If it is done in one, the antennas, the coding schemes, the transmit powers, etc., and the standards, would be chosen in one go. If it is done in two steps, the standard should be selected first, followed by the selection of the MIMO spatial modes within each standard. Each of these two steps have fewer degrees of freedom than the single step case, and can lead to sub-optimum performances as the two selections may depend on each other.

This is the goal of this thesis. In order to achieve it, public software tools were modified and used. Regarding MIMO, a SISO channel model [Marq01] was extended to support MIMO. Regarding the standards convergence, the simulator described in [Agui03] was provided with a physical layer to cope with MIMO capacity enhancements.

A key concept behind the present work is a common core network based on Internet Protocol (IP), to which a variety of wireless access points/technologies will be connected. The selected technologies that will be considered throughout this thesis are GSM/General Packet Radio Service (GPRS), Universal Mobile Telecommunication System (UMTS), and High-PErformance Radio Local-Area Network type 2 (HIPERLAN/2). The combination of these three access technologies provides a broad data rate support, a wide range of mobility, and from the application point of view, voice, data and multimedia support, Figure 1.3.

However, the study of the impact of a propagation technique on the traffic behaviour of a system implies considering the system as a whole and not as a purely stacked protocol with independent layers. The novelty of this thesis is based on the establishment of a relation between the MIMO spatial propagation modes and the multi-standard availability, through the

channel capacity. In a purely layered protocol, the optimisation of the performance of each level is normally sought independently of the preceding and following layers. This is normally done for simplicity and reusability reasons, *i.e.*, one layer can change its attributes without the need to change the other layers. However, this usually leads to sub-optimum performances because the sum of optimised layers does not necessarily lead to an optimised system, *i.e.*, the optimisation of one layer may depend on the characteristics of another one.
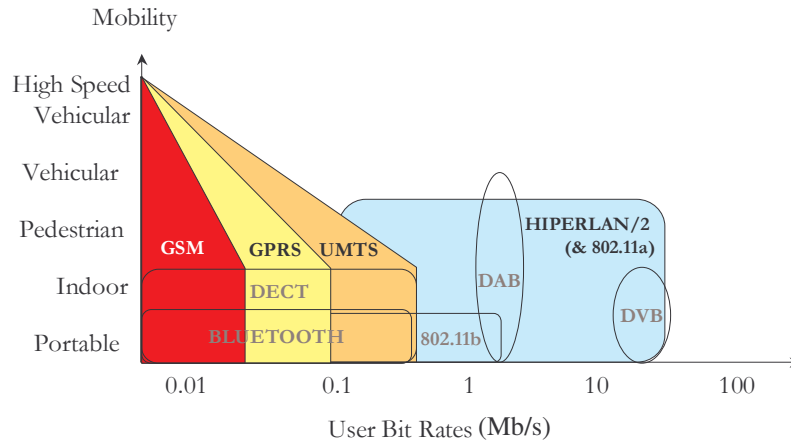
Figure 1.3: Support for User Data Rate versus Mobility of Different Radio Access Technologies (based on [ACGN02]).

After the introduction, this document is initiated with an overview of UMTS and HIPERLAN/2, Chapter 2, where the main focus is put in the capacity aspects of the radio interfaces. Although GSM/GPRS is used, it is not overviewed because it is widely known and it is not provided with multiple antennas. Chapter 3 consists of an overview on MIMO channel modelling: after some historical remarks, the mathematics of the different attempts to model the MIMO channel are described, and the Shannon's capacity formula is generalised for multiple antennas. Chapter 4 presents and discusses the specific MIMO model used, from a description of its baseline SISO model to a capacity-based assessment. Chapter 5 presents the specific model used to simulate the standards convergence. It includes the description of the original implementation, and how it was modified to cope with the MIMO capacity enhancement. After a parameterisation of the scenarios, Chapter 6 illustrates and interprets the simulation results in the following two criteria: a varying number of users benefiting from a fixed set of standards, and a fixed number of users utilising different sets of available standards. Chapter 7 presents general conclusions and suggests future work.

2

Systems Overview

This chapter presents an overview of the technologies under study, i.e., UMTS (Section 2.1) and HIPERLAN/2 (Section 2.2) with a special focus on radio interface issues, even though protocols and architectures are also briefly described. The GSM standard is not addressed because it is widely known, and also because it is not supplied with multiple antennas. The aim is to make the reader comfortable with the basic characteristics of these systems.

2.1   UMTS

2.1.1 Introduction

The overview of the UMTS presented in this section is based on [HoTo01]. UMTS supports two basic modes of operation: FDD and TDD. In the FDD mode, separate 5 MHz frequency bands are used for the Up- and Downlinks (UL and DL respectively), whereas in TDD the same bandwidth is time-shared between UL and DL. The FDD mode is the main one to be used, while TDD was added to extend UMTS to the asymmetric services.

In UTRA, the radio interfaces are defined in such a way that a wide range of services, including speech, data, and multimedia, can be simultaneously used by a subscriber and multiplexed onto a single carrier. Therefore, Circuit and Packet Switched (CS and PS, respectively) services are efficiently supported, and real- and non-real-time operations employing transparent and non-transparent data transport are specified. The Quality of Service (QoS) is an important feature in UMTS, and it is specified to be adjusted in terms of parameters such as delay, Bit Error Rate (BER), Frame Error Rate (FER), and others.

The architecture of UMTS consists of a Core Network (CN), UTRA and User Equipment (UE) or, generally, MT. The versatility provided by UTRA allows the use of the conversational, streaming, interactive, and background traffic classes.

In the next sections, an overview of the UMTS system is provided, with a particular focus on the radio interface of the FDD mode.

2.1.2 System Architecture

UMTS consists of a number of logical Network Elements (NEs), each one having a defined functionality. NEs are defined at the logical level, but this quite often results in a similar physical implementation, especially since there are a number of standardised open interfaces. Functionally, NEs are grouped into the UMTS Terrestrial Radio Access Network (UTRAN), which handles all radio-related functionalities, and the CN, which is responsible for switching and routing calls and data connections to external networks. Finally, the UE bridges the user with the radio interface. Figure 2.1 shows the elements in a UMTS Public Land Mobile Network (PLMN), and, in order to illustrate the connections, also external networks.

From a specification and standardisation viewpoints, both the UE and the UTRAN consist of new protocols, designed upon the needs of the new WCDMA radio technology. On the other hand, the definition of the CN is adopted from the GSM/GPRS one.

The UE consists of the Mobile Equipment (ME) and the UMTS Subscriber Identity Module (USIM). The UTRAN architecture consists of one or more Radio Network Subsystems (RNSs). An RNS is a sub-network within UTRAN, and consists of one Radio Network Controller (RNC) and one or more Node Bs (the BSs). RNCs are connected among each other via an Iur interface; RNCs and Node Bs are connected with an Iub interface. The Iu, Iur and Iub are logical interfaces, which may be provided via any suitable transport network.

The RNC is the NE responsible for the control of the radio resources of the UTRAN. It interfaces the CN with UTRAN, and also terminates the Radio Resource Control (RRC) protocol that defines the messages and procedures between the UE and the UTRAN.

 The main function of the Node B is to perform the air interface Layer 1 processing (channel coding and interleaving, rate adaptation, spreading, etc.) and some basic Radio Resource Management (RRM) operations, such as the inner loop Power Control (PC).

The main elements of CN are the Home Location Register (HLR), Mobile Services Switching Centre/Visitor Location Register (MSC/VLR), Gateway MSC (GMSC), Serving GPRS Support Node (SGSN), and Gateway GPRS Support Node (GGSN).
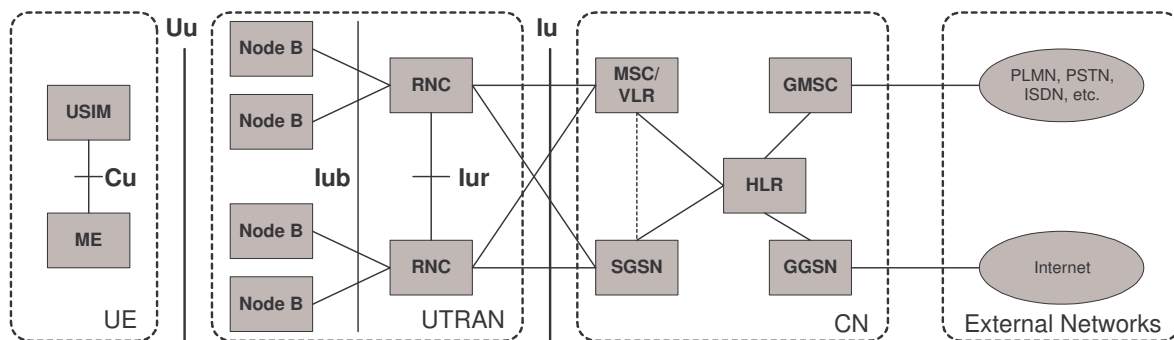
Figure 2.1: NEs in a UMTS PLMN (extracted from [HoTo01]).

2.1.3 Radio Interface

Even though for the overall system performance the protocols in the higher layers have a great deal of impact, the physical layer defines the fundamental capacity limits.

The IMT-2000 spectrum allocation in Europe, Japan, Korea, and the USA is shown in Figure 1.1. In Europe, and in most of Asia, the IMT-2000 bands of 2×60 MHz (1920-1980 MHz and 2110-2170 MHz) are available for UMTS FDD. The availability of the TDD spectrum varies: in Europe, 25 MHz are available for licensed TDD use in the 1900-1920 MHz and 2020-2025

MHz bands. The rest of the unpaired spectrum is expected to be used by unlicensed TDD applications in the 2010-2020 MHz band.

In order to support bit rates up to 2 Mb/s, the use of a variable Spreading Factor (SF) and multicode connection is supported. The constant chip rate of 3.84 Mchip/s leads to a carrier bandwidth of approximately 5 MHz. Subject to operating licenses, the network operator can deploy multiple 5 MHz carriers, possibly in the form of hierarchical cell layers.

UMTS supports highly variable user data rates or, in other words, it supports the concept of Bandwidth-on-Demand (BoD): the capacity among users can change from frame to frame (10 ms long), during which the user data rate is kept constant.

Table 2.1 summarises the main parameters related to the UMTS air interface.

Table 2.1: Main UMTS Parameters.

Maximum Transmission Power	43 dBm
Multiple Access Method	DS-CDMA
Carrier Spacing and Bandwidth	5 MHz
Chip Rate	3.84 Mchip/s (Constant)
Frame Length	10 ms
Power Control	Closed loop 1500 Hz in UL and DL
DL Transmit Diversity	Supported by the Standard to Improve DL Capacity
Packet Data	Load-based Packet Scheduling
Duplexing Method	FDD and TDD
Base Station Synchronism	Asynchronous
Multirate Concept	Variable Spreading Factor and Multicode
Inter-Frequency Handovers	Possible, Measurements with Slotted Mode
Detection	Coherent Using Pilot Symbols or Common Pilot
Multiuser Detection and Smart Antennas	Supported by the Standard, Optional in the Implementation
Quality Control	Provided by RRM Algorithms
Service Multiplexing	Different QoS Services Multiplexed on one Connection

Managing power through PC is of essential importance in WCDMA, since users are sharing the same bandwidth at the same time, thus, interfering with each other.

In the FDD mode, open- and closed-loop PC can be distinguished. The former is used if no direct feedback link between the UE and the Node B is available or to provide a coarse initial power setting at the beginning of the connection, *e.g.*, during connection set-up phase on the random access channel. It assumes similarity between the UL and the DL channels, so the receiver can adjust its transmission parameters by measuring the arriving signal quality. This procedure is not the most appropriate for FDD operation as the channel quality is frequency dependent, and the UL and DL make use of different frequencies. Open loop PC is mainly applied with common channels.

Closed-loop PC involves a feedback link between the UE and the Node B. Despite the increased accuracy this PC mode presents, the delay between the channel quality measure by the receiver and the transmitter reaction can ruin the power adaptation if it is longer than the coherence time of the channel (time interval over which the channel impulse response is essentially invariant). If this were the case, the transmission parameters would be adapted to a past channel state, and not to the channel state they were supposed to be applied to. Closed-loop PC can be characterised by a two-staged process, comprising two feedback loops: the inner and the outer ones. The inner loop control, also referred to as fast power control, aims at combating the fast fading; the SIR value is estimated at reception, and a power up or down command is sent at a rate of 1 500 Hz. The outer loop aims at controlling the target SIR level of the inner loop; for this purpose, the RNC measures the BLock Error Rate (BLER) of the received data, and sets the target SIR around the minimum value that fulfils the required quality.

In UMTS, two channel coding methods have been defined. Half-rate and 1/3-rate convolutional coding are intended to be used with relatively low data rates, equivalent to the date rates provided by 2G cellular networks today, though an upper limit has not been specified. For higher data rates, 1/3-rate turbo coding can be applied, which typically brings performance benefits when large enough block sizes are achieved.

The fact that UMTS is a wideband system (a system using a bandwidth wider than the coherence band of the channel), provides frequency diversity: different frequencies of the signal fade differently, thus, some channel stabilisation is achieved through a frequency averaging effect.

Furthermore, advanced receivers, such as the Rake one, make use of pilot signals to obtain basic knowledge of the channel and to be able to undo the phase rotations suffered by each of the multiple replicas of the signal arriving at different time instants through different paths. In

the end, the phase-rotated replicas are summed constructively to reconstruct the original signal. From this perspective, Inter-Symbol Interference (ISI) is seen as a way to provide multipath diversity (spatial diversity achieved by having single transmit and receive antenna elements, but multiple propagation paths connecting them).

The data generated at higher layers is carried over the air interface in transport channels, which are mapped onto the physical layer via the so-called physical channels. There are two types of transport channels: common and dedicated ones. The main difference between them is that the former serves a group of users (possibly all), whereas the latter, identified by a certain code on a certain frequency, is reserved for a single user only. A list of the transport channels is presented in Table 2.2.

Table 2.2: Transport Channels in UMTS (based on [HoTo01]).

Channel	Type	Link	Channel Identification
DCH	Dedicated	BS↔MT	Dedicated Channel
BCH	Common	BS→MT	Broadcast Channel
FACH	Common	BS→MT	Forward Access Channel
PCH	Common	BS→MT	Paging Channel
RACH	Common	BS←MT	Random Access Channel
CPCH	Common	BS←MT	UL Common Packet Channel
DSCH	Common	BS→MT	DL Shared Channel

The only dedicated transport channel is called DCH. It carries all the information intended for the given user coming from layers above the physical one, including data for the actual service as well as higher control information. The DCH is mapped onto two physical channels: the Dedicated Physical Data Channel (DPDCH) carries higher layer information, including user data, while the Dedicated Physical Control Channel (DPCCH) carries the necessary physical layer control information. Both are needed to efficiently support DPDCH bit rate variations, done on a frame basis.

The common transport channels needed for the basic network operation are RACH, FACH and PCH, while the use of DSCH and CPCH is optional and can be decided by the network operator.

The transmission of the physical channels consists on three main processes: spreading, scrambling and modulation. The spreading transforms each symbol into an SF number of

chips, increasing the signal bandwidth by a factor of SF. The spreading codes are derived from the Welsh-Hadamard orthogonal codes tree. Independently of the SF, the constant chip rate of 3.84 Mchip/s used leads to a carrier bandwidth of approximately 5 MHz. The deployment of multicode connection to transmit to a single user is supported to increase the throughput of a specific user. The final goal of the spreading codes is to separate transmissions from the same source: DL connections from the same cell/sector, and UL transmissions of the dedicated physical control and data channels.

After the spreading, the signal is further multiplied by a so-called scrambling code, not changing the system bandwidth and allowing the signals from different sources to be separable. Finally, the chip sequence generated by the spreading process is modulated (Quadrature Phase Shift Keying –QPSK– in DL and Binary Phase Shift Keying –BPSK– in UL) and transmitted over the radio interface. The functionalities and characteristics of the spreading and channelisation and scrambling codes are summarised in Table 2.3.

Table 2.3: Functionalities of the Channelisation and Scrambling Codes (adapted from [HoTo01]).

	Channelisation Code	**Scrambling Code**
Usage	**UL**: Separation of Physical Data (DPDCH) and Control Channels (DPCCH) from Same Terminal. **DL**: Separation of Transmissions to Different Users within a Cell.	**UL**: Separation of Terminals. **DL**: Separation of Sectors (cells).
Length	**UL**: 4-256 Chips (1.0−66.7µs). **DL**: 4-512 Chips(1.0−133.4µs).	**UL**: (1) 10 ms = 38 400 Chips. (2) 66.7 µs = 256 Chips. **DL**: 10 ms = 38 400 Chips.
Number of Codes	Number of Codes under one Scrambling Code = SF	**UL**: Several Millions. **DL**: 512
Code Family	OVSF	**Long code**: Gold Code. **Short Code**: Extended S(2) Code Family. Allows Independent OVSF Code Tree Usage Between Different Cells/ Sectors.
Spreading	Increases Transmission Bandwidth by a Factor of SF.	Does Not Affect Transmission Bandwidth.

The channelisation codes of UTRA are based on the Orthogonal Variable Spreading Factor (OVSF) technique. The use of OVSF codes allows the SF to be changed, and orthogonality between different spreading codes of different lengths to be maintained.

In the UL, the physical layer control information is carried by the DPCCH with a fixed SF of 256. The higher layer information, including user data, is carried on one or more DPDCHs, with a SF ranging from 256 down to 4.

The maximum user data rate on a single code is derived from the maximum channel bitrate, which is 960 kb/s, without channel coding and a SF of 4. With channel coding, the practical maximum user data rate for the single code rate is in the order if 400-500 kb/s. When higher data rates are needed, parallel code channels are used. Up to six parallel codes can be used, raising the channel bit rate for data transmission up to 5 760 kb/s, which can accommodate 2 Mb/s user data or an even higher data rate if the coding rate is ½. The achievable data rates with different SFs in the UL are presented in Table 2.4. The rates given assume a ½ – rate coding and do not include bits taken for coder tail bits or the Cyclic Redundancy Check (CRC). The relative overhead due to tail bits and CRC bits has significance only with low data rates.

Table 2.4: UL DPDCH Data Rates.

DPDCH Spreading Factor	DPDCH Channel Bitrate [kb/s]	Maximum User Data Rate with ½-rate Coding (approx.) [kb/s]
256	15	7.5
128	30	15
64	60	30
32	120	60
16	240	120
8	480	240
4	960	480
4, with 6 parallel codes	5 760	2 300

In DL, the SF for the highest transmission rates determines the channelisation code to be reserved from the given code tree. As the SF is always fixed in the DPCH, the lower rates are

implemented with discontinuous transmission, by gating the transmission ON/OFF or with repetition of the bits. In the DL, the SF ranges from 4 to 512, with some restrictions on the use of 512 in the case of soft handover.

The DL data rates are given in Table 2.5 with raw bit rates calculated from the QPSK-valued symbols. When higher data rates are needed, parallel code channels are used as in the case of UL transmission. Up to three parallel codes can be used, rising the channel bit rate for data transmission up to 5 760 kb/s, which can accommodate 2 Mb/s user data rate or even higher rate if the coding rate is ½.

Table 2.5: DL Dedicated Channel Bitrates.

Spreading Factor	Channel Bit Rate [kb/s]	DPDCH Channel Bit Rate Range [kb/s]	Maximum User Data Rate with ½-Rate Coding (approx.) [kb/s]
512	15	3-6	1-3
256	30	12-24	6-12
128	60	42-51	20-24
64	120	90	45
32	240	210	105
16	480	432	215
8	960	912	456
4	1 920	1 872	936
4 (3 parallel codes)	5 760	5 616	2 300

In addition to the DL dedicated channel, user data (low rate) can be sent on both the DSCH and FACH. In the DL, services are multiplexed dynamically in a similar way than in UL.

To end this section, a brief description of UMTS handover procedures follows. Apart from the hard handover (that can be used for cell, frequency and/or mode changing), where an MT travels from one cell to another without any diversity increase, there are two main ways for the MT to interact with more than one cell or sector in order to achieve macro diversity: the soft and the softer handover. In the former case, the MT stands in the overlapping area of two cells communicating with two BSs: the DL communication is done concurrently via two different spatial channels using two different spreading codes, and, in the UL, the signals

received by both BSs are combined in the RNC; two PC loops are performed. In the latter, the MT stands in the overlapping area of two sectors within the same cell, communicating with antennas in two different sectors: the DL is similar to the soft handover from the MT perspective, but, in the UL, one single code is used and both signals, received by the corresponding sectors, are transmitted to the same (Rake) receiver as if they were two normal replicas coming from two different paths. Only one PC loop is involved.

While softer handover aims at achieving some extra spatial diversity in the overlapping area of two sectors, soft handover is needed to avoid situations where one MT penetrates deeply into the adjacent cell and the original cell demands an increase of the transmitted power, as this would result in large interference in the cell where the MT actually stands (and by which would not be power controlled if no soft handover was performed). Frequent hard handovers could avoid the problem, but the delays involved and the signalling load would be excessive.

2.1.4 Capacity and Interference

In wireless cellular systems, capacity and interference are related through several different trade-offs, balanced by numerous random variables and system constraints, such as, propagation environments, transmitted powers, traffic loads, bit rates, etc..

Multipath propagation for example, apart from the provided multipath diversity, also entails loss of orthogonality of the spreading codes, the overall effect being advantageous at cell edge and disadvantageous for MTs near the BS. On the other hand, considering a single Power Delay Profile (PDP), *i.e.*, the same multipath propagation environment, increasing the MT's speed enhances the performance of the transmission to users near the cell edge, while close to the BS, low MTs' speeds perform better. Regarding cell range, macro-cells are likely to grant lower throughput than micro-cells, due to the higher vulnerability to inter-cell interference. Besides, the expected maximum achievable DL bitrate is significantly different from the UL one, in the former type of cell (more throughput in UL), while both are quite balanced for the latter. The reason is based on the loss of orthogonality of the spreading codes.

When dimensioning a UMTS network, it is very important to estimate the three main limiting capacity factors: the air interface traffic load, the maximum BS transmitting power, and the number of the OVSF codes (the last one being important only in particular situations, *e.g.*, with all the users next to the BS and demanding low data rates). With a frequency reuse of 1, UMTS capacity is particularly sensitive to the amount of interference. For this purpose, two load measures can be considered: load estimation based on throughput and on power.

For the throughput load based estimation, the following two load parameters are considered: UL Load Factor (LF), $\eta_{T\text{-}UL}$, and DL LF, $\eta_{T\text{-}DL}$. These two parameters are commonly used for

the purpose of predicting cell capacity and planning noise raise in the dimensioning of UMTS networks, and are given by the following two equations:

$$\eta_{T\text{-}UL} = (1+i) \cdot \sum_{j=1}^{N_{UL}} \left(1 + \frac{R_c / R_{bj}}{\left(E_b / N_0 \right)_j \cdot v_j} \right)^{-1} \tag{2.1}$$

$$\eta_{T\text{-}DL} = \left[\left(1 - \overline{\alpha} \right) + \overline{i} \right] \cdot \sum_{j=1}^{N_{DL}} v_j \cdot \frac{\left(E_b / N_0 \right)_j}{R_c / R_{bj}} \tag{2.2}$$

where:

- N_{UL} is the number of users per cell,
- N_{DL} is the number of connections per cell = $N_{UL} \times (1 + \text{soft handover overhead})$,
- v_j is the activity factor of user j at physical layer (usually taken as 0.67 for speech and 1 for data),
- E_b is the signal energy per bit,
- N_0 is the noise spectral density including thermal noise and interference,
- R_c is the WCDMA chip rate (3.84 Mchip/s),
- R_{bj} is the bitrate of user j (dependent on service),
- i is the inter-cell to intra-cell interference ratio seen by the BS receiver,
- $\overline{\alpha}$ is the average orthogonality factor in the cell (depends on the multipath propagation, ranging from 0 up to 1; values of 60 % for vehicular and of 90 % for pedestrian scenarios were used in [Reis04]),
- $\overline{i}$ is the inter- to intra-cell BS power ratio received by user (typically 65 % for macro-cells and 20 % for micro-cells),.

The E_b/N_0 ratio is commonly obtained through complex simulations; the values used for the link budget calculations are extracted from [FCSC02], Table 2.6.

Table 2.6: E_b/N_0 Used for Link Budget Calculations (extracted from [FCSC02]).

E_b/N_0 [dB] / Bearer Service [kb/s]	3 km/h		120 km/h	
	UL	DL	UL	DL
12. 2	6.8	10.4	5.0	6.2
64	3.8	6.2	2.8	4.4
128	3.4	5.0	2.4	4.2
384	3.8	4.6	2.8	4.2

These load equations allow for the prediction of the amount of noise raise over thermal noise due to interference. The noise raise, $N_{i\text{-}UL}$, in the UL is equal to:

$$N_{i\text{-}UL} = -10\log_{10}(1-\eta_{\text{T-UL}}). \tag{2.3}$$

Similarly, the noise raise in the DL, $N_{i\text{-}DL}$, is given by:

$$N_{i\text{-}DL} = -10\log_{10}(1-\eta_{\text{T-DL}}). \tag{2.4}$$

When the LFs become close to 1, the corresponding noise raise approaches infinity and the system has reached its pole capacity. The load estimation based on power for the UL, $\eta_{\text{P-UL}}$, and DL, $\eta_{\text{P-DL}}$, are given by the following two equations:

$$\eta_{\text{P-UL}} = 1 - P_N/I_{Total} \tag{2.5}$$

$$\eta_{\text{P-DL}} = P_{Total}/P_{max} \tag{2.6}$$

where
- P_N is the background and receiver noise power,
- I_{Total} is the received wideband interference power (at the BS),
- P_{Total} is the total DL transmission power,
- P_{max} is the maximum BS transmission power.

I_{Total} can be divided into the interference powers of intra-cell users, I_{intra}, inter-cell users, I_{inter}, and P_N:

$$I_{Total} = I_{intra} + I_{inter} + P_N \tag{2.7}$$

The two load estimation methods (throughput and power) provide different tools for load measuring. In the power-based approach for DL, the total Node B's transmission power P_{Total} does not provide accurate information concerning how close to the DL pole capacity the system is operating, in opposition to the throughput-based one. For example, in a small cell, the same P_{Total} corresponds to higher air interface loads than in a large cell.

In the power-based approach for UL, interference from adjacent cells is directly included in the load estimation, meaning that if the load in adjacent cells is low, this can be seen in the power-based load measurements, and a higher load can be allowed in this cell, *i.e.*, soft capacity can be obtained. In opposition, UL throughput-based load estimation does not take interference from adjacent cells or adjacent carriers directly into account.

On the other hand, the capacity can also be limited by the fact that the BS transmit power is upper bounded by P_{max}:

$$P_{max} = \frac{N_0 \cdot R_c}{1 - \eta_{\text{T-DL}}} \sum_{j=1}^{N_{UL}} \frac{\left(E_b / N_0 \right)}{R_c / R_{bj}} \cdot \overline{L_{pj}} \tag{2.8}$$

where $\overline{L_{pj}}$ is the average attenuation between the BS and user j.

Especially in the DL, it has to be confirmed if the number of available channelisation codes is limiting the system capacity or not. Considering the set of services presented in [Reis04], the corresponding SFs and numbers of codes, Table 2.7, determine the number of users in the system. The channel bit rate is obtained through:

$$\text{Channel Bitrate} = \frac{7\,680}{\text{DL SF}} \tag{2.9}$$

Table 2.7: Services vs. UL/DL Spreading Factors and UL/DL Codes (adapted from [FCSC02]).

Service	UL SF	DL SF	UL codes	DL codes
Speech Telephony	64	128	4	2
Video Telephony	16	32	16	8
Streaming Multimedia Low Quality	128	16	2	16
Streaming Multimedia High Quality	128	8	2	32
Web Browsing	128	32	2	8
Location Based	128	128	2	2
Multimedia Messaging Service	16	32	16	8
Electronic Mail	32	64	8	4
File Download	128	32	2	8

The number of channelisation codes depends directly on the SFs, which are related to the channel bit rates: they may vary between a SF of 4 (960 kb/s) and 256 (15 kb/s) in the UL, and a SF of 4 (1 920 kb/s) and 512 (15 kb/s) in the DL. The utilisation of a specific code causes the unavailability of the sub-tree of higher SFs descending from that code, meaning that a limit on the number of channelisation codes is imposed mainly by high bit rate services with low spreading factors. Consequently, when users demand a mix of services, those requiring fewer codes, *e.g.*, Speech Telephony or Location-Based, will leave more resources to others, letting more MTs to access the system; on the opposite side, code-consuming services, *e.g.*, Streaming Multimedia, utilise the total amount of resources allowing few users to access the system.

2.2   HIPERLAN/2

2.2.1 Introduction

HIPERLAN/2 [ETSI00a] is a standard for high-speed radio communications with typical data rates ranging from 6 to 54 Mb/s, working in the 5 GHz band with 20 MHz bandwidth channels.

Restricted user mobility (up to 10 m/s) is supported within the local service area or cell. Figure 1.3 shows HIPERLAN/2 mobility and capacity in comparison with other wireless technologies.

Apart from the reasonable balance in the mobility versus data-rate trade-off, HIPERLAN/2 presents a few other features that makes it raise above other wireless technologies:

- QoS handling: capable of supporting practically any type of service or application by providing mechanisms to handle QoS.
- Centralised and direct mode: even though the access is primarily done via a fixed access point, ad-hoc network capabilities (direct mode operation) are part of the original BRAN project [ETSI00a].
- Possibility of roaming: roaming could be supported by the standards outside the scope of the BRAN project.
- Convergence layer: offering backbone independence, makes it appropriate for internetworking with other core networks (3G cellular networks, IP or ATM-based networks) and protocols (IEEE 1394, etc.).
- True usable maximum data rate of 42 Mb/s compared to IEEE 802.11a maximum of 18 Mb/s (for Ethernet packets with an average size of 512 bytes), enhanced security and very cost effective [HIPE04].

2.2.2 System Architecture

A HIPERLAN/2 network typically has a topology as depicted in

Figure 2.2: MTs communicate with the Access Points (APs) over a radio interface. There is also a direct mode of communication between two MTs (as previously referred), which is not further considered in this report. The MT may move around freely in the HIPERLAN/2 network; after association has been performed, the MT only communicates with one AP at each moment. The radio network is automatically configured, taking into account changes in the radio network topology, *i.e.*, there is no need for manual frequency planning.
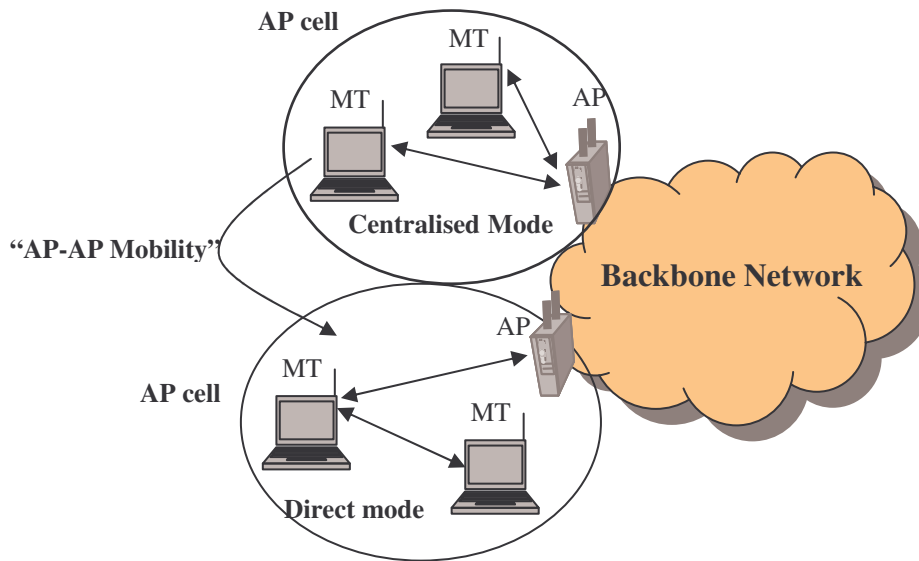
Figure 2.2. HIPERLAN/2 Network Structure (adapted from [KrSa01]).

The cell range depends on the environment: a radius of about 30 m in an indoor environment and about 150 m in an outdoor one is expected [KrSa01]. The AP cell is connected to a Backbone Network (BN) through the AP; the BN can, for example, be a wired Ethernet LAN. Through the BN, different AP cells are interconnected, and an increased coverage is accomplished. The BN also provides specific services for MTs, *e.g.*, access to the Internet. Different AP cells may partially overlap and an MT, which is dynamically associated with an AP cell, can therefore move between two different cells with a handover or a re-association mechanism.

2.2.3 Radio Interface

In Figure 2.3 the protocol reference model for the HIPERLAN/2 radio interface is depicted. The protocol stack is divided into a control plane part and a user plane one following the semantics of Integrated Services Digital Network (ISDN) functional partitioning. User plane includes functions for transmission of traffic over established connections, and the control plane includes functions for the control of connection establishment, release and supervision.

The HIPERLAN/2 protocol has three basic layers: PHYsical layer (PHY), Data Link Control layer (DLC), and Convergence Layer (CL).

PHY delivers a basic data transport function by providing means of a baseband modem and a Radio Frequency (RF) part [ETSI00a]. The baseband modem also contains a Forward Error Correction (FEC) function. The PHY layer breaks down the packets from the Medium Access Control (MAC) function of the DLC layer into Orthogonal Division Frequency Multiplex (OFDM) symbols and transmits them [KrSa01].
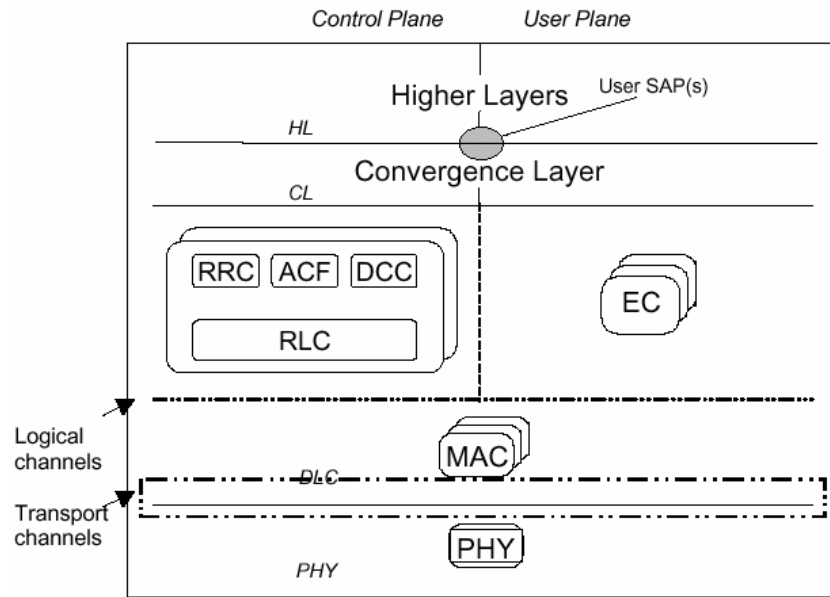
Figure 2.3: HIPERLAN/2 Protocol Reference Model (based on [HIPER01]).

The allocated spectrum is a license exempt band, which means that the frequency bands are free to be used as long as the spectrum rules are fulfilled, Table 2.8. In addition to the spectrum rules shown in this table, there are requirements on implementing PC and Dynamic Frequency Selection (DFS), which are RRM functions.

Table 2.8: Spectrum Allocation and Rules for HIPERLAN/2 in Europe (based on [ETSI00a] and [KrSa01]).

Frequency Band [MHz]	Nominal Carrier Frequencies [MHz]	Number of Channels	EIRP Limit [W]	Usage
5 150 - 5 350	5 180+20·n, $n \in$ [0, 7]	8	0.2	Indoor
5 470 - 5 725	5 200+20·n, $n \in$ [0, 10]	11	1 (0.2 for the Highest Channel)	Indoor and outdoor

The PHY layer provides several transmission modes with different coding rates and demodulation schemes. The benefit of using different schemes is that a scheme supporting a high transmission rate can be used when transmission conditions are favourable. The function of choosing modulation schemes depending on transmission conditions is called Link Adaptation (LA). LA can be based on the estimated carrier to interference ratio, *C/I,* values at the receiver and this of course requires protocols for initiating and sending measurements. Another simpler technique is to select the mode depending on the Packet Data Unit (PDU) Error Rate (PDER). The PHY layer supports other RRM functionalities, besides LA, such as

DFS, PC and handover. The main purpose of these functions is to increase the overall performance of the system.

The DLC layer consists of the Error Control (EC) function, the MAC function and the Radio Link Control (RLC) function. It is divided into the user data transport functions and the control functions. The user data transport function is fed with user data packets from higher layers via the User Service Access Point (U-SAP). This part contains the EC, which performs Automatic Repeat reQuest (ARQ) protocol. The RLC sublayer delivers a transport service to the DLC Connection Control (DCC), the RRC and the Association Control Function (ACF).

The air interface is based on TDD and TDMA, *i.e.*, the time-slotted structure of the PDU allows for simultaneous communication in both DL and UL within the same time frame (MAC frame in HIPERLAN/2). Besides, data meant for different MTs is separated also in time. Time slots for DL and UL communication are allocated dynamically depending on the need for transmission resources.

The basic MAC frame structure has a fixed duration of 2 ms and comprises transport channels for broadcast control, frame control, access control, DL and UL data transmission, and random access, Figure 2.4. All data from both AP and MTs is transmitted in dedicated time slots, except for the Random access Channel (RCH) where contention for the same time slot is allowed. The duration of broadcast control is fixed, whereas the duration of other fields is dynamically adapted to the current traffic situation. A MAC frame comprises a broadcast, DL, UL and random access phases. The broadcast phase comprises fields for Broadcast CHannel (BCH), Frame control Channel (FCH) and Access feedback CHannel (ACH) while the UL and DL phases carry traffic from/to an MT in bursts of packets called Long CHannels (LCH) and Short CHannels (SCH). A LCH contains control or user data and a SCH contains only control data (*e.g.*, acknowledgements and Resource Requests-RRs-in the UL) and is always generated by the DLC layer.

Both logical and transport channels were introduced in the HIPERLAN/2 standard, in order to improve readability and to define the exact terms for the structures that are used to construct the MAC frames [ETSI00b]. The logical channels are mapped onto different transport channels that are the basic elements to construct PDU trains. These represent the interface between the DLC protocol and the PHY layer [ETSI00c]. Transport channels describe the basic message format while its contents and interpretation are subject to the logical channels.

Table 2.9 contains a list of HIPERLAN/2 transport and logical channels (according to [ETSI00b]). The "links" column indicates the possible transmission links on each channel (UL, DL or both).
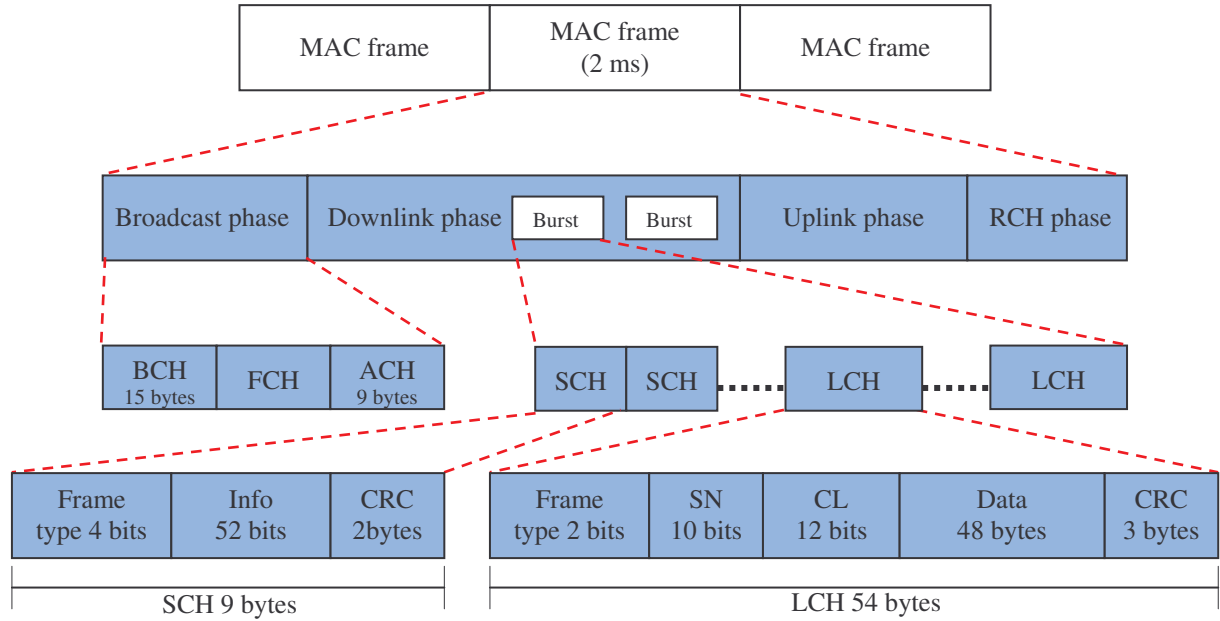
Figure 2.4: A MAC Frame Structure in HIPERLAN/2 (extracted from [KrSa01]).

A PDU train comprises DLC User PDUs (U-PDUs of 54 bytes with 48 bytes of payload) and DLC control PDUs (C-PDUs of 9 bytes) to be transmitted or received by one MT. There is one PDU train per MT (if resources have been granted in the FCH). The C-PDUs are referred to as the SCH, and the U-PDUs are referred to as the LCH.

HIPERLAN/2 supports QoS by allowing the AP to set up and manage the different radio bearers during transmission [KMST00]. The AP selects the appropriate EC mode (acknowledged, unacknowledged and repetition) including detailed protocol settings (*e.g.*, ARQ window size, number of retransmissions, and discarding). Scheduling is performed at the MAC level, where the AP determines how much data and control signalling will be sent in the current MAC frame. For example, by regularly polling a MT for its traffic status (pending data to be transmitted), the AP provides the terminal's radio bearer with short access delay. The polling mechanism provides rapid access for real-time services. Additional QoS support includes LA and internal functions (admission, congestion and dropping mechanisms) to avoid overload situations.

The CL has two main functions: it adapts service requests from higher layers to the service offered by the DLC and it converts higher-layer packets of fixed or variable length into a fixed-length Service Data Unit (SDU) that is used within the DLC [KMST00].

A brief description of HIPERLAN/2 dynamics follows. The system uses a centralised common mechanism, and the AP is responsible for assigning radio resources within the MAC frame. Any MT that wants initial access to the radio network uses the RCH for sending a RR to the AP. If a collision occurs during a RR, the AP will inform the requesting MT in the

following ACH and a back off procedure in the RCH will take place. After a successful RR, which is indicated in the ACH, the MT goes into a contention free mode where the AP schedules the MTs transmissions. A RR contains the number of pending LCHs in the MT and the AP uses this information when assigning radio resources. The FCH sent by the AP contains an exact description of the resource allocation within a MAC frame, *i.e.*, the time slots which an MT shall transmit or receive. The length of the FCH depends on the number of scheduled sessions. The BCH is used by the AP to broadcast cell information such as the identity of the AP, the AP transmission power and the expected received power level at the AP. The transmission mode used in the broadcast phase and the RCH phase is the most robust (mode 1) since this information is supposed to be received by all MTs in the AP cell.

Table 2.9: HIPERLAN/2 Transport and Logical Channels (based on [ETSI00b]).

Type	Links	Channel	Channel Identification
Transport Channels	MT←BS	BCH	Broadcast Channel
	MT←BS	FCH	Frame Channel
	MT←BS	ACH	Access Feedback Channel
	MT↔BS	SCH	Short Transport Channel
	MT↔BS	LCH	Long Transport Channel
	MT→BS	RCH	Random Access Channel
Logical Channels	MT←BS	BCCH	Broadcast Control Channel
	MT←BS	FCCH	Frame Control Channel
	MT←BS	RFCH	Random Access Feedback Channel
	MT↔BS	RBCH	RLC Broadcast Channel
	MT↔BS	DCCH	Dedicated Control Channel
	MT↔BS	UBCH	User Broadcast Channel
	MT↔BS	UMCH	User Multicast Channel
	MT↔BS	UDCH	User Data Channel
	MT↔BS	LCCH	Link Control Channel
	MT→BS	ASCH	Association Control Channel

2.2.4 Capacity and Interference

HIPERLAN/2 is a standard with an LA mechanism to adapt its bitrate to the channel's conditions, granting low PDER in unfavourable channels, while exploiting the channel's potential in propagation environments with superior conditions. In Table 2.10, the different transmission modes, their modulation and coding schemes are presented, together with their

achievable bitrates and requirements on receiver sensitivity. This sensitivity is defined as the power level needed at the receive antenna at which the PDER is below 10 %. The data rate ranging from 6 to 54 Mb/s can be varied by using the several transmission modes for each OFDM sub-carrier.

Table 2.10: Transmission Modes, Modulations, Code Rates, Bitrates, and Receiver Sensitivities for HIPERLAN/2 (based on [ETSI00c] and [KrSa01]).

Mode	Modulation and Coding Rate	Code Rate	PHY Layer Transmission Rate [Mb/s]	Receiver Sensitivity [dBm]
1	BPSK	$\frac{1}{2}$	6	-85
2	BPSK	$\frac{3}{4}$	9	-83
3	QPSK	$\frac{1}{2}$	12	-81
4	QPSK	$\frac{3}{4}$	18	-79
5	16-QAM	$\frac{9}{16}$	27	-75
6	16-QAM	$\frac{3}{4}$	36	-73
7	64-QAM	$\frac{3}{4}$	54	-68

However, the capacity of a HIPERLAN/2 system in a realistic environment is normally known through simulations or measurement campaigns. It depends upon a number of factors, such as the available number of frequencies, the propagation conditions, and the presence of interference, *e.g.*, another HIPERLAN/2 network in close vicinity.

The performance of two standard environments has been evaluated in [ToMa99], *i.e.*, a five storey office building and an open exhibition hall. The office building includes attenuation from walls and floors, and the exhibition hall consists only of LoS propagation. The performance with LA is compared with a reference fixed PHY mode (mode 4). The system throughput is calculated as the mean throughput of all users, Table 2.11.

In the office environment, the reference case with a fixed PHY mode and omnidirectional antennas reaches a maximum of 18 Mb/s system throughput. However, when link adaptation is used, the throughput is close to 35 Mb/s. In the exhibition hall, the throughput exceeds the 25 Mb/s when LA is used. It can be read that the use of multi-beam antennas increase the throughput even further.

Also in [ToMa99], LCH PDER and throughput versus *C/I* are shown for all the 7 modes of Table 2.10.

Table 2.11: HIPERLAN/2 User Throughput for Different Environments.

Throughput [Mb/s]	Office Building	Exhibition Hall
Omni fixed Mode 4	17	16
Omni with LA	35	27
Beamforming with LA	−	30

3

MIMO Overview

This chapter presents the state-of-the-art on systems using multiple antenna elements at both transmission and reception. After a short motivation and notation remarks, Section 3.1, a discussion is made on the main efforts accomplished to model the channels plugged with several inputs and outputs, from the brute-force and extremely site-specific approach of measurements campaigns, to the sophisticated and highly reusable correlation-based model with 3 correlation matrices, Section 3.2. The discussions on the capacity increase through the use of multiple antennas carried out since the mid 90s are addressed in Section 3.3.

3.1   Introduction

Multipath propagation is one of the typical features of a radio channel. This phenomenon implies that the received signal level is time, frequency and/or space dependent. Since the beginning of the last century, reception diversity is used to combat the severe impairments caused by multipath fading. In 1901, Guglielmo Marconi used four antennas to increase the gain of the cross-Atlantic transmissions of Morse codes. The idea of diversity is based on the processing of two or more uncorrelated signals obtained in the receiver by the usage of different antennas. The systems that exploit several transmit and receive antennas are called MIMO. Their main advantage is the usage of space as an additional degree of freedom, which is possible due to the multipath propagation. The propagation of signals from different antennas along different paths enables detection of particular bit streams on the basis of the signals received by several antennas. MIMO effectively takes advantage of random spreading, and when available, multipath delay spread. Sometimes MIMO systems are treated as extensions of adaptive antenna arrays; nevertheless, MIMO systems and smart antennas differ in the approach to multipath propagation. The former exploits its effect, while the latter combats them.

From this point onwards, $\mathbf{H} \in \mathbb{C}^{M \times N}$ represents the transfer matrix of a MIMO system whose Receiver (Rx) and Transmitter (Tx) deploy respectively M and N antennas. The elements of $\mathbf{H}$ are represented as h_{mn}, with $m \in [1, M]$ and $n \in [1, N]$, Figure 3.1.
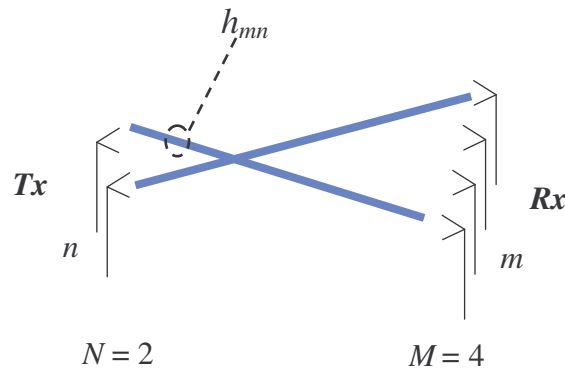
Figure 3.1: 2×4 MIMO System (based on [Chan04]).

Furthermore, h_{mn} are considered independent and identically distributed (i.i.d.), which is a realistic approximation as the antenna spacings increases. They have zero-mean real and imaginary Gaussian components. Their modules follow a Rayleigh distribution, and their phases a uniform one ranging from 0 to 2π. The received signal $\mathbf{y}(t) \in \mathbb{C}^M$ is

$$\mathbf{y}(t) = \mathbf{H}(t) * \mathbf{x}(t) + \mathbf{n}(t) \tag{3.1}$$

where:
- $\mathbf{x}(t) \in \mathbb{C}^N$ is the transmitted vector,
- $\mathbf{n}(t)$ is the zero-mean complex Gaussian noise with independent real and imaginary part. It is assumed that the noise of each receiving antenna is independent, *i.e.*, the covariance matrix of $\mathbf{n}$ is $E[\mathbf{nn}^H]=\mathbf{I}_M$,
- * stands for the convolution operation,
- $(\cdot)^H$ stands for the hermitian operation.

MIMO can provide three main different gains:
- array gain, by shaping the array pattern of the antenna array,
- diversity gain, by transmitting the same signal through all antennas,
- spatial multiplexing gain, by sending different data streams through different antennas.

These three approaches are meant for different goals, and the system configuration is shaped according to specific needs. Even though all may be present in a real situation, the system is designed to achieve one of those types of gain; therefore, this thesis only considers the spatial multiplexing approach with independently fed antennas.

3.2   MIMO Channel Modelling

In a simplistic way, the results of the efforts that have been done to model MIMO channels can be split into *deterministic* and *stochastic* models. Within the former category, *recorded impulse responses* and the *ray tracing technique* are included, while for the latter, the *geometrically-based*, the *parametric* and the *correlation-based* can be found, Figure 3.2
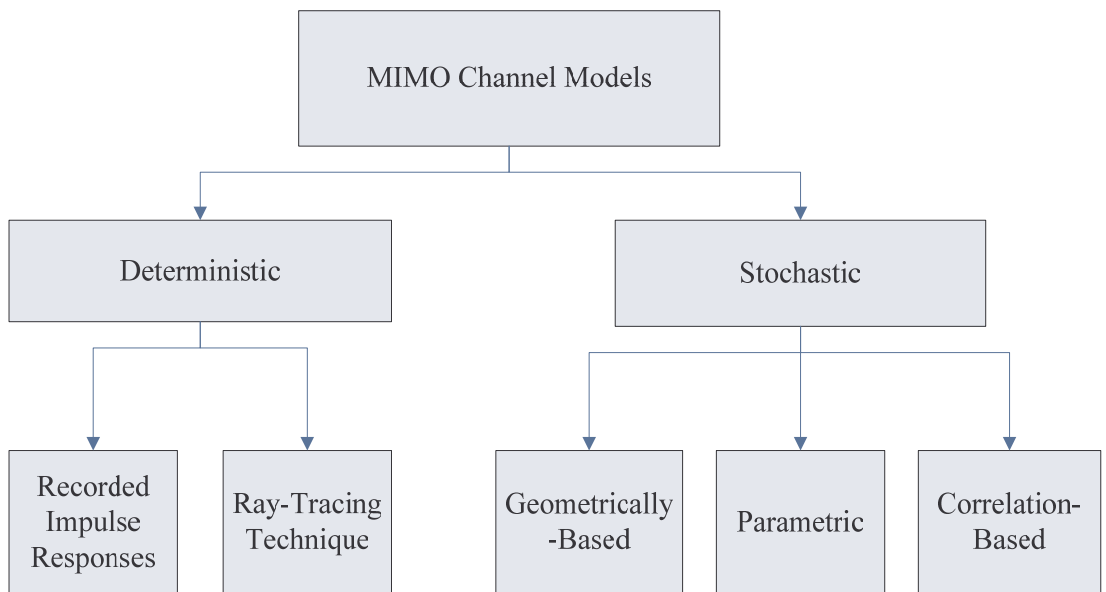
Figure 3.2: Categories of MIMO Channel Models.

The deterministic models characterise the environments in a non-probabilistic way, achieving high accuracy, but very little flexibility to reuse the results in other scattering environments.

In the so-called Recorded Impulse Responses (RIR), typical sets of parameters are extracted from measurement campaigns. In the literature, [KSBO01],

[KCVW03], surveys can be found of MIMO measurements for single and dual polarisation including representative ranges on the number of receive and transmit antennas, their minimal spacing, carrier frequency, bandwidth, time resolution and environment. The fact that the measured channel responses are rather site-specific and that it requires significant amount of memory, makes these models to be rarely used to simulate MIMO radio channels.

The Ray Tracing Technique (RTT), based on the geometric optics approximation, consists of the reconstruction of the propagation paths. It is able to estimate the signal strength, Direction of Departure (DoD) and Direction of Arrival (DoA), but its results cannot be reused for other environments, since they are highly dependent on the scatterers' distribution and on the electromagnetic properties of their surfaces. A ray-based propagation MIMO channel simulator has been proposed in [CoPa03], and two examples of ray-tracing applied to MIMO are given in [GSLV01] and [Burr02].

Contrary to deterministic models, stochastic models do not rely on a site-specific description. They rather aim at reproducing observed phenomena by statistical means. Therefore, they reflect the propagation environment in an indirect way, either by assuming a stochastic distribution of the scatterers around both ends of the connection, considering the different arriving signals as a superposition of waves, or by studying their spatial correlation.

The most comprehensive attempt to statistically model directional channels until now is, most likely, the COST 259 Directional Channel Model [Corr01]. It has a three-level top-bottom structure consisting of the cell type (macro-, micro- or pico-cells), the Radio Environment (RE) and the Local Parameters (LPs) of the detailed propagation scenario. A given set (cell type/RE/LP) fully characterises a simulation environment. It is not a model implementation as such, but rather a framework enabling to tune the parameters of a specific implementation.

The Geometrically-Based Stochastic Models (GBSM) [Chan04] derived from the positions of the scatterers, by applying the fundamental laws of specular reflection, diffraction and scattering of electromagnetic waves. Macro-, micro-, and pico-cells are distinguished as basic scenarios, Figure 3.3.

Usually, macro-cells are simulated by distributing scatterers around the UE only, micro-cells involve ellipses whose foci are the BS and MT locations, while pico-cells are represented by a

circumference centred on the BS embracing the UE. Their maximum linear distances are approximately 10 km, 1 km and 100 m, respectively.

a) Macro-cell   b) Micro-cell   c) Pico-cell
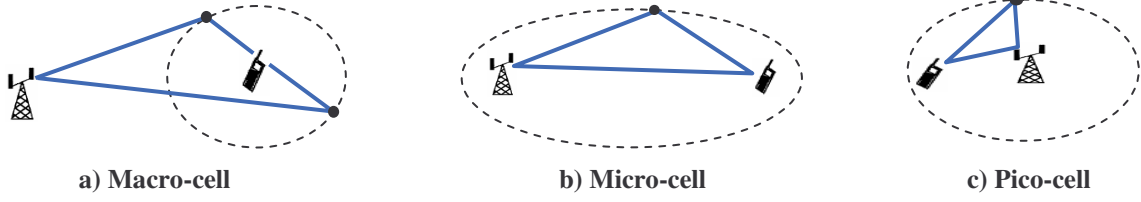
Figure 3.3: GBSM Cell Categories.

The number of scatterers within a scattering area, and also their gathering into clusters are user-defined parameters that help to achieve a more trustworthy simulation of the propagation scenario. In an attempt to model a N_p-tap PDS, the remote scatterers are distributed on N_p delay ellipses, as shown in Figure 3.4.

A known example of GBSM, called Wideband Directional Channel Model (WDCM), is presented in [MaCo01]. It is parameterised for micro- and macro-cells, using the corresponding circular and elliptical distribution areas of scatterers. The size of these areas is derived from the dimensions of the propagation environment. The scatterers are grouped into clusters uniformly distributed in space, in which the location of the scatterers follows a Gaussian distribution around the centre of the cluster. The model considers only a single specular reflection. Besides, neither scattering, nor diffraction are taken into account.
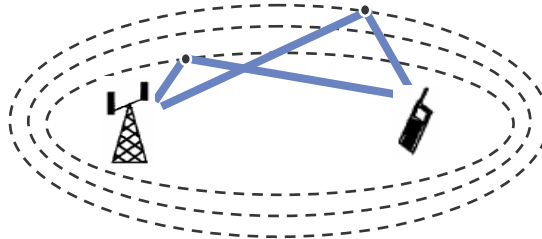
Figure 3.4: Frequency Selective GBSM.

A Parametric Stochastic Model (PSM) describes the received signal as a superposition of waves. It often assumes the form of a tapped delay line, where each tap represents a propagation path.

The Double Directional Channel Model (DDCM) [StMB01] is a PSM, which parameters are a delay-angle distribution or a spatial scatterer distribution. [StMB01] also specifies the output of DDCM as a tapped delay line where the resolvable paths are characterised by their own complex gain, delay, and the (DoD, DoA) pair. The Rx and Tx antenna characteristics and the number of bounces are not taken into account. DDCM is therefore described as [THRS01]:

$$\mathbf{H}\left(t,\tau,\vartheta_{Tx},\zeta_{Tx},\vartheta_{Rx},\zeta_{Rx}\right)=$$

$$\sum_{k=1}^{N_p}\boldsymbol{\xi}_k(t)\delta\left[\vartheta_{Tx}-\vartheta_{Tx,k}(t)\right]\delta\left[\zeta_{Tx}-\zeta_{Tx,k}(t)\right]\delta\left[\vartheta_{Rx}-\vartheta_{Rx,k}(t)\right]\delta\left[\zeta_{Rx}-\zeta_{Rx,k}(t)\right]\delta\left[\tau-\tau_k(t)\right] \quad (3.2)$$

where:

- t is the time variable,
- τ stands for the delay or ToA,
- ϑ stands for the azimuthal angle,
- ζ is the elevation angle,
- N_p is the number of taps,
- $\boldsymbol{\xi}$ is a 2×2 matrix whose elements are the complex gains of the orthogonal polarisations and the cross-coupling between them,
- $\delta[\cdot]$ is the delta function.

Other flavours of DDCM are described in the literature. The authors in [SJBF00] propose a so-called Virtual Ray Model (VRM), where the wavefronts arriving within a given delay bin are collapsed into a space-time fading coefficient; by adding the path loss and the shadowing, the channel impulse responses can be constructed. In [Saye02], a further evolution of the VRM is proposed easing the combination of beamforming with space-time coding: instead of DoDs and DoAs representing the actual angles, they now represent virtual ones periodically sampling the azimuth domain.

Despite the referred variety of models, the need for a more direct and intuitive insight into the capacity increase of MIMO systems lead to the development of models based on the spatial correlation of the multiple paths as well as of the Tx and Rx elements. By analysing the propagation of the waves in a single-bounce GBSM, which assumes that the spatial correlation between antenna elements is a result of the scattering on their immediate surroundings, one comes to the conclusion that the spatial correlation of the wavefronts can be characterised independently at the connection terminations [SFGK00]: the correlation among the receiving elements is independent of the transmitter, and vice-versa. A narrowband correlation-based environment was therefore proposed in [CRLL00], extended to a wideband perspective in [YBOM02], making use of two different spatial correlation matrices capturing the spatial correlation properties seen from the two ends of the connection, as in:

$$\mathbf{H}(\tau)=\sum_{k=1}^{N_p}\left(\mathbf{R}_{Rx}^k\right)^{1/2}\mathbf{A}^k\left[\left(\mathbf{R}_{Tx}^k\right)^{1/2}\right]^{\mathrm{T}}\delta\left[\tau-(k-1)\Delta\tau\right] \quad (3.3)$$

where:
- $\mathbf{R}_{Rx}^k$ and $\mathbf{R}_{Tx}^k\in\Re^{M\times N}$ are the spatial correlation matrices of the kth tap, at the receiver and at the transmitter, respectively,

- $\mathbf{A}^k \in \Re^{M \times N}$ is a matrix of independent, circularly symmetric complex Gaussian variables, representing samples of the fading induced by the channel on the kth tap,
- $(\cdot)^{\frac{1}{2}}$ and $(\cdot)^{\text{T}}$ denote the matrix square root and the matrix transpose [Agud89], respectively.

Consequently, the correlation between two paths is assumed to be the product of the correlation between the antennas connected by these paths at each end. Generalising this assumption to the whole channel, [PAKM00] introduced a wideband correlation-based model where the spatial correlation properties of the MIMO system are derived from a Kronecker product of the separately defined spatial correlation matrices $\mathbf{R}^k_{Rx}$ and $\mathbf{R}^k_{Tx}$. The matrix decomposition of this product, delivers a shaping matrix $\mathbf{C}$ which multiplies a column vector of independent fading samples $\mathbf{a}$ to emulate spatial correlation. Mathematically, using the vect$(\cdot)$ operator to reshape a matrix into a column vector, each channel coefficient can be written as:

$$\text{vect}(\mathbf{H}) = \mathbf{Ca} \tag{3.4}$$

where, with the help of the Kronecker product $\otimes$, the channel correlation matrix $\mathbf{R}^k$ is given by, for each k,

$$\mathbf{R} = \mathbf{R}_{\text{Tx}} \otimes \mathbf{R}_{\text{Rx}} \tag{3.5}$$

The promoters of this model have validated it, both analytically [YBOM01] and by comparison against narrowband measurement results [KSPM02]. However, the use of the Kronecker product has been much discussed: the authors in [ÖHWW03] argue that for large array geometries, where selective shadowing at the array elements can occur, the Kronecker product fails to render the multipath propagation, as it forces the joint DoD-DoA spectrum to be separable. [ÖHWW03] presents some experimental cases where this separability is not achieved, resulting in a capacity underestimate of 10-20 % when using the Kronecker product. A novel MIMO radio channel model was built [WeÖz03] based on the coupling between eigenmodes, still relying on the Kronecker product, no longer between correlation matrices, but between eigenvectors. To model the spatial properties on the channel, this model requires:

- $\mathbf{U}_{Tx}$ and $\mathbf{U}_{Rx}$, the spatial eigenbases at the Tx and Rx side respectively,
- Ω, the eigenmode coupling matrix.

One of the main interests of correlation-based models is the direct insight into the capacity increase of MIMO systems, since they suggest the existence of a direct link between the rank of $\mathbf{R}$ and the capacity increase: the more decorrelated the channel, the higher the ideal capacity [Tela95]. Nevertheless, a counter-example has been identified, called *pinhole* or

keyhole [GBGP00], where the expected capacity increase is not delivered despite exhibiting spatially uncorrelated fading at both connections terminations, because its transfer matrix **H** is rank-deficient. These situations occur in waveguide-like environments, such as hallways, tunnels, or for very large distances between the UE and the BS, where the particular electromagnetic characteristics of wave propagation limit the number of possible propagation modes, leading to a reduction of the multiplexing gain (gain provided by the exploitation of parallel, orthogonal subchannels in MIMO systems). Reference [GBGP00] also proposes an improved MIMO channel model that accounts for these environments, the novelty being to model separately the diversity gain related to the channel's spatial correlation, and the multiplexing gain, related to the rank of the transfer matrix. From a geometric perspective, three regions are defined, Figure 3.5: two that include the scatterers in close proximity to the Tx and Rx antenna arrays, and one that embraces the propagation paths between the previous two. This way, the elements of the transfer matrix depend on the triad ($\mathbf{R}_{Tx}$, $\mathbf{R}_S$, $\mathbf{R}_{Rx}$), where $\mathbf{R}_S$ controls the multiplexing gain.
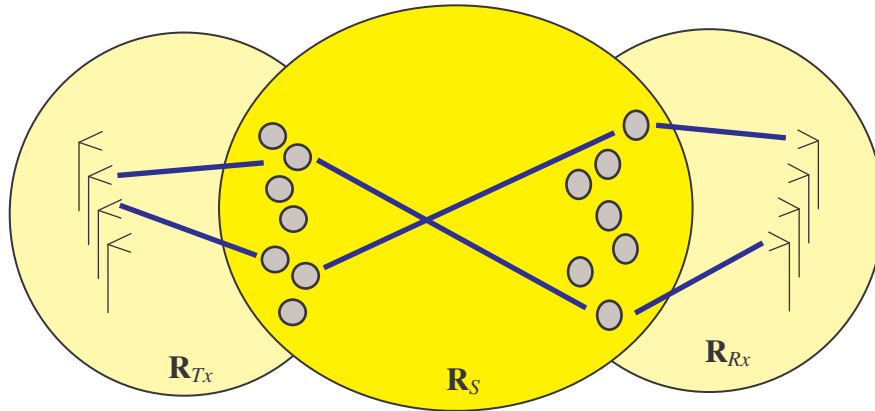
Figure 3.5: Correlation-based Model with Three Regions.

The narrowband transfer matrix is given in this case by:

$$\mathbf{H} = \left(\mathbf{R}_{Rx}\right)^{\frac{1}{2}} \mathbf{A}_r \left(\mathbf{R}_s\right)^{\frac{1}{2}} \mathbf{A}_t \left[\left(\mathbf{R}_{Tx}\right)^{\frac{1}{2}}\right]^T \qquad (3.6)$$

where:

- $\mathbf{R}_{Rx}$ is a $M \times S_R$ matrix, representing the correlation of the propagation paths between the M receive antennas and the S_R scatterers that bounce the signal directly to the receiver,
- $\mathbf{A}_r$ and $\mathbf{A}_t$ are $S_R \times S_R$ and $S_T \times S_T$ diagonal matrices, representing the fading caused by the scatterers around the receiver (S_R) and the transmitter (S_T), respectively,
- S_T is the number of scatterers that are directly illuminated by the transmitter,
- $\mathbf{R}_S$ is a $S_R \times S_T$ matrix representing the correlation of the propagation paths between the S_R and the S_T scatterers.

- $\mathbf{R}_{Tx}$ is a $S_T \times N$ matrix, representing the correlation of the propagation paths between the N transmit antennas and the S_T scatterers directly illuminated by the transmitter.

Therefore, despite having uncorrelated antenna elements and consequently full-rank $\mathbf{R}_{Tx}$ and $\mathbf{R}_{Rx}$, a "low rank channel" could be experienced due to the low Scatterer-to-Scatterer (STS) rank of matrix $\mathbf{R}_S$. Other approaches to overcome keyholes have been proposed [Sibi01], where the transfer matrix connects transmitted waves to received ones through a diffracting slit.

Although correlation-based models have been first suggested for Non Line-of-Sight (NLoS) scenarios, *e.g.*, under the assumption of zero-mean complex Gaussian-distributed channel coefficients, a small modification enables them to account for the presence of a Rice component [LUCE01]. The channel matrix of the first tap then takes the form:

$$\mathbf{H} = \sqrt{\frac{K}{K+1}}\mathbf{H}_{LoS} + \sqrt{\frac{1}{K+1}}\mathbf{H}_{Stochastic} \tag{3.7}$$

where:
- K is the Rice factor,
- $\mathbf{H}_{LoS}$ represents the product of the coherent wave component by a steering matrix,
- $\mathbf{H}_{stochastic}$ stands for the channel transfer matrix as derived from correlation-based models.

Excess delay taps are characterised only by the $\mathbf{H}_{stochastic}$ matrix.

Finally, a comprehensive MIMO channel model has been recently formulated in [XCHV04] that tries to gather the benefits of the previously described models. It is based on a combination of the correlation and wave superposition approaches and it can cope with polarizations, channel transitions, keyholes, uplink and downlink differentiation.

3.3   Theoretical MIMO Capacity

Information theory has shown that with multipath propagation, multiple antennas at both the transmitter and the receiver can establish essentially multiple parallel channels that operate simultaneously on the same frequency band and at the same time. The theoretical maximum capacity for a point-to-point communication has been derived in [Tela95] and [FoGa98].

The highest rate at which information can be sent with an arbitrarily low probability of error or capacity C, in the single transmitter and receiver case for an additive white Gaussian noise channel, is given by (in b/s/Hz) [Proa01]:

$$C = \log_2(1+\rho^2) \tag{3.8}$$

where ρ is the average signal to noise ratio at the receive antenna. In this 1-dimensional case (SISO channel), the channel transfer function is a (complex) scalar and (3.8) can also be put as:

$$C = \log_2\left(1 + \frac{P_{Total}}{\sigma^2}\alpha^2\right) \tag{3.9}$$

where:

- σ^2 is the noise power at the receive antenna,
- α is the (complex) gain of the channel.

[FoGa98] generalises the capacity expression for the multiple channel case, assuming (apart from the assumptions referred in the introduction of this chapter):

- that the transmitted signal is composed of N statistically independent equal power components each with a Gaussian distribution, and M is the number of the received signal components,
- that the channel is fixed during a burst and randomly changing from burst to burst,
- that the bursts are long enough so that information theory infinite time horizon approach is applicable,
- $h_{mn} = \text{Normal}\left(0, \frac{1}{\sqrt{2}}\right) + \sqrt{-1} \cdot \text{Normal}\left(0, \frac{1}{\sqrt{2}}\right)$, where $|h_{mn}|^2$ is a normalised random variable so that $E[|h_{mn}|]=1$,
- that the channel characteristics are not known at the transmitter (robust codes are possible that can cope with a wide range of possibilities for different channel realisations) but known at the receiver, leading to a uniform power distribution among the transmit antennas,
- a fixed total transmit power (independently of the number of transmit antennas) and equal power components of the transmitting stream.

In these circumstances, MIMO capacity is given by (3.10) in terms of the non-normalised channel transfer matrix $\mathbf{T}$, which incorporates the channel transfer gains from each transmit to each receive antenna.

$$C = \log_2\left\{\det\left[\mathbf{I}_M + \left(\frac{E_x}{\sigma^2}\right)\mathbf{T}\mathbf{T}^H\right]\right\} \tag{3.10}$$

where:

- $\mathbf{I}_M$ is the M-dimensional identity matrix,

- E_x is the energy[1] sent by each transmit antenna.

Similarly to the Shannon formula for the single transmitter/single receiver case, the MIMO channel capacity can be expressed as [Kyri01]:

$$C = \log_2 \left\{ \det \left[\mathbf{I_M} + \left(\frac{\rho}{N} \right) \mathbf{HH^H} \right] \right\}$$
(3.11)

where:

- ρ is defined at each receive antenna by:

$$\rho = \frac{P_{Total}}{\sigma^2} g^2$$
(3.12)

- $\mathbf{H}$ is the normalised channel transfer matrix related to $\mathbf{T}$ as:

$$\mathbf{H} = \mathbf{T}/g$$
(3.13)

- g is defined as:

$$g^2 = \mathrm{E}\left[|\mathbf{T}|^2 \right] = \frac{1}{MN} \sum_{m=1}^{M} \sum_{n=1}^{N} |\mathbf{T}_{mn}|^2$$
(3.14)

On average, upper and lower bounds for the capacity can be established corresponding to channels that present a spatial correlation among the antennas of zero and one, respectively. For the former case with $X = \min(N, M)$,

$$C_{\mathrm{corr}=0} = X \cdot \log_2(1+\rho)$$
(3.15)

while for the latter,

$$C_{\mathrm{corr}=1} = \log_2(1 + X \cdot \rho)$$
(3.16)

If $\mathbf{H}$ is unitary, *i.e.*, $\mathbf{H}$ is square ($M=N$) and $\mathbf{HH^H} = \mathbf{H^H H} = \mathbf{I}$, and the channel is not known at the transmitter, then:

$$C_{unitary\,\mathbf{H}} = N \log_2 \left(1 + \frac{\rho}{N} \right)$$
(3.17)

One illustrative channel modelled by a unitary $\mathbf{H}$ matrix is the one where each transmit antenna illuminates a different group of scatterers and each of these groups illuminate a different receive antenna without power loss. The $\mathbf{H}$ matrix would then be the identity one representing multiple parallel paths that do not interfere among them. In real scenarios close

---

[1] E_x can also be the power sent by each transmit antenna if $\mathbf{T}$ represents the channel transfer matrix in terms of power. E_x and $\mathbf{T}$ must agree in their magnitudes.

to this one, the transmitter should exploit the spatial multiplexing approach, which would provide a gain upper-bounded by (3.17).

When the transmitter ignores the characteristics of the channel, it distributes the power among the antennas uniformly. In this case, assuming a large and equal number of antennas, it can be seen that the MIMO capacity increases linearly with ρ (not logarithmically as in the 1-dimensional case) as (3.18) shows.

$$C = N \log_2 \left\{ 1 + \frac{\rho}{N} \right\} \xrightarrow{N \to \infty} \frac{\rho}{\ln(2)} \tag{3.18}$$

If **H** is unitary and known at the transmitter, a power distribution known as waterfilling [ATEM02] can be performed, and the maximum achievable capacity is simply the sum of the individual capacities of the channels:

$$C = \sum_{m=1}^{M} C_m = \sum_{m=1}^{M} \log(1 + \rho_m) \tag{3.19}$$

On average, this leads to:

$$\overline{C} = N \cdot \log_2(1 + \rho) \tag{3.20}$$

Waterfilling is the optimum power allocation that aims at allocating power to the propagation eigenmodes that present the highest ρ at reception. Therefore, the power is not "wasted" in modes that have a ρ below a certain threshold. The general expression using waterfilling is:

$$C = \log_2 \left\{ \det \left[\mathbf{I}_M + \left(\frac{\rho}{N} \right) \mathbf{HPH}^H \right] \right\} \tag{3.21}$$

where **P** describes the power distribution.

The capacities shown so far are stationary ones, *i.e.*, capacities for a (spatial or temporal) stationary channel. The ergodic capacity is the expected value of the stationary capacity over a set of independent channel realisations (spatial or temporal channel samples):

$$C_{ergodic} = \mathrm{E}[C] \tag{3.22}$$

As it has become clear so far, the MIMO capacity depends on several aspects, namely on the number of antennas at both ends of the connection (*M* and *N*), the received ρ, the channel characteristics through **H** and knowledge of the channel by the transmitter and receiver, through **P**.

Recalling the spatial multiplexing approach (different data streams sent through different antennas), the influence of the knowledge of the channel by the transmitter and by the receiver is shaped in (3.11) and (3.21). On the other hand, if **H** is unknown at the transmitter and known and the receiver, Bell-labs LAyered Space-Time architecture (BLAST) [Fosc96] is normally used to successively decode and cancel the interference at reception. In these situations, the capacity scales linearly with the min(*M*, *N*, *S*), where *S* is the number of scatterers. If **H** is unknown at both transmission and reception, the so-called matrix modulation technique [AMSH01] is robust enough to achieve proper stream separation at reception. Regarding ρ, it can be clearly observed in (3.18) that the capacity increases linearly with it for large antenna arrays. Regarding **H** itself, [FeMa03] illustrates how the channel correlation (defined separately at the receive and transmit antennas) and the spectral selectivity influences the capacity of a 2×2 MIMO system: the capacity is highly dependent and inversely proportional to the correlation levels of the propagation paths, and moderately dependent and also inversely proportional to spectral selectivity.

4

MIMO Channel Model

This chapter describes the MIMO channel model used in this thesis, from its mathematical outline to the practical issues of implementation. Starting with the description of the SISO model that has been extended to support MIMO, Section 4.1, the main advantages and limitations of the proposed model are discussed, Section 4.2, and a channel capacity-based assessment is presented, Section 4.3.

4.1   The Baseline SISO Channel Model

4.1.1 Underlying Models

The MIMO channel model employed throughout this study is based on the SISO one described in [Marq01]. This is a Wideband Double Directional Channel Model (WDDCM), supported on the Geometrically-Based Single Bounce (GBSB) model with additional contributions from two other models: the Elliptical Sub-regions Model (ESM) and the combined GBSB and Gaussian Wide-Sense Stationary Uncorrelated Scattering (GWSSUS) models. This combination provides a particularly good balance between simulation realism and complexity by gathering some of the benefits of the previously mentioned models.

The GBSB model [LiRa99] defines a planar spatial Probability Density Function (PDF) that rules the random positioning of the scatterers within a confined scattering area. Its shape is defined according to the considered cell type (macro- or micro-cells). The scatterers are regarded as omnidirectional point-like elements, re-radiating the signal coming directly from the transmitter, *i.e.*, no multiple bounces, diffraction, or rough surface scattering is accounted for. They are characterised by their complex reflection coefficients, which have uniformly distributed magnitudes and phases.

The implementation of the models is based on the application of the specular reflection laws to each bouncing ray, assuming that all scatterers offer a contribution to the received signal. Thus, the model provides spatio-temporal information at arrival, *i.e.*, Angles and Times of Arrival (AoAs and ToAs).

The environment under consideration defines the shape of the scattering region, Figure 3.3: circular shapes centred at the MT use the GBSB Circular Model (GBSBCM) accounting for the scattering region of macro-cells, while elliptical shapes with foci at the BS and MT use GBSB Elliptical one (GBSBEM) describing micro-cells. Macro-cells are typically considered when the BS antenna height is relatively large compared with that at the MT, so that the scatterers are mostly placed around the latter. Nevertheless, the BS-MT distance is considered much larger than the difference of the BS and the MT antenna heights so that the planar assumption of the scattering region is reasonable. In micro-cells, the BS antenna height is of the same order of the MT one (typically below rooftops) so the scatterers are predominantly placed in the proximities of the BS-MT axis, and around these.

Some other characteristics of this model are:
- wideband with Doppler effect accounted for,

- Channel Impulse Response (CIR) obtained through simulation,
- joint and marginal ToA and AoA PDFs can be obtained through algebra,
- the scattering region sizes must be based on measurements,
- the LoS component is assumed in the elliptical model, but not mentioned in the circular one,
- although Doppler power spectrum is taken into account, it is not clear how motion affects the spatial PDF.

The ESM [LuLL97] also relies on a two-dimensional (2D) elliptical scattering region, but divides it into a given number of elliptical belts or crowns. Within each belt, the number of scatterers follows a Poisson distribution, with mean based on measured data. To reproduce the fact, observed in measurements, that the multiple signal replica tend to arrive in clusters, each scatterer is considered to have a number of reflecting points also given by Poisson distribution. The reflection coefficient of each of these points has the same amplitude but random uniformly distributed phase. In order to cope with macro-cell environments, a circular area around the BS antenna can be defined as scatterer free.

Other characteristics can be summed as:
- wideband accounting for Doppler effect,
- CIR obtained from simulations,
- scatterers assumed to be single bounce specular reflectors,
- the LoS component is not mentioned,
- although statistically very complete, time variation is not explored,
- it is not clear how the MT motion affects the scatterers' spatial PDF.

The combined GBSB and GWSSUS model [PiTs99] embraces the simulation methodology of the GBSB models, while being in compliance with one of the assumptions of the GWSSUS: scatterers grouped into clusters. The GBSB does not account for the temporal evolution of the MTs, and successive realisations of the channel are therefore totally uncorrelated, which is unrealistic. On the other hand, the GWSSUS is completely dependent on measured data (number of clusters, number of scatterers per cluster, etc.), and therefore, its results can hardly ever be reused. The combination consists in considering the GBSB model with scatterers gathered in clusters, uniformly distributed, and fixed in space. As the MT moves, the scattering region moves with it, and more clusters are included in the scatterer region while others leave it. The authors have derived the distribution of the time-varying number of multipath components as well as the distribution of their lifetime.

Other model features are:
- 2D wideband model accounting for Doppler,
- CIR computed through simulations,

- dependence of path loss is mentioned and LoS is included depending on the considered environment,
- it is able to cover several environments: macro-cell urban, bad urban, suburban, and micro-cell urban.

The intention in [Marq01] was to build a WDDCM suited for simulations and exploitable for general scenarios instead of particularly well defined ones, where a balanced trade-off between compliance with measurement results and computational burden was achieved. The result was a GBSB model, modified to include the gathering of scatterers in clusters (in compliance with the ESM and the combined GBSB and GWSSUS models), that reproduces the multiple reflecting points of each scatterer, Table 4.1.

Table 4.1: Characterisation of the Model.

Scattering Region	Shape		Ellipse (2D) with foci at the BS and MT
	Delay limit		Given by (Effective) Street Width
Clusters	Distribution		2D-Uniform
	Range		Scattering Region
	Density		User Defined
Scatterers within Cluster	Distribution		Gaussian
	Standard deviation (cluster half-size)		User Defined
	No. of scatterers per cluster	Distribution	Poisson
		Average	User Defined
Scattering Coefficients	Magnitude	Distribution	Uniform
		Range	]0, 1]
	Phase	Distribution	Uniform
		Range	$[0, 2\pi[$
Path Loss Exponent			User Defined
LoS Path			Always Present
Doppler Shift			Accounted for
MT Velocity			User Defined
Delay Resolution			User Defined
Angle Resolution			User Defined
Noise Margin			User Defined

The number of scatterers per cluster is given by the Poisson distribution (as in the number of scatterers per crown of the ESM). The movement of the MT results in a smaller or larger scattering region, depending on the movement being towards the BS or not, respectively, with scatterers naturally entering or leaving the region. This way, the scatterers' spatial PDF changes with the MT movement as it does in the combined GBSB and GWSSUS model.

The model assumes scatterers gathered in uniformly distributed clusters, following a Gaussian PDF within each cluster. Path loss, shadowing, and fast-fading affect every signal including

the always present LoS. The model has been extended to cope with macro- and pico-cells, by shaping the scattering region [GVCM03], and to handle antenna arrays, by shaping the radiation pattern [VGCC03]. Multiple bounces are also accounted by considering an effective scattering region. In the micro-cell, street type scenario, this region is obtained by artificially widening the real scattering region by the so-called "street width ratio" factor. Other features as Doppler shift, different angular and temporal resolutions, noise margin, etc., are also considered.

4.1.2 Mathematical Model

The simulator channel model uses a semi-statistical approach that provides realistic insight into the channel's behaviour by statistically reconstructing the scattering environment, while providing deterministic spatio-temporal information of the signal. The goal of this approach is to characterise the channel realistically enough in order to obtain directional and temporal information of the transmitted signals, which can help in the study of MIMO and adaptive beamforming, while keeping the burden on the computational effort within reasonable levels.

Assuming a planar scattering region, the ToA and AoA joint PDF of the GBSB model derived in [LiRa99] can be applied to our model, since the finite angular and temporal resolutions make the rays coming from scatterers of the same cluster to be summed coherently at reception.

The joint PDF is the same for the BS and for the MT, and is given for the macro-cell environment by:

$$\rho_{\tau,\varphi}(\tau,\varphi) = \frac{\left(d^2 - \tau^2 c^2\right) \cdot \left(d^2 c - 2d\tau c^2 \cdot \cos\left(\varphi - \varphi_0\right) + \tau^2 c^3\right)}{4\pi R^2 \cdot \left(d \cdot \cos\left(\varphi - \varphi_0\right) - \tau c\right)^3}$$

(4.1)

where

- τ is the ToA,
- φ is the AoA,
- c is the speed of light,
- d is the BS to MT distance,
- φ_0 is the angle from the BS-MT vector to a reference axis,
- R is the radius of the circular scattering region.

However, the validity region for the BS:

$$\frac{d^2 - 2d\tau c \cdot \cos\left(\varphi - \varphi_0\right) + \tau^2 c^2}{\tau c - d \cdot \cos\left(\varphi - \varphi_0\right)} \leq 2R \wedge \tau > \frac{d}{c}$$

(4.2)

is different from the one of the MT:

$$\frac{d^2 - \tau^2 c^2}{d \cdot \cos(\varphi - \varphi_0) - \tau c} \leq 2R \wedge \tau > \frac{d}{c}. \tag{4.3}$$

Out of these validity regions, the PDF's value is zero. To adjust the performance of the model, R can be set to match the angle and time spreads of the model with measured ones.

In micro-cell environments, the joint PDF and the validity region for the BS and MT are the same:

$$\rho_{\tau,\varphi}(\tau, \varphi) = \begin{cases} \dfrac{\left(d^2 - \tau^2 c^2\right) \cdot \left(d^2 c - 2d\tau c^2 \cdot \cos(\varphi - \varphi_0) + \tau^2 c^3\right)}{\pi \tau_{max} c \sqrt{\tau_{max}^2 c^2 - d^2} \left(d \cdot \cos(\varphi - \varphi_0) - \tau c\right)^3}, & \dfrac{d}{c} < \tau \leq \tau_{max} \\ 0 & , \text{otherwise} \end{cases} \tag{4.4}$$

where τ_{max} determines both the maximum delay and angle spreads.

4.1.3 Model Discussion, Inputs and Outputs

The scatterer's planar PDF assumes the DoAs confined to the horizontal plane, *i.e.*, considers AoAs in the azimuthal plane. Consequently, the ToAs are confined to those that result from bounces inside the planar scattering region. This might seem a strong simplification of the reality, as scatterers positioned at different heights (floor, car, building, etc.) can equally contribute to the received signal. Nevertheless, the model does not ignore the three-dimensional (3D) space, but projects it onto a planar region, where the scatterers do not block each other's signals, as if they had different elevations. However, this projection does neglect the propagation time differences due to different heights.

The spatial distribution of the clusters follows a uniform PDF, because this distribution is the only one that maintains its statistical coherence as the scattering region enlarges or shrinks, *i.e.*, when the MT moves, clusters will keep their distribution without the need of repositioning them. The disadvantage is that it yields to an abrupt signal power variation at the maximum delay. On the other hand, within each cluster, scatterers follow a Gaussian distribution with the same standard deviation in both spatial axes, so their orientation is meaningless.

The amplitude and phase of the scatterers' reflection coefficients are uniformly distributed in space over]0,1] and [0,2π[, respectively. In this way, the ambiguity regarding the reflecting materials and Angles of Incidence (AoI) is added. Furthermore, the fact that scatterers are omnidirectional re-radiators with random reflection coefficients is a coarse way to simulate propagation phenomena, like diffraction and rough surface scattering. Even though it is

known that the reflection coefficient changes with the AoI, scatterers keep it throughout the MT movement, because clusters may assume any orientation and are made of any material, so they can be seen as average ones. However, the dependence of the amplitude on frequency is accounted for by reassigning different random values in the UL and DL of FDD modes.

In this thesis, only the micro-cell accounting for the LoS rectangular street environment with the BS and the MT aligned in the same street is considered. The receiver and the transmitter are positioned in the centre of the transversal street axis, and, although the model allows the MT to move along the longitudinal one, that shall not be considered here. The shape of the scattering region should be one that is:

- coherent with the received signal,
- compliant with the scenario under consideration.

If a channel modeller wants to map each of the arriving taps of a wideband system onto a scatterer, the set of possibilities for each scatterer location defines an ellipse with foci at the BS and the MT. With a sufficiently high time resolution, the set of ellipses forms an elliptical region bounded by the ellipse of maximum delay. In the street scenario with the BS and MT antennas at the same (low) height, and if only single bounces were considered, the ellipse would represent faithfully the scenario as it embraces the relevant part for the connection of the street; the ellipse and the street widths would naturally be the same. However, it was shown in [MaCo01] that the street environment presents a waveguide like behaviour, where multiple bounces play an important role. The model attempts to cope with this effect by widening the ellipse beyond the street width so that longer delays are considered. The simplification here is that multiple bounces are not necessarily on ellipses. One might think that the ellipse widening results in a misinterpretation of the AoA spreads in the sense that it artificially modifies the PAS. Yet, the multiple bounces also widen the PAS by reaching the receive antennas with higher AoAs (the higher the number of bounces, the higher the AoA).

Besides, the model assessment has shown accurate results for the ToAs, AoAs and powers, after tuning its parameters. For example, the street width ratio is chosen so that the delay spread given by the model resembles the one of measurement campaigns. The authors in [MaCo01] have lately agreed on a value of 4 for this parameter in a street scenario.

Even though the simulator outputs information on every transmitter-scatterer-receiver ray, only the filtered results are meaningful, because of the inherent finite angle and time resolutions of the receiver. Besides, if the resolution is low enough so that scatterers in the same cluster are not resolvable, their coherent sum at reception will naturally keep the correlation between consecutive time/space samples of the fast-fading within clusters. Furthermore, signals whose power falls below a user-defined noise margin are discarded. One should note that this can also limit the scattering region, no longer based on the street width

but on the receiver sensitivity. Finally, the philosophy of the model is based on Monte-Carlo simulations to achieve the desired statistical results on the geometry of the environment. Seen as a black box, the simulator is depicted in Figure 4.1, where inputs are grouped into four categories.
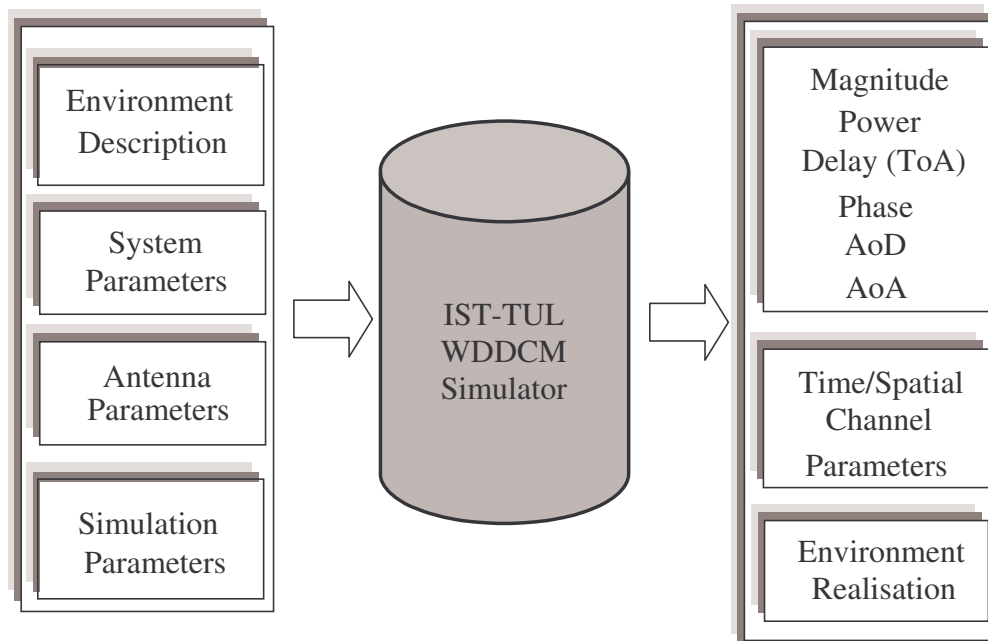
Figure 4.1: SISO Simulator Structure, Inputs, and Outputs (based on [FiGC03]).

This information should be tuned with the reality of measurement campaigns [MaCo01]. These main inputs are:

- Environment description: macro-, micro- or pico-cells, cell dimensions, cluster sizes and densities, scatterers' reflection coefficients, MT positioning and speed, path loss exponent, and path loss exponent corrective factor,
- System parameters: mean transmitted power, UL or DL, bandwidth, carrier frequency, angle and time resolutions, and noise level (below which scatterer contributions are discarded),
- BS and MT antenna parameters: type of antenna array (if an array is considered), number of antennas elements, their separation, magnitude, and phase excitation of each element,

Simulation parameters are: number of channels realisations, option for outputting several spatio-temporal indicators, such as the environment data (spatial coordinates of the scatterers), the filtered and unfiltered scatterers' contributions, delay and angular spread, and Rice factor. The simulator outputs are regular text files to enable easy post-processing. The first two blocks of outputs can be sorted in filtered and unfiltered results. The first block includes magnitude, power, phase, ToA, AoA, and AoD for every ray and for their coherent sum, according to the user-defined angle/time resolution. The time/spatial channel parameters

block includes mean delay, delay spread, angular spread, Rice factor, mean power gain, and standard deviations for all these parameters, also for the filtered and unfiltered results. Finally, the environment description provides the characteristics and locations of each cluster and scatterer.

4.2   The MIMO Model

4.2.1 Underlying Model and Extension to MIMO

The MIMO channel model used in this investigation is based on the SISO one described in Section 4.1. The extension to MIMO was done by post-processing the CIR obtained from the single antenna element case. Once the spatio-temporal characteristics of the signals are known for a reference transmit-receive antenna pair, pure geometric calculations can be used to derive the CIRs between all the other antenna pairs. Theoretically, all the spatio-temporal characteristics of the signals depend on the specific antenna pair from which they have been transmitted and received. However, it is not realistic to consider that the receiver is able to resolve different time delays from signals that have reflected in the same scatterers, but that have been transmitted and/or received by different antennas. The same reasoning is taken for the AoDs, AoAs, and amplitudes. Therefore, this MIMO model assumes differences only in the phases of the signals that have bounced on the same scatterers in compliance with the so-called *narrowband array assumption* [JeBF00] or *source-point model* [Chan04].

In other words, it is assumed that scatterers are in the far-field zone of the antennas. The received signals that have bounced in the same scatterers are therefore planar waves with no difference in delay, power, AoAs or AoDs. The only difference is the phase rotation $\Delta\Phi$ due to the slightly different path lengths covered by the signals in their transmit antenna-scatterer-receive antenna trip:

$$\Delta\Phi = k \cdot d_a \cdot \cos(\varphi) \tag{4.5}$$

where:

- $k = 2\pi/\lambda$ is the wave number,
- d_a is the inter-antenna spacing,
- φ is the angle between the array axis and the direction of the propagation of the signal.

Another implicit assumption of the source-point model is the consideration of inexistent coupling effects among the antennas of each array. Mutual coupling, defined as the effect that each antenna has on the neighbouring ones (*e.g.*, re-radiation), in the WDDCM of [Marq01]

was addressed in [GVCM03]. The conclusions were that no significant differences in the radiation pattern were observed when coupling effects were considered.

Figure 4.2 illustrates the narrowband array assumption for a single propagation path of a signal being transmitted (received) from (at) the BS. At the MT, this assumption is similarly applied. If the downlink (uplink) is considered, φ represents the AoD (AoA).
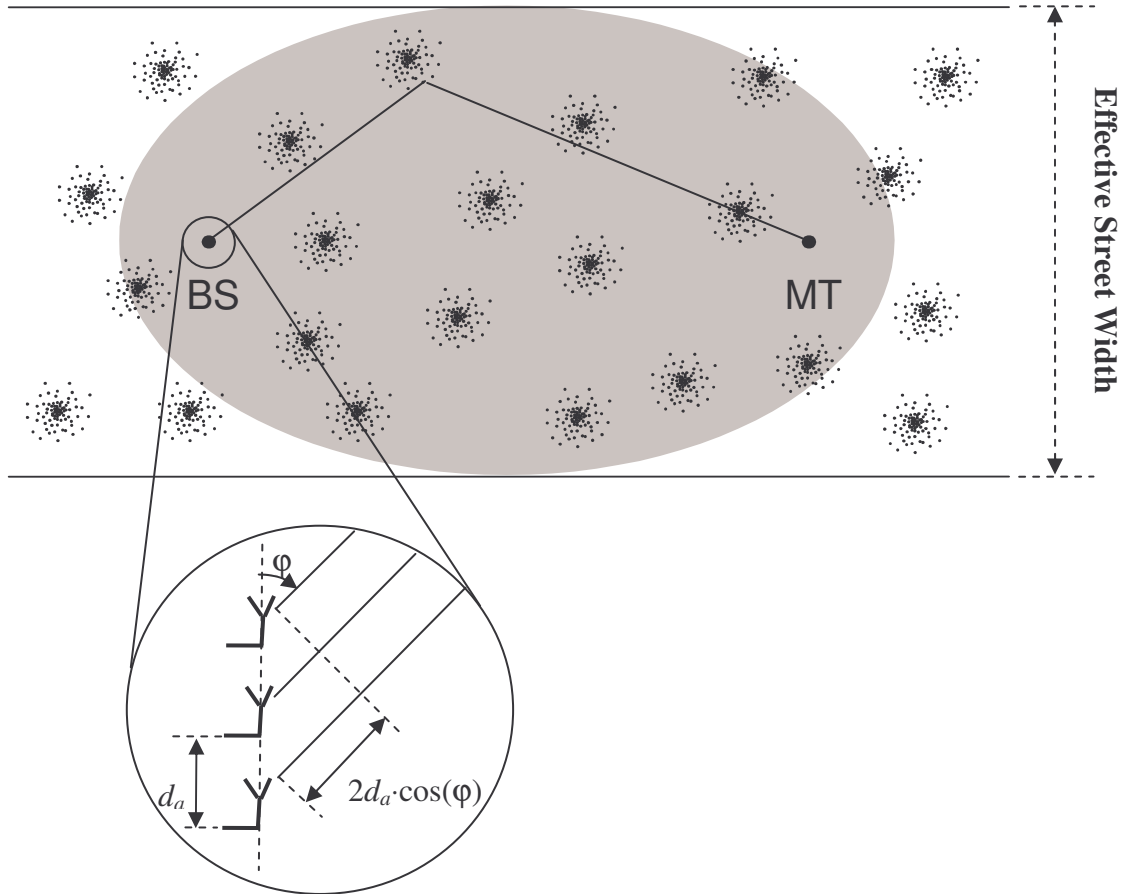
Figure 4.2: Narrowband Array Assumption.

The set of the wideband CIRs from all antenna pairs is gathered in a matrix **H,** obtained for each environment realisation, *i.e.*, for each specific set of locations of scatterers and their reflection coefficients. Nevertheless, the randomness of the environment entails multiple Monte-Carlo loops, and thus multiple **H** matrices. The capacity becomes then a random variable and statistical tools should be used to model it. In this thesis, the Cumulative Distribution Function (CDF) was used to study the ergodic capacity given by (3.22), where *C* is the stationary capacity of (3.11).

The scattering attributes to be changed from one environment realisation to another depend on the aim of the study. If a general channel is envisaged, where only the scattering region shape is fixed, the location of the scatterers and their reflection coefficients change according to the distributions of Table 4.1. On the other hand, if a quasi-static channel is to be modelled,

where only small movements of the scatterers are accounted for, mere random changes on the phase of the reflection coefficients reproduce the phase shifts the signal would suffer. Changes in path loss, delays, AoDs and AoAs would not be significant. The reflection coefficient Γ is then expressed by (4.6), where the dependence on time (τ) is discrete, corresponding to realisations of the channel.

$$\Gamma(\tau) = |\Gamma| \exp\{j \cdot \gamma(\tau)\}$$
(4.6)

where *j* is the imaginary unit.

4.2.2 Mathematical Model

For the considered *M*×*N* MIMO system, the entries of the wideband channel transfer matrix (h_{mn}) for each channel realisation are given by:

$$h_{mn}(t, \varphi) = \sum_{k=1}^{N_p} a_{mnk} e^{j\theta_{mnk}} \cdot \delta(t - \tau_{mnk}) \cdot \delta(\varphi - \varphi_{mnk})$$
(4.7)

where:

- $m \in [1, M]$ is the receive antenna index,
- $n \in [1, N]$ is the transmit antenna index,
- N_p stands for the number of multipath components (taps),
- *a* is the amplitude of each tap,
- τ is the delay of each tap,
- θ is the phase of each tap,
- φ is the AoA.

Each entry represents the channel between a receive and a transmit antenna pair and has a joint ToA and AoA PDF given by (4.1)–(4.4). However, in MIMO, an additional focus is put on the similarity (spatial correlation) between the channels h_{mn}, and not only on the statistics of each one. Therefore, the joint PDF of all h_{mn} is also important to model.

In [Debb03], it is claimed that the best theoretical model for a MIMO channel can be achieved with the recursive algorithm represented in Figure 4.3. It mainly consists on using the entropy maximisation over the supposed known information of the channel a priori. In this way, the constraints of the *channel prior state of knowledge* are imposed, while the model is general about the prior unknowns. The channel capacity resulting from this model should be compared with the one of measurement campaigns, and the modeller should return to the starting point refining the prior known information if the derived capacity did not show accuracy. It is claimed that the theoretical models that are not compliant with this algorithm are not as general with the prior unknowns of the channel as the ones that are.

The originality of the methodology is the fact that the model is constructed using three mathematical tools, namely matrix modulation, Bayesian probability, and, mainly, entropy maximisation. To exemplify the methodology, models for several typical prior states of knowledge of the channel were derived in [Debb03].
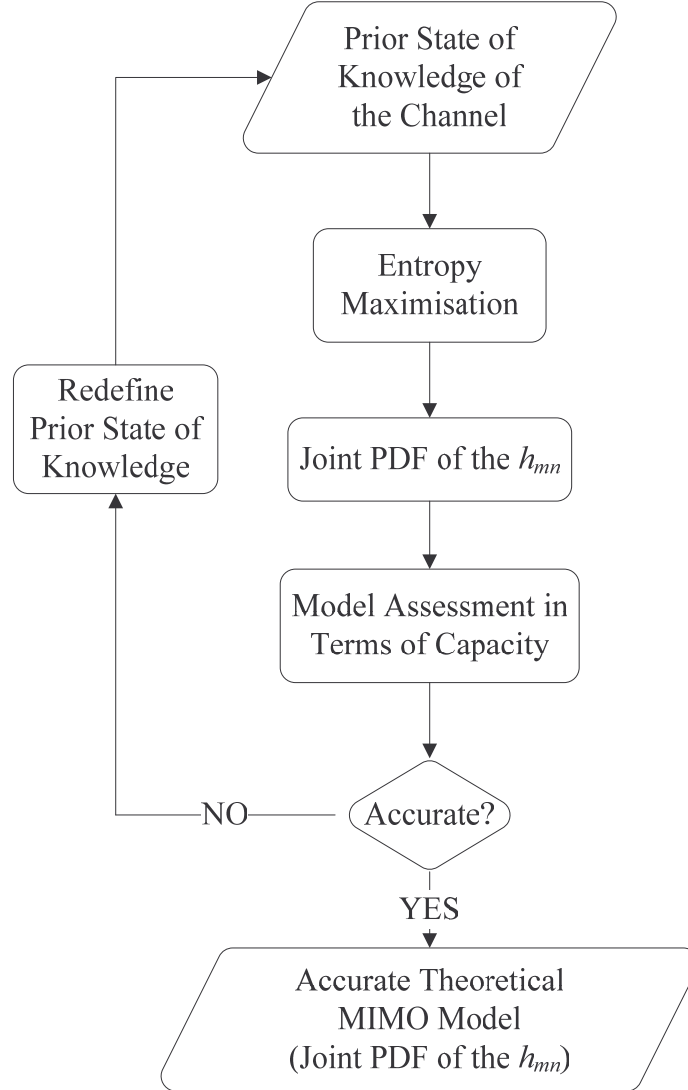
Figure 4.3: Flowchart of the Theoretical MIMO Channel Modelling Algorithm.

For the single bounce, quasi-static channel, mere random changes on the phases of the reflection coefficients reproduce the small movements of the scatterers. Thus, the prior state of knowledge of the channel consists of:

- all the AoDs, AoAs and ToAs,
- the transmitted and received powers from and to the scatterers,
- the MT speed,
- the carrier frequency and bandwidth,
- the magnitudes of the scatterers' reflection coefficients ($|\Gamma|$ in (4.6)).

because these are fixed from one environment realisation to another. What is left as random, and therefore unknown, are the $\gamma(t)$ of (4.6). For a single bounce WDDCM, the application of the previous algorithm delivers:

$$\mathbf{H} = \frac{1}{S}\mathbf{\Phi} \cdot \mathbf{\Delta_{Rx}} \cdot \mathbf{\Theta} \odot \mathbf{D} \cdot \mathbf{\Delta_{scat}} \cdot \mathbf{\phi} \qquad (4.8)$$

where:

- S is the number of scatterers, corresponding to the L number of multipath components in (4.7) because of the single bounce assumption,
- $\mathbf{\Phi}$ is a $M{\times}S$ matrix whose complex elements $\Phi_{ms}(t)=\exp\{j\cdot(\psi_{ms}+2\pi\cdot f\cdot\mathbf{u}_{ms}\cdot v_r\cdot t/c)\}$ characterise the AoAs from the sth scatterer to the mth receive antenna,
- $\mathbf{u}_{ms}$ is the unitary vector with direction of the sth scatterer $-$ m^{th} receive antenna axis,
- $\psi_{ms}=\mathbf{k}_{ms}\cdot\mathbf{d}_{ms}$ is the scalar product between the wave vector $\mathbf{k}_{ms}=(2\pi/\lambda)\cdot\mathbf{u}_{ms}$ and the distance vector between the sth scatterer and the mth receive antenna, $\mathbf{d}_{ms}$,
- f is the carrier frequency,
- v_r is the scalar speed of the receiver,
- $\mathbf{\Delta_{Rx}}$ is a $S{\times}S$ diagonal matrix whose real elements are the powers that arrive to the receive antennas from the scatterers,
- $\mathbf{\Delta_{scat}}$ is a $S{\times}S$ diagonal matrix whose real elements are the powers that arrive to the scatterers from the transmit antennas,
- $\mathbf{\Theta}$ is a $S{\times}S$ diagonal matrix whose complex elements characterise the reflection coefficients,
- $\mathbf{D}$ is a $S{\times}S$ diagonal matrix whose complex elements characterise the ToAs,
- $\mathbf{\phi}$ is a $S{\times}N$ matrix whose complex elements $\phi_{sn}(t)=\exp\{j\cdot(\psi_{sn}+2\pi\cdot f\cdot\mathbf{u}_{sn}\cdot v_t\cdot t/c)\}$ characterise the AoDs from the nth transmit antennas to the sth scatterer,
- $\psi_{sn}=\mathbf{k}_{sn}\cdot\mathbf{d}_{sn}$ is the scalar product between the wave vector $\mathbf{k}_{sn}=(2\pi/\lambda)\cdot\mathbf{u}_{sn}$ and the distance vector between the nth transmit antenna and the sth scatterer, $\mathbf{d}_{sn}$,
- v_t is the scalar speed of the transmitter,
- $\odot$ is the Hadamard product, *i.e.*, element by element multiplication of the matrices' elements.

As a consequence of the narrowband array assumption, $\Phi_{ms}=\Phi_s$ and $\phi_{sn}=\phi_s$, for any m and n.

In order to model $\mathbf{H}$, a statistical distribution should now be applied to $\mathbf{\Theta}$, as it is the only unknown of (4.8). In a quasi-static channel, $\mathbf{\Theta}$ represents the phases of the scatterers' reflection coefficients since the magnitudes are part of the prior state of knowledge. The entropy maximisation leads to an i.i.d. Gaussian distribution for the entries of $\mathbf{\Theta}$. Since Gaussian complex variables have uniform phases and so do the Γ in (4.6), it can be concluded that the proposed MIMO model is compliant with the entropy maximisation principle and the algorithm in Figure 4.3.

If the general channel approach was taken, the prior state of knowledge of the channel would be confined to:

- the scattering region shape and dimensions,
- the carrier frequency and bandwidth,
- the MT speed.

Therefore, a new mathematical model should be derived from the methodology of Figure 4.3, which is out of the scope of this thesis.

4.2.3 Model Discussion, Inputs and Outputs

As in Section 4.1.3, the inherent limitations and assumptions of the (now MIMO) model are discussed.

Some propagation phenomena, such as diffraction, rough surface scattering, the dependence of Γ on the AoIs, and the fact that the scatterers may have small displacements and rotations even when the BS to MT distance is constant, are not directly accounted for in the SISO baseline model, as discussed in Section 4.1.3. Despite the narrowband array assumption (that considers the antenna arrays as point-like), their influence might be significant in MIMO systems as they may illuminate each antenna differently and provide extra sources of decorrelation among the propagations paths. One way to statistically account for these phenomena is to set an additional randomness on the phases of the reflection coefficients. It would not only change in time (τ) from one channel realisation to another but it would also change from one propagation path to another, *i.e.*, from one receive–transmit (m, n) antenna pair to another. The new reflection coefficient for any scatterer Γ_d is then:

$$\Gamma_d(\tau, m, n) = |\Gamma|\exp\left\{j\cdot\left(\gamma(\tau)+\omega(\tau, m, n)\right)\right\}$$

<div align="right">(4.9)</div>

where

$$\omega(\tau, m, n) \sim U\left[-\frac{\Omega}{2}, +\frac{\Omega}{2}\right]$$

<div align="right">(4.10)</div>

is a random variable following a uniform distribution with user-defined range Ω. Unlike (4.6), the dependency of the reflection coefficients on the propagation path exists. The goal is to statistically account for all the phase shifts induced by the mentioned propagation phenomena, since the richness (and therefore the spatial decorrelation) of the signals at reception comes from the variety of constructive and destructive interference, solely ruled by the phases. The reader may argue that these phenomena were neglected in the SISO model, *e.g.*, the differences in the AoIs when the MT moved. The reason to consider it here has to do with the goal in hands: to gauge the influence of the environment in the MIMO capacity, highly sensitive to the spatial correlation among antennas, and thus to the phases. Since the study of

the spatial correlation around the receiver's antenna was not the main goal in the baseline SISO model, the hypothesis was then legitimate. Furthermore, no movement of the MT relatively to the BS is considered in this thesis, and though there is no conflict of assumptions as far as AoIs are concerned. The model with the new reflection coefficient is still compliant with the entropy maximisation principle since ω is uniformly distributed. This additional randomness was initially implemented in [MGFC01] to simulate non-stationarity of the MT and small displacements and rotations of the scatterers. The Ω parameter was then set as a function of the MT speed with values between 2.6º and 62.3º for speeds between 5 and 120 km/h, respectively.

As a consequence of the narrowband array assumption, the scattering region dimensions do not vary with the presence of multiple antennas; for micro-cells for example, the ellipse is not rotated, shifted or widened as the whole set of antennas is considered point-like. The individual antennas are seen as omni-directional, independently fed, point-like elements. The influence of their spacing at each end of the connection was subject of study in terms of capacity (Section 4.2.4). The temporal resolution of the receiver was set according to the bandwidth of the system under study, while the angular resolution is 0.5º [GVCM03]. Effects of polarisation were not studied, and thermal noise is only considered to establish a noise level under which the scatterers' contributions are not taken into account.

The inputs are grouped into the same categories as they were in Figure 4.1, with the following differences:
- the environment description now includes:
  - the parameter Ω of (4.10),
  - the average ρ at each receive antenna;
- the antenna parameters category now includes:
  - the number of the transmit and receive antennas (supposed independently fed with isotropic radiation patterns),
  - the antennas' spacings.

The outputs are grouped into the following categories:
- the **H** matrix category, which includes:
  - the normalised transfer matrices of the MIMO channels converted from the SISO simulator (hereafter called *simulated channels*),
  - the **H** matrix from two hypothetical channels: a totally uncorrelated (*ideal*) channel and a totally correlated (*worst-case*) one[2]; these are further filtered in time and angle;

---

[2] The *ideal* and *worst-case* designations were chosen having in mind the spatial correlation among the sub-channels that form the MIMO channel. It has nothing to do with the attenuation of the signal through these sub-

- the correlation matrix category, that includes:
  - o the coefficients of the simulated channels;
- the capacity category, that includes:
  - o the PDFs and CDFs of the narrowband and wideband capacities of the simulated, ideal and worst-case channels,
  - o the variation of these capacities with ρ per antenna branch, the number of transmit and receive antennas, the antennas' spacings, and the Ω parameter,
  - o the relative gain provided by the use of a certain *M×N* antenna array size in relation to another array size.

The flowchart of the MIMO simulator is depicted in Figure 4.4.
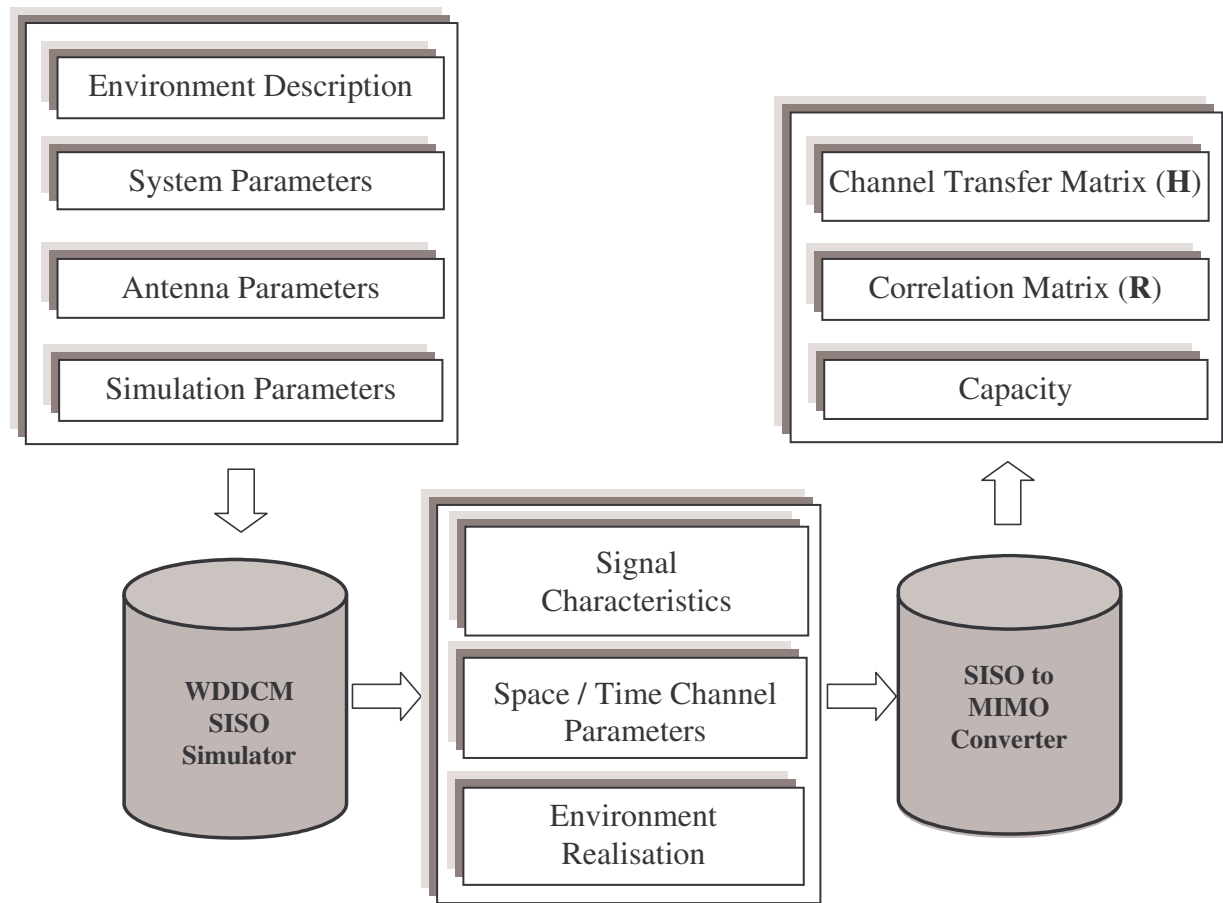
Figure 4.4: MIMO Simulator Structure, Inputs, and Outputs.

The outputs of the original WDDCM SISO simulator are now inputs of the SISO to the MIMO converter. The ideal and worst-case channels arise by direct manipulation of the **H** matrix: $h_{mn}(t)$ in the worst-case channel are random i.i.d. for each channel realisation (τ) and equal for all (m,n), whereas the ones of the ideal channel are random i.i.d. for each channel

---

channels. Therefore, the reader should be aware that the worst-case channel could outperform the ideal one if their channel gains, $|h_{mn}|$, were sufficiently different.

realisation (τ) and for each sub-channel (m,n). In both cases, the real and imaginary parts of $h_{mn}(t)$ are independent, following a Gaussian distribution with zero-mean and ½-variance as in [Tela95]. This is the usual *Rayleigh fading model*, in which the $h_{mn}(t)$ have Rayleigh distributed amplitudes and uniform phases.

Mathematically,

$$h_{mn\text{-worst case}}(t) = h_{mn\text{-worst case}}(\tau, t) \in \mathbb{C}^2 \tag{4.11}$$

where

$$\text{Re}\{h_{mn\text{-worst case}}(t)\} \sim \text{Normal}(0, \text{½})$$
$$\tag{4.12}$$
$$\text{Im}\{h_{mn\text{-worst case}}(t)\} \sim \text{Normal}(0, \text{½})$$

and

$$h_{mn\text{-ideal}}(t) = h_{mn\text{-ideal}}(\tau, t, m, n) \in \mathbb{C}^2 \tag{4.13}$$

where

$$\text{Re}\{h_{mn\text{-ideal}}(t)\} \sim \text{Normal}(0, \text{½})$$
$$\tag{4.14}$$
$$\text{Im}\{h_{mn\text{-ideal}}(t)\} \sim \text{Normal}(0, \text{½})$$

A flowchart of the SISO to MIMO converter is depicted in Figure 4.5. The simulator was written in C (WDDCM SISO Simulator) and Matlab[®] (SISO to MIMO Converter) programming languages. The average amount of memory involved in the input and output files and the processing times for a simulation run of 1 000 channel realisations with a single value of M, N, d_a, Ω and ρ, in a computer equipped with a Intel Pentium IV[®] processor at 2.4 GHz are in Table 4.2.

Table 4.2: Memory and Processing Times for 1 000 Channel Realisations for Single Valued M, N, d_a, Ω, and ρ.

	WDDCM SISO Simulator	**SISO to MIMO Converter**
Average Occupied Memory [MB]	11.8	18.15
Average Processing Time [min]	2.5	15

According to Table 4.2, the processing times to obtain the Figure 4.7 to Figure 4.12, range from 4 to 10h.
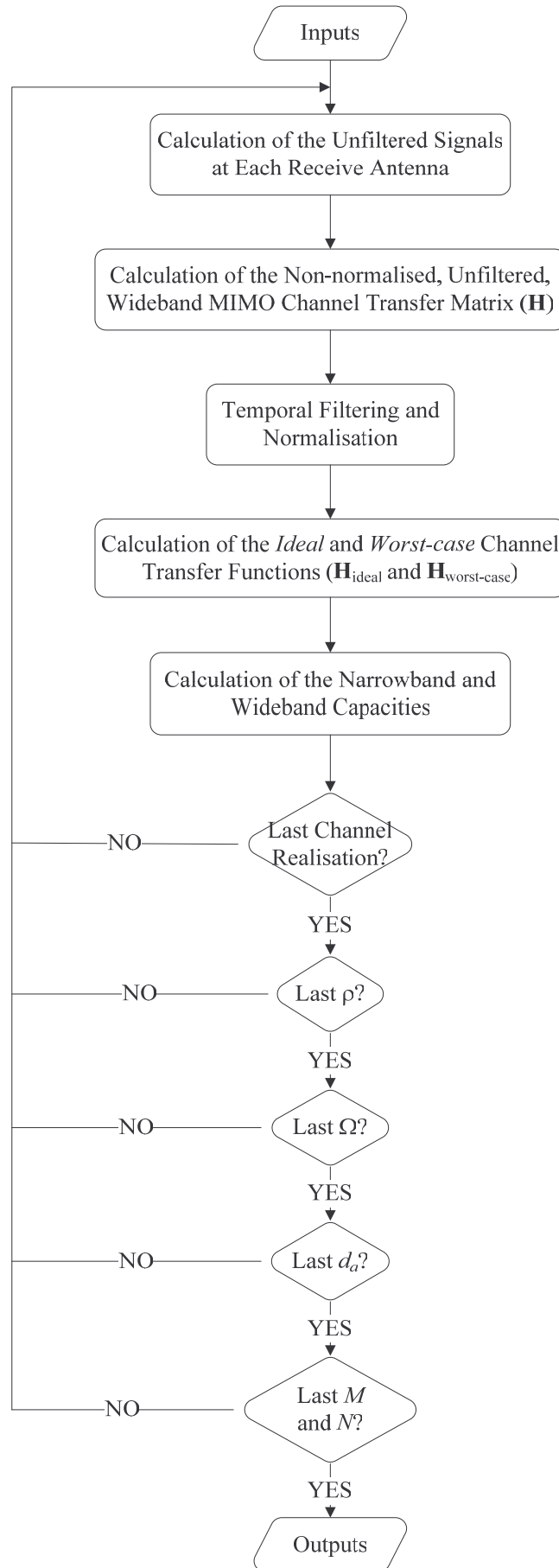
Figure 4.5: SISO to MIMO Converter Flowchart.

4.2.4 Model Assessment

The proposed MIMO model was assessed in terms of capacity. The reference environment for the assessment is the micro-cell accounting for a typical street, Table 4.3. The simulator has been tested as a function of the number of scatterers, number of clusters, Angle Spread (AS) − through the variation of the street width ratio −, M, N, d_a, and Ω. The assessment was done varying only one parameter at a time.

All simulated capacities are plotted against the capacities of the ideal and worst-case channels to show how the latter ones bound the former. These results are further compared with published work.

Table 4.3: Parameters of the Reference Environment.

Scattering Environment	BS to MT distance [m]	100
	Real street width [m]	20
	Street width ratio	4
	Average number of clusters	7
	Clusters' spatial density [m^{-2}]	0.000875
	Av. no. scatterers per cluster	20
	Standard deviation of the scatterers within clusters [m]	1
MIMO System	$M \times N$	3×3
	d_a [m]	0.075 (λ/2)
	Ω [rad]	π/5
System Parameters	f [GHz]	2
	Bandwidth [MHz]	5
	ρ [dB]	10
	Path Loss Exponent	2
	Mobility	Not considered[3]
	Delay resolution [ns]	200
	Angle resolution [^{o}]	0.5
	Noise Margin [dBm]	-150
	Number of channel realisations	1 000

---

[3] It is not considered the mobility of the MT relatively to the BS. However, this does not mean that the channel is stationary in time as scatterers can move relatively to the MT and BS. These movements will be later characterised by a coherence time of the channel.

Regarding the scattering environment, it was statistically characterised in Table 4.1, while its parameters have been optimised in [GVCM03] to fit the reality of measurement campaigns.

Regarding the MIMO system, a 3×3 configuration was chosen to clearly view the capacity increase of multiple antenna enabled systems, while bearing in mind basic space limitations. The antennas at each end of the connection were put half wavelength apart, since it is shown in [PFMC02] that this achieves a good balance between signal decorrelation and occupied space. Finally, Ω was set to $\pi/5$, so $\omega \sim$ Uniform$[-\pi/10, +\pi/10]$ as in (4.10). Later in this section, a study of the influence of Ω is shown.

Regarding the system parameters, the carrier frequency and bandwidth were set to 2 GHz and 5 MHz, respectively, to meet the system's requirements. The average received ρ per antenna branch was set to 10 dB, as it is one of the most frequent values in the literature, and the noise margin was picked from [GVCM03]. The number of channel realisations was such that provided sufficient averaging (*i.e.*, more channel realisations would not significantly modify the results) while keeping the computational burden within reasonable levels.

In the following, the MIMO capacity is shown under the variation of some of the reference environment characteristics. In order to study the variation of the capacity with the channel's richness, Figure 4.6, a set of environments have been defined, Table 4.4, that vary in the number of scatterers, clusters, and effective street widths. It is important to note that the ideal and worst-case channel capacities do not depend on the scattering richness of the environment.

Table 4.4: Environments with Different Degrees of Scattering Richness.

	Average No. Scatterers / cluster	**Average No. Clusters**	**Street Width Ratio**
Env. 1	20	7	4
Env. 2	1	7	4
Env. 3	1	1	4
Env. 4	1	1	1

These environments are only defined in this thesis for assessment purposes, they do not try to identify new propagation scenarios. Environment 1, which corresponds to the reference environment of Table 4.3, provides a rich scattering channel and a wide AS. Environment 2 presents a much lower number of scatterers than Environment 1 and provides very little clustering (as clusters have in average only one scatterer); the scatterers are therefore distributed uniformly in the scattering region. Environment 3 has one scatterer on average, which can have AoD and AoA set within a wide range, while Environment 4 resembles Environment 3 with a much lower AS.
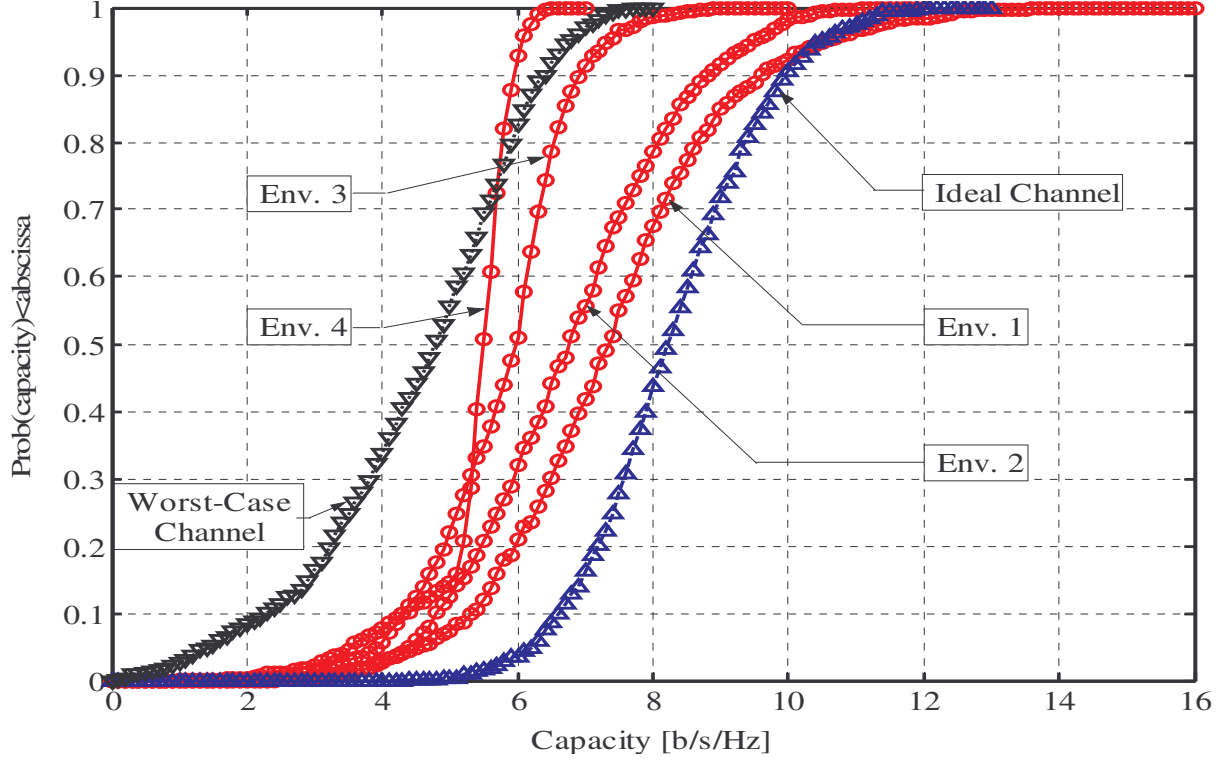
Figure 4.6: Channel Capacity CDF with Different Levels of Correlation.

As expected, Figure 4.6 shows that the capacities of the simulated channels are confined by the ones of the ideal and worst-case channels. The fact that the set of **H** matrices for the ideal and worst-case situations were derived with the same statistical distribution delivers the same shape for both CDF curves, only differing in a shift along the capacity axis. On the other hand, the simulated CDFs have different shapes because their statistical richness varies with the channels' scattering richness. For some sets of parameters, this is well expressed in the curves' steeper slope and consequent narrower range of achievable capacities. Therefore, when there is a very low number of scatterers (Env. 4), the CDF is nearly vertical. Furthermore, one can note the natural decrease of the capacity as the scattering richness is reduced (spatial correlation increased).

These curves can be compared to the ones in [GeAk02] and [Debb03] having in mind that in this thesis the entries of **H** are always complex (not the case in the mentioned references), which normally leads to higher capacities than the ones of real-valued **H.**

Until the end of this section, the capacity shown for each configuration, antenna spacing and/or Ω is the ergodic capacity calculated from 1 000 channel realisations.

The variation of the capacity with the number of transmit and receive antennas is displayed in Figure 4.7.
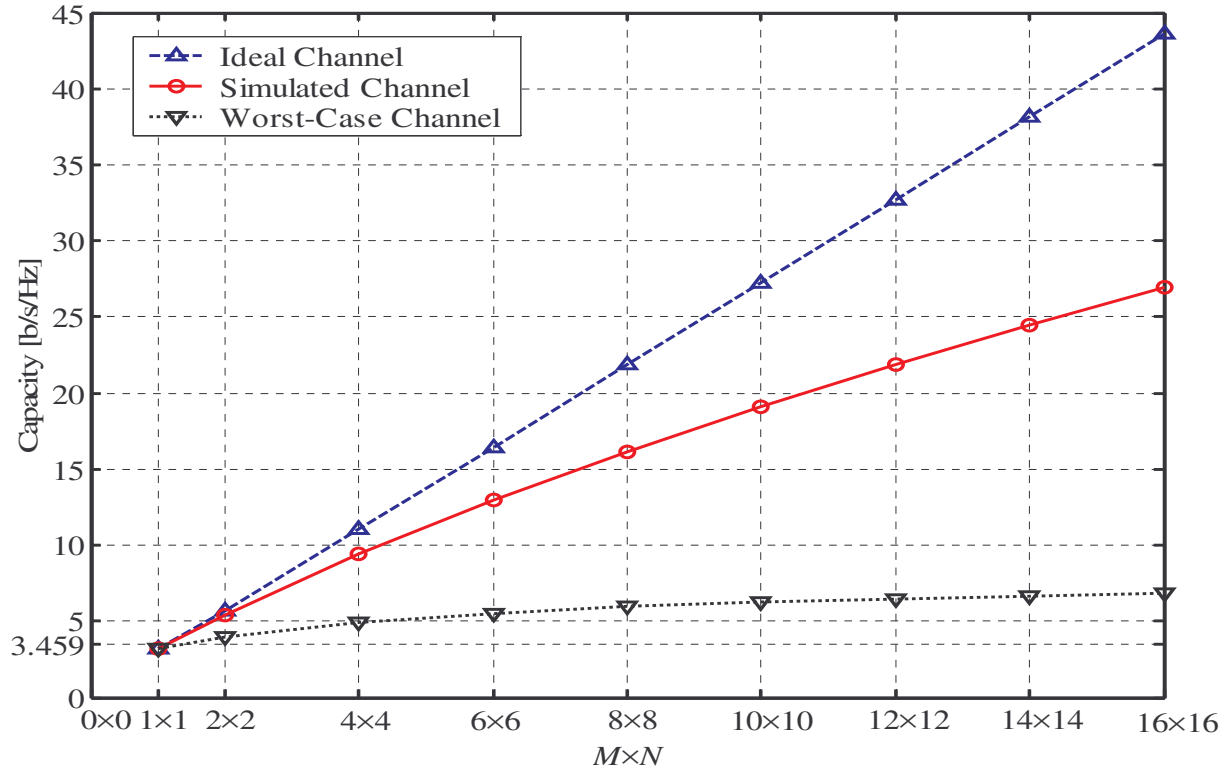
Figure 4.7: Mean Channel Capacities for Different MIMO Configurations in Env. 1 with *M=N*.

As depicted in Figure 4.7 and as it is expressed in (3.15) and (3.16), the capacity of the ideal channel increases linearly with the number of antennas, while the worst-case one does it logarithmically. The simulated channel has a behaviour in-between. For the single transmitter, single receiver case, the capacities practically coincide, which was expected, since the only difference between the 3 cases is the spatial correlation between the antennas: the differences on the particular **H** of each channel realisation were eliminated with sufficient averaging. The single antenna configuration provides a capacity given by (3.8). For $\rho=10$ dB, it is found that:

$$C_{1\times1}=\log_2(1+10)\approx 3.459 \text{ b/s/Hz} \tag{4.15}$$

The capacity scaling with the array size can be found in [HoTW03] for real-valued **H** and $\rho=0$ dB, and in [Kyri01] for complex-valued **H** and $\rho=20$ dB. The capacity variation with the antenna spacings at both ends of the connection is depicted in Figure 4.8.

The first observation is the constant capacity of the ideal and worst-case channels that bound the simulated one: their correlation is null or total, independently of the antenna spacings. The specific constant values they assume are the mean values given by (3.11) with **H** following the distributions given by (4.11)-(4.14). In fact,

$$C_{av} = \left\langle \log_2 \left\{ \det\left[\mathbf{I_M} + \left(\frac{\rho}{N}\right)\mathbf{H_{ideal}}\mathbf{H_{ideal}^H} \right] \right\} \right\rangle \approx 8.28 \text{ b/s/Hz} \tag{4.16}$$

and

$$C_{av} = \left\langle \log_2 \left\{ \det\left[\mathbf{I_M} + \left(\frac{\rho}{N}\right)\mathbf{H_{worst\text{-}case}}\mathbf{H_{worst\text{-}case}^H} \right] \right\} \right\rangle \approx 4.61 \text{ b/s/Hz}$$
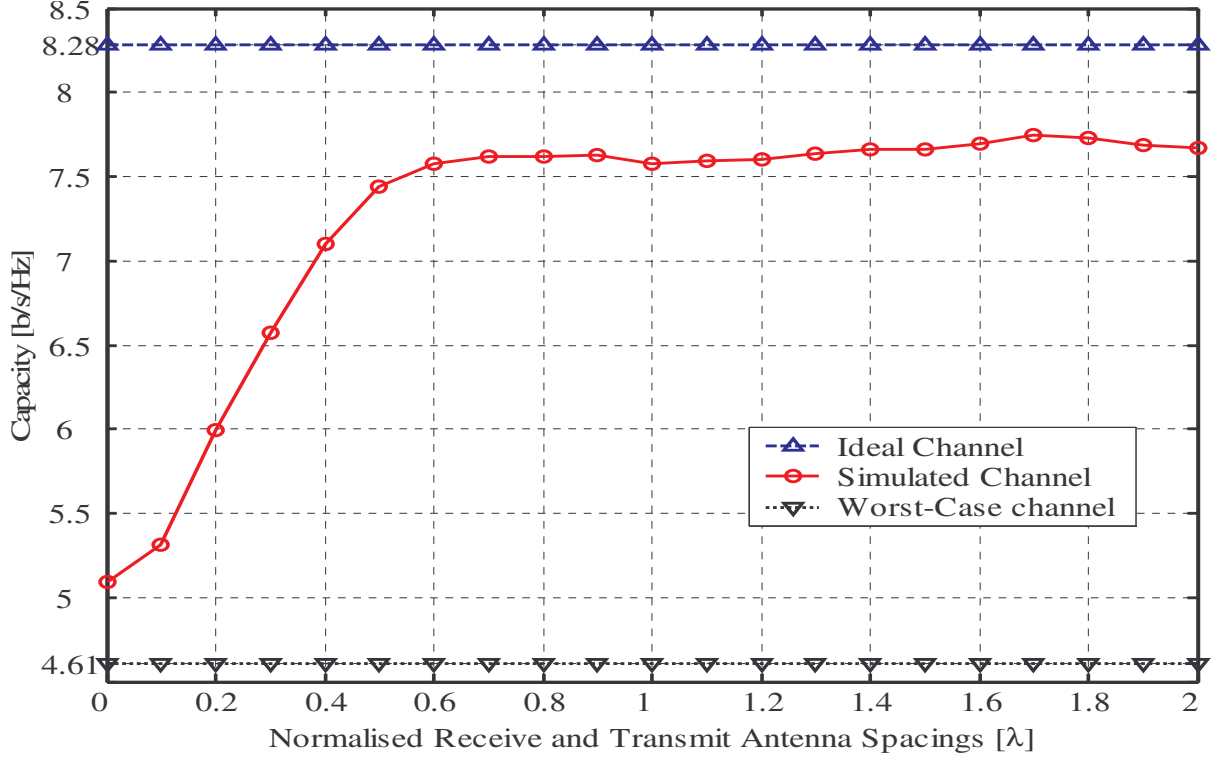
(4.17)

Figure 4.8: Channel Capacity for Different Antenna Spacings in Env.1.

In the purely conceptual case of 3 antennas with zero spacing, the capacity gap between the simulated and the worst-case channels is due to the presence of $\omega(\tau,m,n)$ in (4.9).

While the increase of the capacity for the first values of the simulated channel was expected, one could wonder why its asymptotic behaviour does not reach the ideal capacity. The reason is that the statistical characteristics of the environment are independent of the antenna spacings and they impose a minimum correlation of the signals at arrival. The mean number of scatterers and clusters, their spatial distribution, and the shape and dimensions of the scattering region prevent the channel from being i.i.d. Gaussian, independently of the characteristics of the antennas (the reader should remember that the i.i.d. Gaussian model represents the least restrictive channel [Debb03]). However, it is expectable that the capacity curve that would be obtained through measurement campaigns would not flatten as much as the one in Figure 4.8 for 0.5λ onwards. The reason for this total flattening has to do with the validity of the narrowband array assumption for high antenna's spacings: the variation of the AoDs and AoAs becomes important as antennas are much separated apart. The different AoDs and AoAs for each antenna is a source of spatial decorrelation that is not accounted for in this MIMO model due to the narrowband array assumption. In one word, as the array size increases, the near field region enlarges and some scatterers may not be illuminated with

planar waves any longer but with spherical ones. The effect of the antenna spacings for LoS indoor environments is much better modelled by the *distributed-point source model* [Chan04], where the signals at each antenna element have different spatio-temporal characteristics.

Previously, it was referred that the disparities between the signals in different antennas were mostly due to their phases, Figure 4.2. By showing the capacity as a function of Ω, Figure 4.9 corroborates this by illustrating the potential of the variation of the phases: they can provide all the decorrelation needed to reach the ideal channel capacity. This makes the choice of Ω critical. Given that the reference channel (Environment 1) represents a very rich scattering environment, the role of Ω in it does not seem so important. However, it is shown that the use of poorer environments, Table 4.4, unbury the effect of Ω, Figure 4.9.
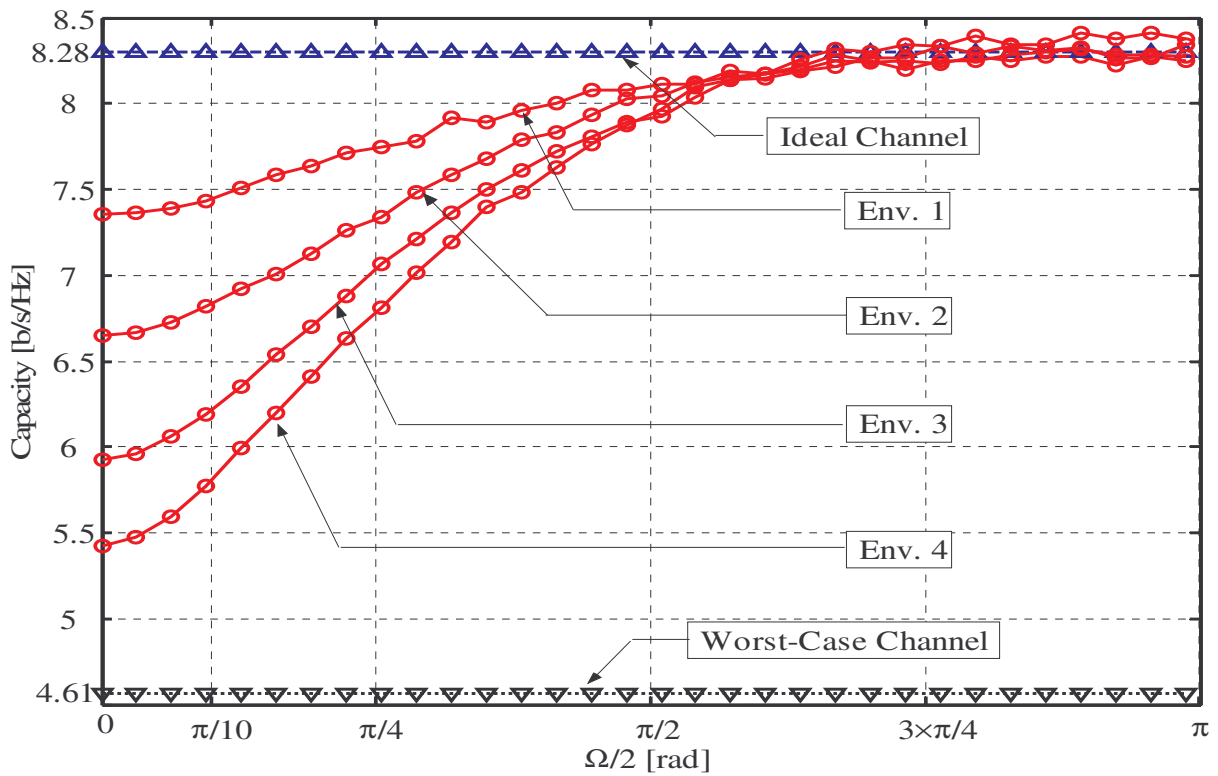
Figure 4.9: Channel Capacity for Different $\Omega/2$.

The gap between the worst-case channel capacity and the simulated ones for $\Omega=0$ is due to the variety of phases provided by different path lengths, strongly dependent on the scattering richness. The choice of Ω tunes the behaviour of the MIMO model between one that does not account for any other propagation phenomena than free space propagation and reflection, and one that provides complete signal decorrelation. It is shown here that the chosen value for Ω ($\pi/10$), Table 4.3, provides some extra decorrelation from the provided solely by the phase shifts due to different path lengths, but still sufficiently low as the effects that ω encompasses are supposedly not predominant. However, to have more accuracy in this parameter, measurement campaigns would have to be carried out to assess the model. Unfortunately, this is out of the scope of this thesis because of time limitations.

4.3   Simulated MIMO Capacity Increase

In this section, the reference environment of Table 4.3 was considered with slight changes that distinguish the UMTS channel from the HIPERLAN/2 one, Table 4.5.

Table 4.5: Reference Environment for UMTS and HIPERLAN/2.

		UMTS	HIPERLAN/2
Scattering Environment	BS to MT Distance [m]	100	100
	Real Street Width [m]	20	20
	Street Width Ratio	4	4
	Average Number of Clusters	7	7
	Scatterers Density in Clusters [m^{-2}]	0.000875	0.000875
	Av. No. Scatterers per Cluster	20	20
	Standard Deviation of the Scatterers within Clusters [m]	1	1
MIMO System	$M \times N$	2×2	2×2
		16×16	16×16
		4×2	4×2
		8×2	8×2
		16×2	16×2
		2×4	2×4
		8×4	8×4
		16×4	16×4
	d_a [m]	0.15 ($\lambda_{UMTS}/2$)	0.06 ($\lambda_{HL/2}/2$)
	Ω [rad]	$\pi/5$	$\pi/5$
System Parameters	f (Bandwidth) [GHz (MHz)]	2 (5)	5 (20)
	ρ [dB]	10	10
	Path Loss Exponent	2	2
	Mobility	Not considered[4]	Not considered[3]
	Delay(Angle) Resolution [ns(^{o})]	200 (0.5)	50 (0.5)
	Noise Margin [dBm]	-150	-150
	No. of Channel Realisations	1 000	1 000

---

[4] See footnote 2 in page 61.

The capacity enhancement at propagation level provided by the use of MIMO in UMTS and HIPERLAN/2 was simulated. The capacity increase of one configuration $M{\times}N$ in relation to another $M'{\times}N'$ is characterised by its relative gain $G_{M{\times}N/M'{\times}N'}$ as:

$$G_{M{\times}N/M'{\times}N'} = \frac{C_{MIMO}\big|_{M{\times}N} - C_{MIMO}\big|_{M'{\times}N'}}{C_{MIMO}\big|_{M'{\times}N'}}$$

(4.18)

where C_{MIMO} denotes the capacity of the MIMO channel (3.11). Like C_{MIMO} itself, $G_{M{\times}N/M'{\times}N'}$ is a random variable, defined for each channel realisation as expressed in (4.18).

Figure 4.10 and Figure 4.11 illustrate the CDF of the capacity gains for the reference environment of UMTS and HIPERLAN/2, respectively. In these figures, $M'=N'=1$, *i.e.*, they illustrate the gain of MIMO in relation to SISO, $G_{M/S}$. The MIMO configurations include 2, 4 and 16 antennas, among others, since these are foreseen to be the most optimistic number of antenna elements in mobile phones, Personal Digital Assistants (PDAs), and portable computers, respectively [ACGN02]. The potential to have larger antenna arrays at the BS motivates Figure 4.11, where the number of antenna elements at each end of the connection is different.

It can be seen how the relative gains increase with the number of antennas: the larger the array size, the lowest the respective CDF gain curve. The asymptotic behaviour slowly approaching 1 indicates that the relative gains can be very high. This is due to the possibility of a nearly zero capacity of the SISO configuration and not to extremely high MIMO capacities.
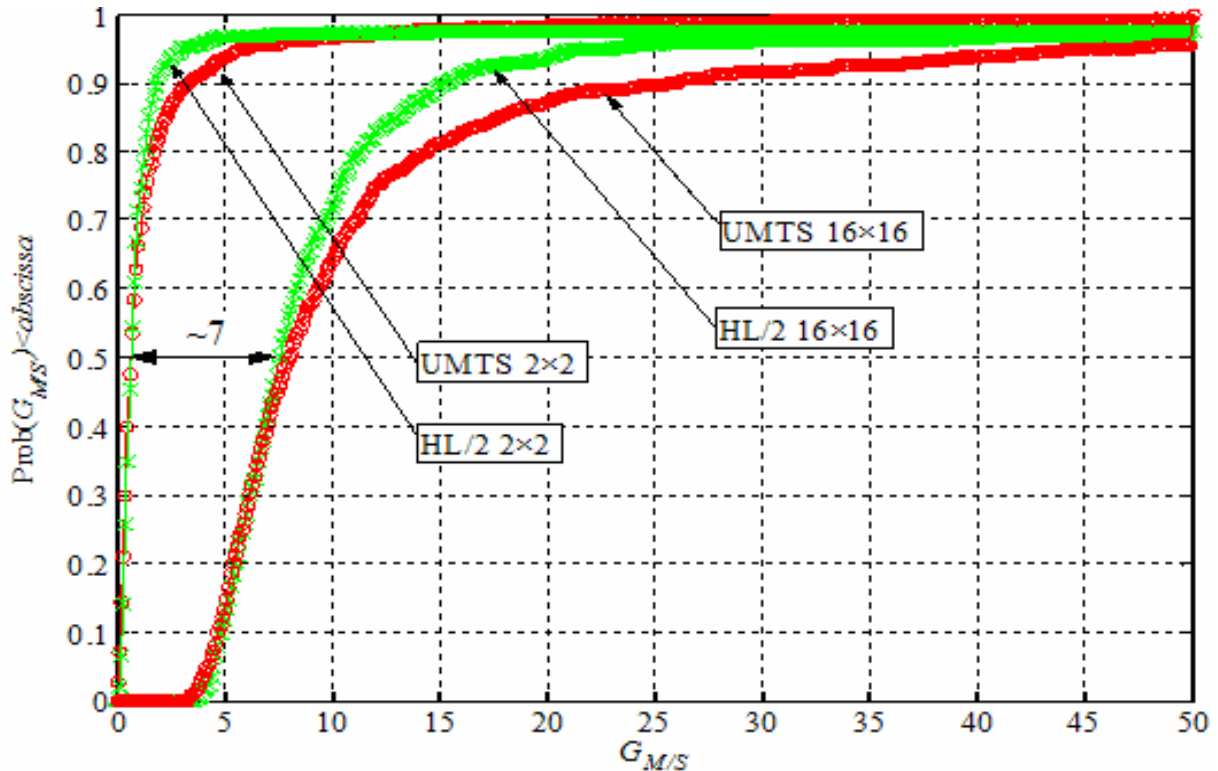

Figure 4.10: MIMO Relative Capacity Gain for $M=N=\{2, 16\}$ and $M'=N'=1$.
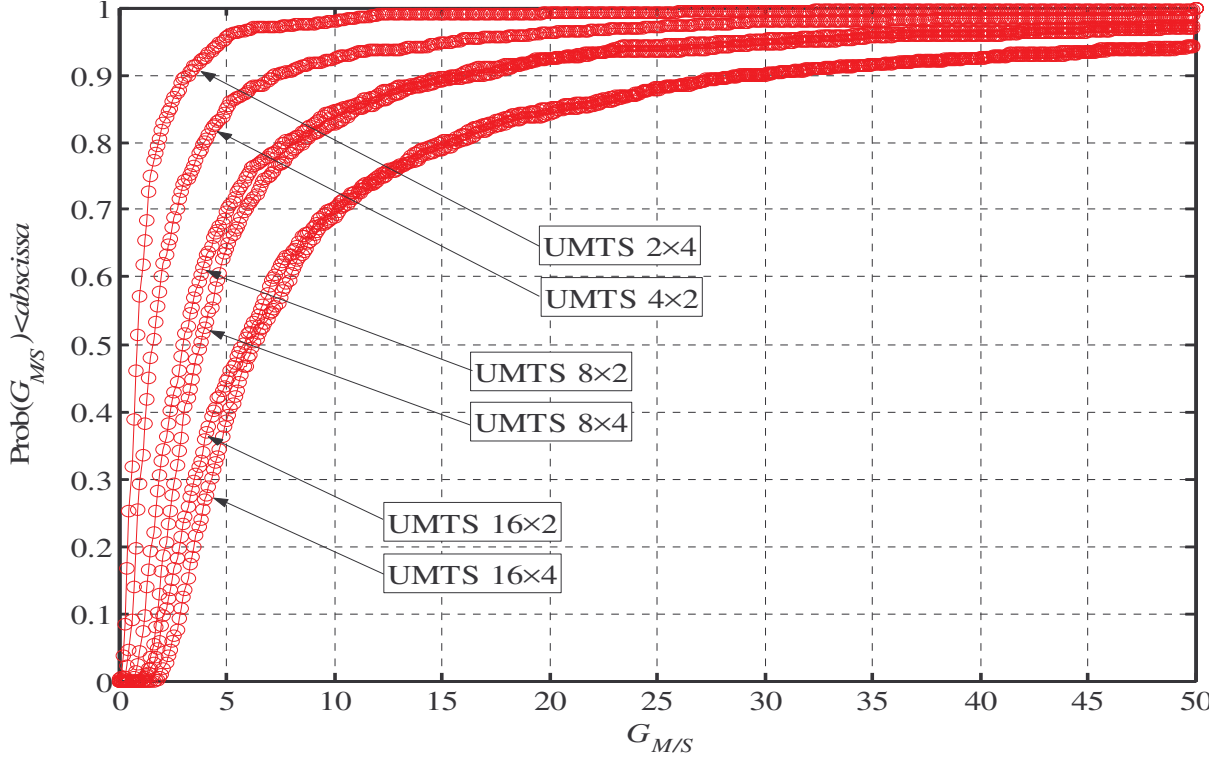
Figure 4.11: MIMO Relative Capacity Gain for *M≠N* and *M'=N'=1*.

The mean gain obtained by using a specific configuration in relation to using any other one can be calculated through (4.18) and Figure 4.7. For the simulated channel of Figure 4.10, the following values can be read from Figure 4.7:

$$<C_{2\times2}>\approx5.36 \text{ b/s/Hz,} \tag{4.19}$$

$$<C_{16\times16}>\approx26.99 \text{ b/s/Hz,} \tag{4.20}$$

and therefore,

$$<G_{16\times16/2\times2}>\approx6.25 \tag{4.21}$$

The median of $G_{16\times16/2\times2}$ (~7) can be read directly in Figure 4.10.

It is also of interest to compare the behaviour of $G_{M/S}$ in UMTS and HIPERLAN/2. It would be natural to think that the system using the smallest wavelength achieves higher spatial decorrelation for the same inter-antenna spacing, as the phase shifts $\Delta\Phi$ would be larger (4.5). Secondly, since the bandwidth is directly proportional to the time resolution of the systems, HIPERLAN/2 would have the means to resolve more propagation paths than UMTS and provide more decorrelation. Quite surprisingly, the superior gains of HIPERLAN/2 over UMTS are not reflected in Figure 4.10: their CDF gain curves are either on top, above or below of each other. In the 2×2 configuration, for example, the crossing point occurs for a

$G_{M/S}$ of approximately 15; in the 16×16 it happens for a value greater than 50, which it is not represented due to illustration difficulties[5].

The sensitivity of the decorrelation on the wavelength is a fact that can be seen in Figure 4.8, since, according to (4.5), varying the wavelength is equivalent to varying the antenna spacings. However, this sensitivity cannot be seen in Figure 4.10, because it supposes an inter-antenna spacing of λ/2, no matter the λ of each system, as stated inTable 4.5. On the other hand, the different bandwidths have very little effect on the $G_{M/S}$ due to two main reasons: not even the HIPERLAN/2 bandwidth is large enough to accurately resolve the paths, and the SISO capacity also benefits from the augmentation of the bandwidth. In fact, Table 4.6 shows that HIPERLAN/2 resolution can only distinguish two sets of signal replicas on average, while the UMTS one can hardly ever resolve any propagation path.

Table 4.6: Systems' Time Resolutions and Signals' Maximum Relative Delay.

	UMTS	HIPERLAN/2
Time resolution (=bandwidth^{-1}) [ns]	200	50
Av. Maximum Signals' Relative Delay [ns]	87.29	

Figure 4.12 shows how the SISO capacity also benefits from the augmentation of the bandwidth so the ratio in (4.18) does not suffer large changes.
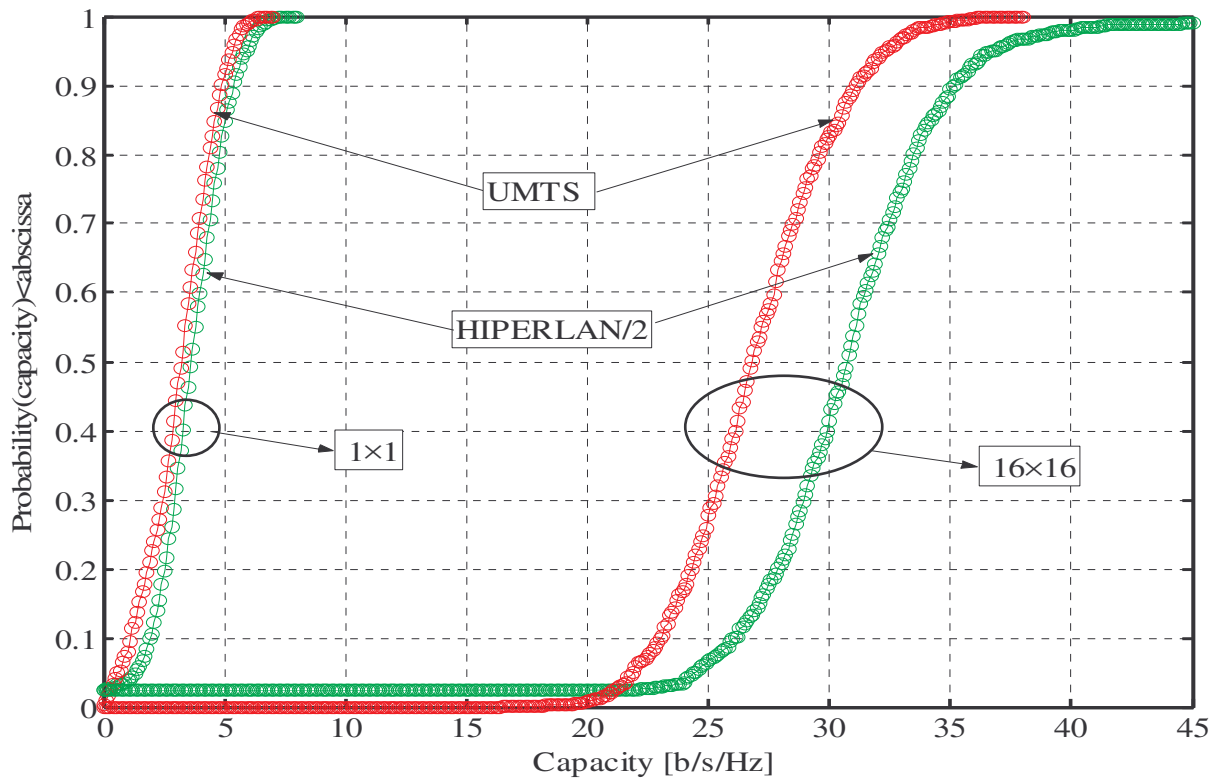
Figure 4.12: UMTS and HIPERLAN/2 Channel Capacity CDF for SISO and MIMO 16×16.

---

[5] For an X-axis ranging from 0 to 200, the 2×2 and 16×16 curves are practically undistinguishable.

The assessment in terms of capacity has shown accuracy when compared with published work, and expected behaviours when varying its main parameters. Therefore, as long as it is capacity what it is aimed to obtain from the model, one can trustworthily use it.

5

Systems Convergence Model

A specific model for wireless systems convergence has been provided with a simple physical layer to cope with channel capacity enhancements. This chapter describes a MIMO-enabled model of traffic convergence, from the philosophy behind the convergence of standards, Section 5.1, to a proposal of studying the influence of the physical layer on the traffic, Section 5.2.

5.1 Systems Convergent Simulator Description

For the purpose of evaluating the benefits of the convergence of GSM/GPRS, UMTS (FDD Mode), and HIPERLAN/2 access technologies, mainly from the capacity/traffic viewpoint, the model described in [Agui03] was used. This section provides an overview of the original model's implementation, *i.e.*, without MIMO. More details can be found in the mentioned reference.

The main goal underlying the development of the simulator was to build a platform enabling the following tasks:
- analysis of the impact of the convergence on the radio network's overall performance,
- evaluation of different convergence perspectives/strategies,
- analysis of the impact of the different traffic distributions in a convergence scenario.

The simulator is constituted by the following two functional blocks, Figure 5.1:
- User Traffic Generation Module (UTGM),
- Traffic Processing Engine (TPE).
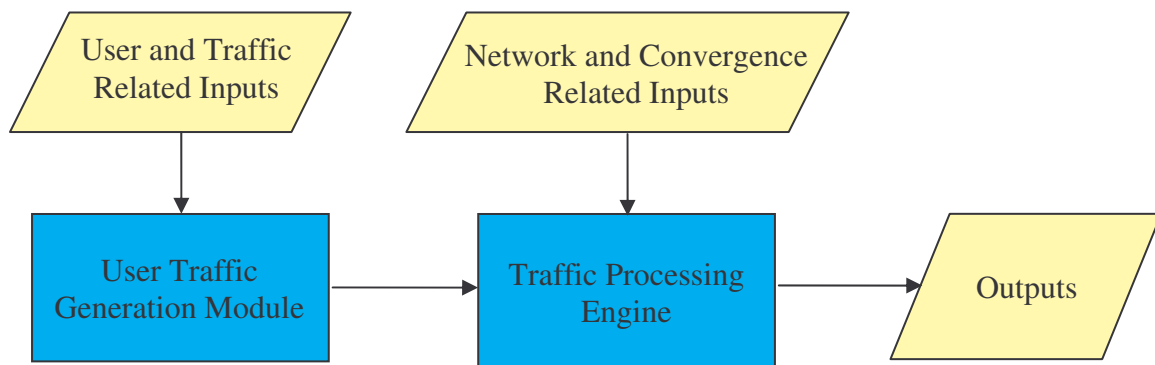
Figure 5.1: General Structure of the System Convergent Simulator (based on [Agui03]).

The UTGM is responsible for generating the user traffic that will be routed to all active users. For each user (or MT), the traffic is generated in the form of User Traffic Vectors (UTVs). The TPE is the "brain" of the simulator, receiving and routing the UTVs, according to a convergence criteria/strategy. For this purpose, Access Technology Traffic Processing Modules (ATTPMs) are implemented in it, for simulation of different access technologies available to users. The TPE's outputs, corresponding to the simulator outputs, include the overall performance indicators to evaluate the convergence benefits. Both the UTGM and TPE receive user-defined input parameters, allowing the simulation of different user, applications and technological scenarios.

For simplicity reasons, the simulator only considers DL user traffic, disregarding the UL components. From a capacity viewpoint, this approach is taken since:

- nearly all of the considered applications are asymmetric, with a higher capacity demand in DL,
- in general, the DL component is capacity limited, in opposition to the UL one that is usually interference/power limited.

The UTGM's functional process is depicted in Figure 5.2, and described in the following paragraphs.

The UTGM initially generates a user-defined (simulator input) number of users. Each user is then given a user type classification. A user type corresponds to a particular user profile (simulator input), with specific traffic usage characteristics, namely Busy Hour Call/session Attempt (BHCA) and average call/session durations per application. In the present simulator, three user types were considered, differing in how they exploit the applications of Table 5.1, although other user types can easily be added. The allocation of a specific user type to each user is randomly performed, and depends on the penetration of each user type (simulator input).

Figure 5.2: UTGM's Functional Process (based on [Agui03]).
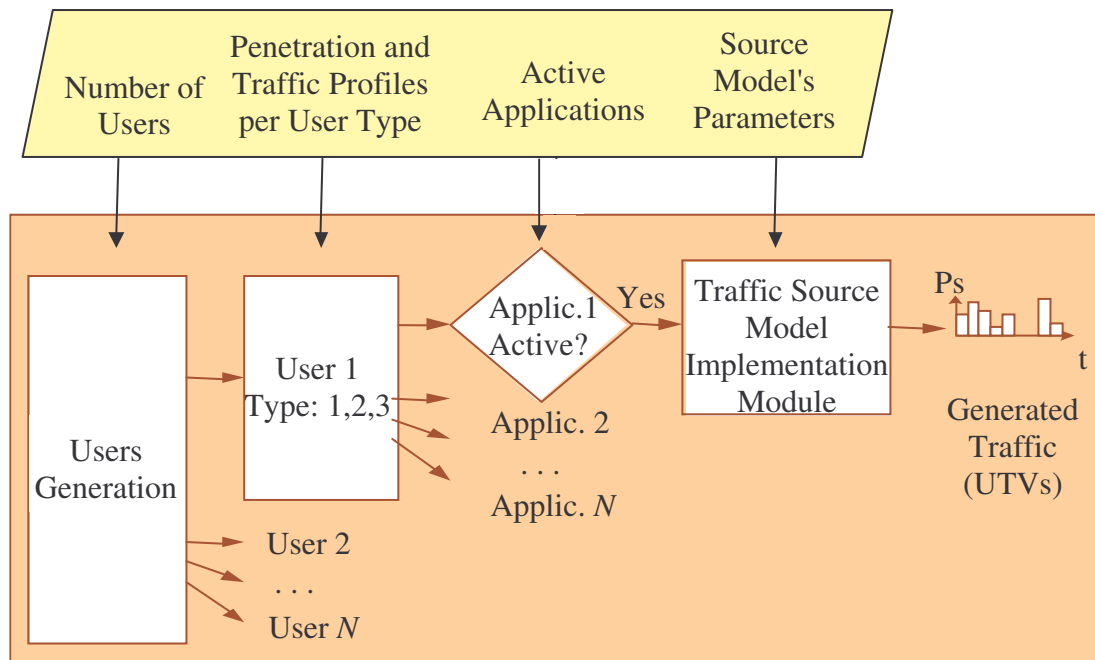
Six different applications, Table 5.1, are supported by the simulator, which can be individually enabled or disabled for analysis of the impact of different traffic mixtures. The last and most elaborate task of the UTGM is to generate the UTVs for each active application of each user. This task is performed by the Traffic Source Model Implementation Modules (TSMIMs).

Table 5.1: Applications Supported by the Simulator.

Applications	Services	Service Class
Voice Call	Speech Telephony	Conversational
Video Call	Video Telephony	Conversational
Video on Demand	Video Streaming	Streaming
Web Browsing	Multimedia Communication Service	Interactive
Email	Messaging Service	Background
FTP	Unrestricted Data Transfer Service	Background

The mapping of the supported applications onto the CS and PS types (as a function of the access technologies) that was adopted in the simulator implementation is presented in Table 5.2. As one can observe, only the Voice Call and Video Call (voice component), when transmitted over GSM or UMTS, were considered to be of the CS type, requiring a constant capacity usage during the complete call transmission. In the remaining cases, the applications traffic is processed as of a PS type.

Table 5.2: Classification of Applications (CS and PS) per Access Technology.

Application		Access Technology		
		GSM/GPRS	**UMTS**	**HIPERLAN/2**
Voice Call		CS	CS	PS
Video Call	**Voice Component**	CS	CS	PS
	Video Component	PS	PS	PS
Video on Demand	**Video Component**	PS	PS	PS
Web Browsing		PS	PS	PS
Email		PS	PS	PS
FTP		PS	PS	PS

The TPE is the main functional entity of the simulator as it performs all the "convergence" and traffic processing tasks. It is assumed that this converged network is supported by a common IP backbone, offering access to different services via several mobile and wireless technologies.

From a functional point of view, the TPE receives the UTVs generated by the UTGM and processes them according to different convergence perspectives/strategies. The traffic is then routed to the MTs through one of the three access technologies. Each access technology is implemented in the simulator as an ATTPM.

All MTs are considered to be "convergence" capable, *i.e.*, capable of receiving traffic through all available access technologies. The main functional building blocks of the TPE and their interactions are depicted in Figure 5.3.
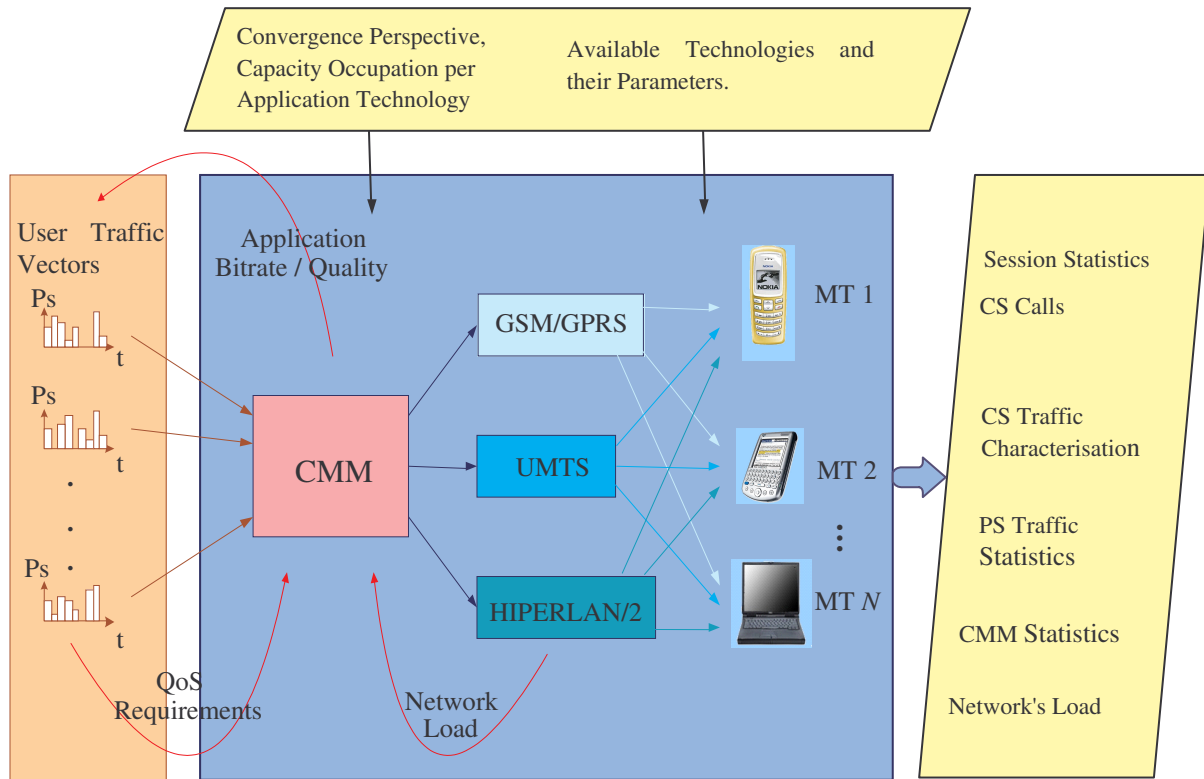
Figure 5.3: Traffic Processing Engine (based on [Agui03]).

The UTVs generated by the UTGM are firstly analysed by a new functional entity here referred to as the Convergence Manager Module (CMM), Figure 5.4. The main functions of the CMM are to detect new sessions and to route the associated traffic to different ATTPMs according to a user-defined (simulator input) convergence criteria/strategy. For this purpose, the CMM considers several parameters, such as the loads of the different access technology networks and the different application's priorities/QoS requirements.

The Priority Table (PT) establishes priority criteria for routing each application through one or another access technology and with one or another bitrate/quality. Thus, for each PS and CS application, a specific order of access technologies and bitrate/qualities is established that rules the way they are transmitted to the user. It is based on a *highest throughput/best system* approach. The *highest throughput* concept means that for data and video applications, the highest available/possible transmission bitrate is selected based on the current networks' loads. In respect to the *best system* approach, priority is given to the most appropriate application-oriented access technology (*e.g.*, data applications first priority – WLAN; Voice Calls first priority – GSM). A detailed description of each TSM of Table 5.3 can be found in [AgCo04].

Table 5.3: Priority Table of the Convergence Manager Module.

Application	Priority	Access Technology	Traffic Source Model
Voice Call **Video Call** **(Voice Component)**	1	GSM/GPRS	Classical ON-OFF
	2	UMTS	CDMA MSVM
	3	HIPERLAN/2	VoIP
Video Call **(Video Component)**	1	HIPERLAN/2	GBAR H.263 VBR
	2	UMTS	H.263 TBR 32 kb/s
	3	GSM/GPRS	H.263 TBR 32 kb/s
Video on Demand **(Video Component)**	1	HIPERLAN/2	GOP GBAR MPEG-4 HIGH Quality
	2	HIPERLAN/2	GOP GBAR MPEG-4 LOW Quality
	3	HIPERLAN/2	H.263 TBR 64 kb/s
	4	UMTS	H.263 TBR 64 kb/s
Web Browsing	1	HIPERLAN/2	WWW 2 Mb/s
	2	HIPERLAN/2	WWW 384 kb/s
	3	HIPERLAN/2	WWW 144 kb/s
	4	UMTS	WWW 384 kb/s
	5	UMTS	WWW 144 kb/s
	6	UMTS	WWW 64 kb/s
	7	UMTS	WWW 32 kb/s
	8	UMTS	WWW 8 kb/s
	9	GSM/GPRS	WWW 64 kb/s
	10	GSM/GPRS	WWW 32 kb/s
	11	GSM/GPRS	WWW 8 kb/s
Email	1	HIPERLAN/2	Email 384 kb/s
	2	HIPERLAN/2	Email 144 kb/s
	3	UMTS	Email 384 kb/s
	4	UMTS	Email 144 kb/s
	5	UMTS	Email 64 kb/s
	6	GSM/GPRS	Email 64 kb/s
FTP	1	HIPERLAN/2	FTP 384 kb/s
	2	HIPERLAN/2	FTP 144 kb/s
	3	UMTS	FTP 384 kb/s
	4	UMTS	FTP 144 kb/s
	5	UMTS	FTP 64 kb/s
	6	GSM/GPRS	FTP 64 kb/s
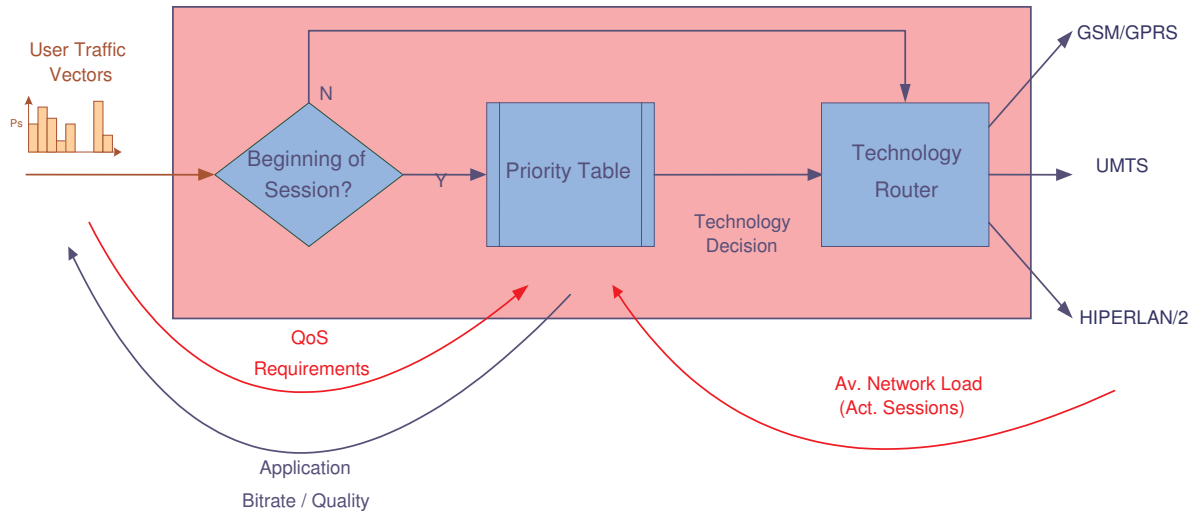
Figure 5.4: Convergence Manager Module (extracted from [Agui03]).

The UTVs are all processed by the CMM before being routed to the different ATTPMs. The CMM constantly monitors the incoming UTVs, performing the following process:

- If a request for beginning of session is detected, the CMM decides to which access technology the traffic must be routed (by the Technology Router - TR), and at what bitrate/quality must the application be delivered (interaction with the application source). The basis for these decisions are user-defined (simulator input) and are represented as a PT. A description of the PT functionalities is presented below. In a real system, all interactions between the CMM and other entities/network elements will have to be performed via new signalling protocols/channels.
- During a session (after CMM decisions) the traffic is constantly routed by the TR to the selected ATTPM and at the selected bitrate/quality.

The main input of the CMM is the instantaneous load of each access technology. For each new session, the CMM decision process takes into account the overall load (capacity occupation) of each access technology, based on the current active sessions, and verifies the existence of free capacity for the incoming session. This process respects the priorities defined in the PT, and tries to "fit" the new session into the most prioritised available possibility.

Simple capacity models were defined for each individual access technology, depending on the:

- number of TSs (GSM/GPRS),
- SF (related to the available number of codes) and DL LF[6] (UMTS),

---

[6] The UMTS power based load estimation is not considered due to the relatively small physical area of the simulated scenarios (Section 4.3), and therefore, in this case, the limiting load measurement is the DL LF.

- number of LCHs (HIPERLAN/2).

The traffic processing algorithms implemented in the ATTPMs for CS and PS applications work as follows:

- For CS applications, each ATTPM monitors the routed traffic from the CMM in order to detect new calls. If a new call is detected, the ATTPM verifies if there is enough capacity in the respective network (TSs for GSM/GPRS, SF and DL LF for UMTS) for its transmission. If there is enough capacity, the ATTPM reserves capacity in the network for the whole duration of the call. If there is not enough capacity, the call is blocked.
- For PS applications, a similar process to the CS case is applied, but on a packet basis rather than a session basis. After detecting an incoming session, the ATTPM checks for available capacity for each packet transmission. Capacity is reserved during each packet complete transmission or, if there is no available capacity, the packet is discarded.

The construction of a specific PT is influenced by the three components above identified and illustrated in Figure 5.5, *i.e.*, it contemplates radio access technology aspects (*e.g.*, available technologies with convergence capabilities), users preferences (*e.g.*, user defined applications, priority/quality requirements, costs issues), and applications' requirements (*e.g.*, maximum delay, bitrate).
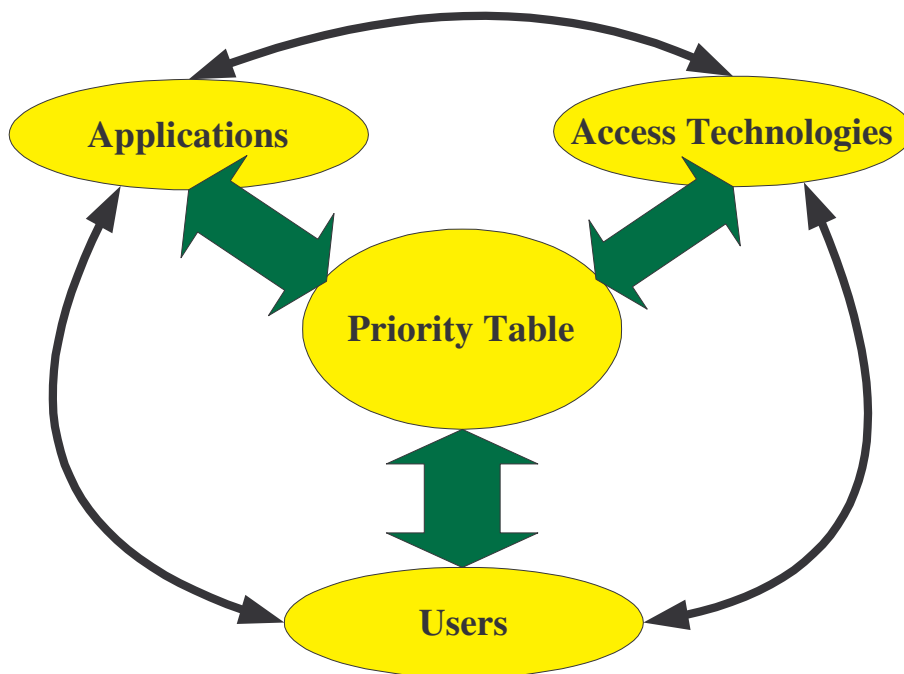
Figure 5.5: Traffic Components of a Convergence Scenario.

5.2   MIMO-enabled Systems Convergence Model

The key concept of this thesis is "MIMO-enabled convergence". Underlying the ideas of the introductory chapter, two different approaches to MIMO-enabled convergent systems can be found in [Burr04]: "MIMO system as enhanced single link" and "MIMO system for diverse spatial modes".

"MIMO system as enhanced single link" provides a single undifferentiated link between the transmitter and the receiver, Figure 5.6. The advantage of MIMO over SISO is that it improves the performance of the link in terms of throughput, reliability (when MIMO is considered in its broader sense, *i.e.*, MIMO with space-time coding and/or SIMO, MISO) or both by (dynamically) trading-off between them. In this approach, the spatial physical modes of a MIMO system are exploited within each standard. The MIMO version of each standard is represented as including a coder and/or demultiplexer that distributes the incoming data over the available modes either by demultiplexing them (to increase rate, as in spatial multiplexing) or encoding them (to increase diversity, as in space-time coding). These are then mapped in some form to the multiple antennas.
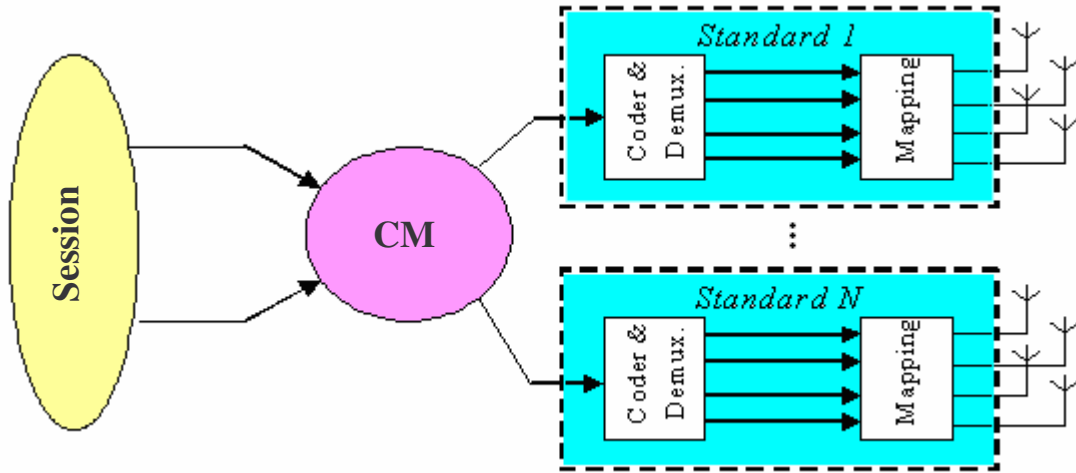
Figure 5.6: MIMO System as Enhanced Single Link (based on [Burr04]).

This approach may be used to match the performance of multiple standards used for the transmission of a single session. For example, a session consisting of two data streams, (*e.g.*, the speech and video signal of a video telephony session). These two streams must exhibit consonant quality in order to maintain overall QoS: the additional flexibility of the MIMO standard could reduce the outage probability of one standard to match the other. For another example, consider a single stream being transmitted over multiple standards, one after another, to extend the range of the communication. If one of these has rather lower bitrate, overall performance can be improved by using MIMO techniques to avoid buffering large amounts of data in one node of the communication.

"MIMO system for diverse spatial modes" considers all the MIMO spatial modes as being available to the multi-standard MIMO system and hence directly to the CM, either by arranging connections to each mode for each standard, Figure 5.7, or by mapping to the modes outside the standard, Figure 5.8. This approach allows the diversity modes available through MIMO within the standard to be combined with the multi-standard diversity, fully under the control of the CM. Moreover, the approach illustrated in Figure 5.8 may allow single antenna versions of the standards to be used, and applied in several different MIMO mappings. Both approaches significantly increase the diversity modes available to the CM.
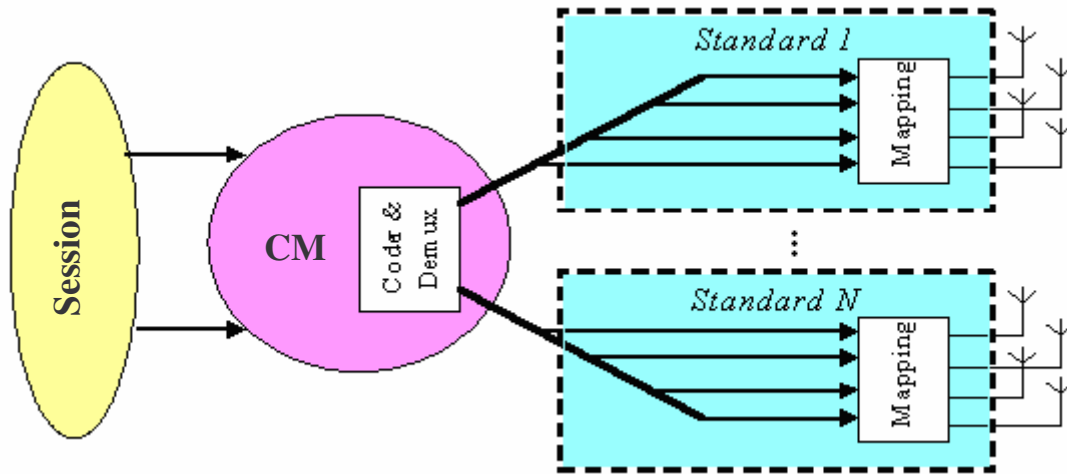
Figure 5.7: MIMO System for Diverse Spatial Modes: Multimode Standards (based on [Burr04]).
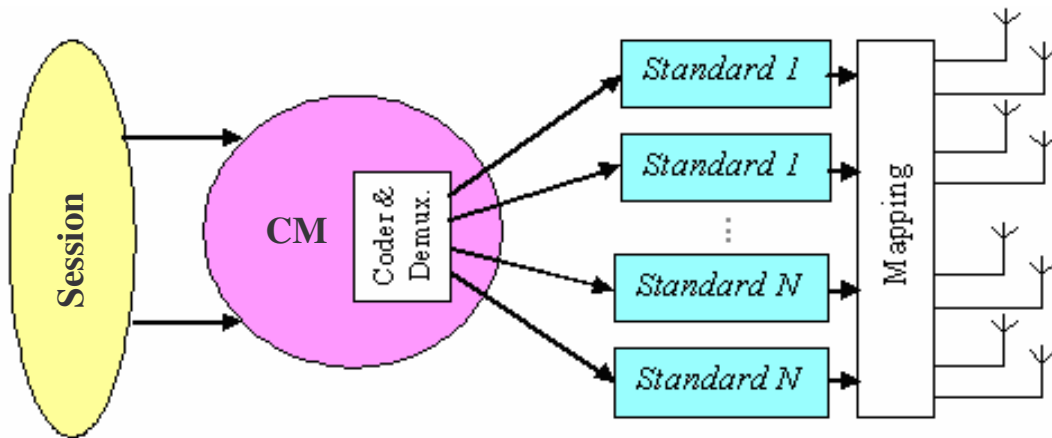
Figure 5.8 MIMO System for Diverse Spatial Modes: Mapping Outside Standards (based on [Burr04]).

In this thesis, the "MIMO system as enhanced single link" approach was taken due to its implementation simplicity. The MIMO versions of the ATTPMs were implemented assuming that the capacity enhancement provided by MIMO at link level (4.18) is the performance enhancement of the standard, as a whole, supplied with multiple antennas. This implies that the layers from the physical to the convergence one relay the gain of MIMO unchanged. However, it is expected that the extra signalling and coding that MIMO requires at the data link layer, etc., would decrease the gain provided by the channel itself. Furthermore, the

Physical, Data Link and the Network layers[7] of the ATTPMs are supposed to dynamically and perfectly adapt to the varying achievable bitrate of the MIMO channel, Figure 5.9.
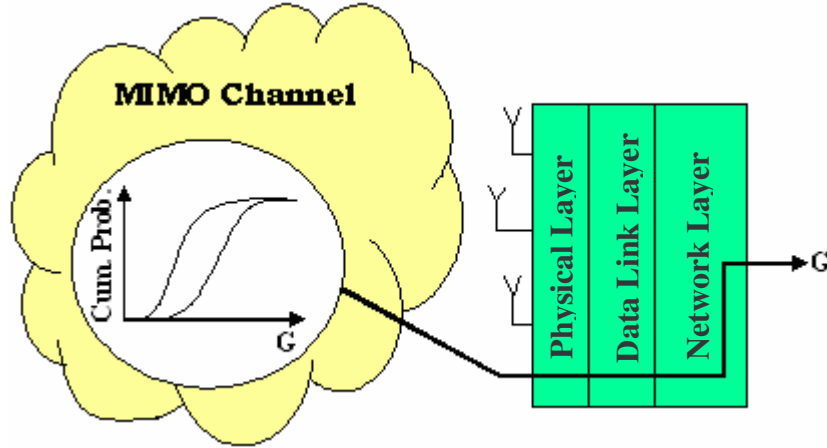
Figure 5.9: The MIMO Channel Capacity Gain is Relayed Unchanged by Each Layer.

The gain provided by simply increasing the capacity of the ATTPMs is two-fold: more sessions accepted for transmission (less are discarded or blocked) and more sessions routed through the most prioritised technology and quality/bitrate of the PT. Both contribute to improve the QoS (reduction of the call blocking rate and discarded packet rate) for the same number of users, or to increase the number of users that can be served with the same QoS. They also contribute for the increase of the bitrate as for the same time durations more sessions/calls are successfully transmitted.

Other approaches, not listed in [Burr04], would foresee changes in the traffic models of the UTGMs to include higher capacity demanding services and applications, which would maintain the number of served users and their perceived QoS, but improve the offer of the service provider.

MIMO was brought only to UMTS and HIPERLAN/2, Figure 5.10: GSM/GPRS is not likely to be supplied with multiple antennas, as it is not part of the future of mobile communications. The implemented capacity models in the traffic convergent simulator are based on DL LF and SF for UMTS, and on the number of LCHs for HIPERLAN/2.

The $\bar{\alpha}$ and $\bar{i}$ parameters of the DL LF (2.2) were set to 0.95 and 0.2, respectively, to meet the micro-cell scenario, instead of the originals of a macro-cell one (0.5 and 0.65, respectively). Therefore, $\eta_{T\text{-}DL}$ is now lower for the same bitrates and activity factors than in [Agui03], and a performance enhancement of UMTS is expected due the lower probability of reaching the maximum allowable value for $\eta_{T\text{-}DL}$.

---

[7] Layers from the OSI Model.
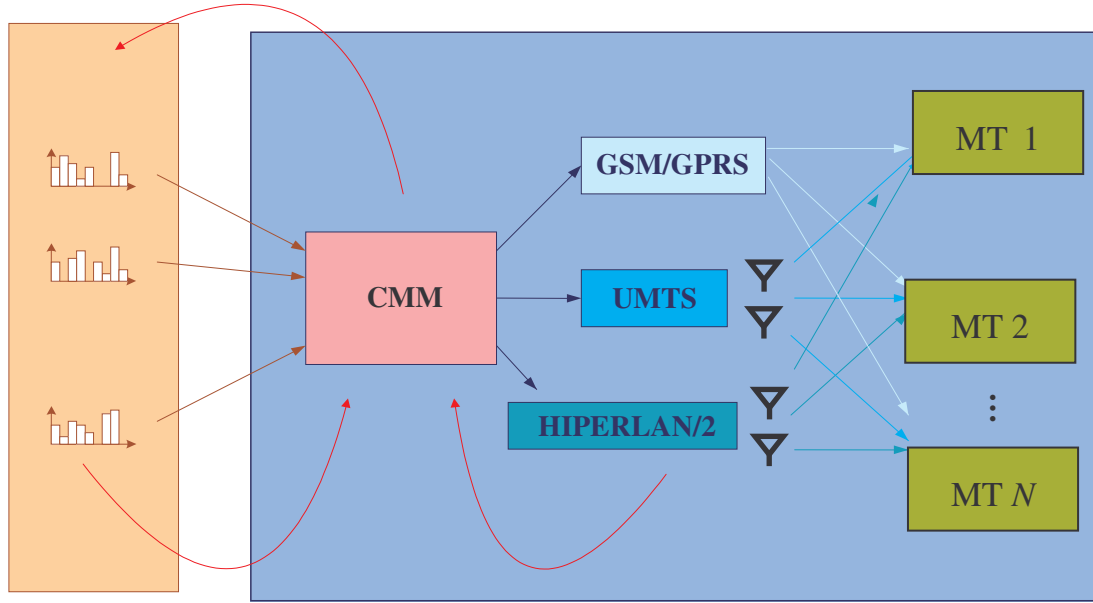
Figure 5.10: Simplified MIMO-Enabled TPE (based on [Agui03]).

For the particular case of $M'=N'=1$, the total number of available spreading codes or LCHs per MAC frame and AP for an $M \times N$ MIMO configuration $I_{M \times N}$ is, from (4.18):

$$I_{M \times N} = I_{1 \times 1} \cdot (G_{M \times N/1 \times 1} + 1) \tag{5.1}$$

where $I_{1 \times 1}=512$ for the spreading codes of UMTS, and 47 for the LCHs of HIPERLAN/2 [Agui03], and $G_{M \times N/1 \times 1}$ is calculated as explained in what follows.

The time variance of the SISO and MIMO channels randomises G (and consequently I) following the CDFs of Figure 4.10 and Figure 4.11. Therefore, $G_{M \times N/1 \times 1}$ is randomly picked from the CDF of UMTS or HIPERLAN/2 of these figures and kept constant during the time interval for which the channel can be regarded as static. The channel's coherence time, T_c (defined with a correlation coefficient ≥ 0.5) can be approximated by [Rapp01]:

$$T_c \approx \frac{9}{16 \pi f_{D\max}} \tag{5.2}$$

where

$$f_{D\max} = \frac{v}{\lambda} \tag{5.3}$$

is the maximum Doppler frequency, and $v=3$ km/h is the speed of the MT relatively to the scatterers (quasi-static channel assumed). This delivers the values of Table 5.4.

Table 5.4: Approximate Coherence Time of the Channel for UMTS and HIPERLAN/2.

	T_c (Approx.) [ms]
UMTS	32.4
HIPERLAN/2	19.9

Finally, the output parameters that were chosen to describe the gain of one MIMO configuration $M{\times}N$ over another $M'{\times}N'$, in terms of the convergence of wireless standards are the relative gains of:

- the mean bitrate, G_{R_b} :

$$G_{R_b} = \frac{R_b\big|_{M{\times}N} - R_b\big|_{M'{\times}N'}}{R_b\big|_{M'{\times}N'}}$$ (5.4)

- the discarded packets/frames rate, G_{η_D} :

$$G_{\eta_D} = \frac{\eta_D\big|_{M{\times}N} - \eta_D\big|_{M'{\times}N'}}{\eta_D\big|_{M'{\times}N'}}$$ (5.5)

- the call blocking rate, $G_{R_{CB}}$:

$$G_{R_{CB}} = \frac{R_{CB}\big|_{M{\times}N} - R_{CB}\big|_{M'{\times}N'}}{R_{CB}\big|_{M'{\times}N'}}$$ (5.6)

- the number of sessions routed through the 1st priority of access technology and quality/bitrate, $G_{\eta_{1PD}}$,

$$G_{\eta_{1PD}} = \frac{\eta_{1PD}\big|_{M{\times}N} - \eta_{1PD}\big|_{M'{\times}N'}}{\eta_{1PD}\big|_{M'{\times}N'}}$$ (5.7)

Only the successfully transmitted packets/frames contribute for the calculation of the mean bitrate. The definition of these parameters is similar to (4.18) so that a parallelism between the channel capacity increase and the increase of the performance of the convergent system can be established. In the next chapter, M, M', and N, N' will be given values and the respective results shown to provide a clear picture of the MIMO impact in a convergent system.

Since user traffic is statistically generated (call/session beginning instants, call/session durations, session volumes, packet sizes and inter-arrival times, etc.), it is necessary to analyse the statistical behaviour of the model to have an accurate idea of the number of simulation runs needed to obtain means of the performance indicators with reasonably low error margins.

This study was done in [Agui03], where means and error margins were calculated for 1, 10, and 100 simulation runs (each simulation run corresponding to 1 BH). As a general conclusion, it was considered that 10 simulation runs per convergence scenario provided a reasonable statistical behaviour, and therefore one can extrapolate from them error margins for results later obtained from a single simulation run. Nevertheless, an extra randomness was added to the process: the changing propagation environment. Every coherence time, the channel capacity changes and so do the radio access technologies' capacities. Therefore, the

total number of sessions and packets that each ATTPM can deal with becomes also a random variable. In fact, it would be necessary to redo the statistical analysis to assess if the same number of simulation runs were enough to obtain the error margins below 10 % as in [Agui03]. However, due to the very long simulations needed, the conclusion in [Agui03] was partially extended to the new situation. In this thesis, 10 simulation runs were always done (and not only to extrapolate error margins) per access technology and user scenario. This increases significantly the processing times, but ensures that the error margins of the means presented in Chapter 6 are kept as low as possible within the thesis timeframe.

To assess the dispersion of the performance indicators relatively to their means obtained with 10 simulation runs, Table 5.5 and Table 5.6 show the standard deviation per user and access technology scenario, respectively, when a 2×2 MIMO configuration is used.

Table 5.5: Standard Deviations per Performance Indicator and User Scenario.

	Number of Users									
	500	**600**	**700**	**800**	**900**	**1 000**	**1 100**	**1 200**	**1 300**	**1 400**
G_{R_b} [%]	1.08	0.67	1.01	1.23	1.87	1.36	2.22	3.25	3.26	4.83
G_{η_D} [%]	1.44	0.26	5.17	7.08	5.10	45.17	58.88	59.88	52.90	72.85
$G_{R_{CB}}$ [%]	0	0	0	0	0	0	0	0	56.88	56.30
$G_{\eta_{LPD}}$ [%]	0.09	0.23	0.48	0.42	0.77	1.00	0.98	1.76	1.13	1.94

The higher the number of users, the higher the standard deviation, *i.e.*, the higher the dispersion of the values of each BHCA relatively to their means. The number of randomly generated applications is directly proportional to the number of users demanding for data; consequently, as the cell becomes more crowded, more randomness is added to the whole process and higher statistical variations are more likely. In fact, for some indicators, when the number of users is high the standard deviation is very significant. This does not necessarily mean that the averages illustrated in Chapter 6 are inaccurate; it means that, in order to achieve the same accuracy in all user scenarios, more simulation runs should be carried out in the scenarios with larger number of users.

Table 5.6: Standard Deviations per Performance Indicator and Access Technology Scenario.

	Access Technology Scenarios						
	G	**U**	**H**	**G+U**	**G+H**	**U+H**	**G+U+H**
G_{R_b} [%]	0	8.52	4.09	22.34	3.64	1.37	1.32
G_{η_D} [%]	0	0	61.14	0	63.55	0	0
$G_{R_{CB}}$ [%]	11.64	51.00	0	155.92	75.71	0	0
$G_{\eta_{LPD}}$ [%]	0	0	1.67	41.81	1.76	1.62	1.05

The standard deviations per access technology scenario do not present a increasing or decreasing trend, they are generally higher when the performance indicators are high, as it will be later seen in Chapter 6.

As mentioned before, high standard deviations indicate that many BHCAs should be simulated and averaged out to obtain accurate means, but they do not inform if the ones performed are enough, *i.e*., if more simulation runs would change the means. Knowing in advance that the MIMO relative gain is, on average, positive, negative values of the relative gains of the performance indicators would reveal lack of statistical averaging. These are seldom depicted, mainly for low values of the indicators of the SISO performance, since low-valued denominators in (5.4)–(5.7) can boost the (possibly negative) relative gains. However, it is shown in Chapter 6 that they hardly ever reach 7 % for the user scenarios and 10 % for the access technology scenarios. It has been observed that, as more and more BHCAs were included in the average, the negative values tended to vanish.

The simulation of 10 BHCAs, one per user scenario, with the three technologies available, lasts approximately 23 hours on a personal computer equipped with an Intel PIV® processor at 3 GHz and 512 MB of RAM memory. On the other hand, the simulation of 7 BHCAs, one per technology scenario, with 1 000 users, lasts approximately 10 hours with the same equipment. Therefore, with the above statistics, figures from Figure 6.1 to Figure 6.7 last 460 hours (23h×20, as 10 simulation runs for SISO and 10 for MIMO were needed), which is more than 19 days each, and figures from Figure 6.8 to Figure 6.14 last 200 hours (10h×20), which is more than 8 days each.

6

Analysis of Results

The performance of a MIMO-enabled traffic convergent system in relation to its SISO version is analysed in this chapter. The simulated scenarios are parameterised in Section 6.1. Two general approaches were considered in order to realise the MIMO gain: a fixed set of access techniques serving a varying number of users, Section 6.2, and a fixed number of users benefiting from different sets of available access technologies, Section 6.3. In addition, the MIMO gain per application and for two different antenna array sizes is shown.

6.1 Scenarios Description

A *convergence scenario* is defined in this thesis as a particular combination of propagation and traffic characteristics.

The propagation characteristics of any convergence scenario considered here are the ones in Table 4.5 for UMTS and HIPERLAN/2. The basis for the overall network configuration is therefore a "public street" type scenario, assuming collocated BSs (*e.g.*, in one of the ends of the street), one per access technology. As mentioned in the previous chapter, the way that MIMO was implemented in the traffic simulator was by assigning an extra capacity to the ATTPMs of UMTS and HIPERLAN/2, Figure 5.10. The CMM and the UTGMs are not aware of the presence of any capacity enhancement technology at propagation level. This strategy corresponds to a particular approach to the problem of studying the propagation and traffic aspects of a mobile communication system as a whole and not as two independent subjects.

Two MIMO configurations (antenna array sizes) were chosen to illustrate the results, Table 6.1. *Configuration 1* provides the lowest gain, while *Configuration 2* is more optimistic, realistic for PDAs or portable computers, Section 4.3. Besides, the larger number of antennas at the transmitter exploits the fact that larger antenna arrays can be collocated at the BS than the ones that can be integrated into an MT.

Table 6.1: MIMO Configurations for UMTS and HIPERLAN/2.

	UMTS ($M{\times}N$)	HIPERLAN/2 ($M{\times}N$)
Configuration 1	2×2	2×2
Configuration 2	2×8	4×16

As mentioned before, three different access technologies were considered in the development of the simulation platform: GSM/GPRS, UMTS and HIPERLAN/2. Table 6.2 contains the parameters for these three radio access technologies.

For the GSM/GPRS system (which is not supplied with MIMO), 30 TSs were considered available for user traffic (in a similar configuration as presented in Chapter 2 for a medium-capacity cell with four Tx frequencies, with 2 TSs reserved for signalling and control). For data applications via GPRS, a maximum user bitrate of 67 kb/s is adopted, corresponding to an allocation of 5 TSs with CS-2 (on average). A free TS allocation scheme between CS and PS applications was considered, although assuming higher priority for the CS traffic.

Table 6.2: Parameterisation of Each Radio Access Technology.

Access Technology	Parameter	Value
GSM/GPRS	No. BSs	1
	No. Tx Frequencies per BS	4
	No. TSs for User Traffic per BS	30 (Remaining 2 TSs Used for Signalling and Control)
	TS Allocation Scheme	Free (All TSs Usable for Voice and data Application)
	GPRS Average Coding Scheme	CS-2 (13.4 kb/s Throughput per TS)
	Maximum No. of TSs per MT	5 (Maximum Supported Bitrate per MT: 5×13.4 kb/s = 67 kb/s)
UMTS	No. BSs	1
	No. Carriers per BS	1 (5 MHz Bandwidth)
	Duplex Mode	FDD
	Target DL E_b/N_0 Values per Application	See Table 6.3
	Power Control	Ideal
	% Pseudo-Random Codes	$I_{M \times N}$ (5.1)
	% Codes Reserved for Soft Handover	30 %
	Activity Factor	0.55 for Voice and 1.0 for Data Applications
	Ratio Inter- to Intra-cell Interference	0.2 (Micro-cell)
	Orthogonality Factor	0.95 (Micro-cell)
	Downlink Load Factor	Max. Allowed Value: 0.7
	Channel Coding Rates	1/2 Rate for Voice Applications and 1/3 Rate for Data Applications
	Code Allocation Scheme	Ideal/Optimised Allocation
HL/2	No. APs	1
	Average PHY Mode	PHY Mode 3
	No. LCHs per 2 ms MAC Frame per AP	$I_{M \times N}$ (5.1)

Regarding UMTS, a single 5 MHz bandwidth carrier was considered available at the BS for the DL. The target E_b/N_0 values per application used in the simulations are the ones presented in Table 6.3. These values were obtained from [FCXV03] for the particular case of a 3 km/h mobility scenario. The maximum allowed value for the DL LF was set to 0.7, a 1/2 rate channel coding rate was considered for voice, and a 1/3 rate for video and data applications. The values for these parameters and for the remaining ones, listed in Table 6.3 for UMTS, were selected from the common value presented in literature (*e.g.*, [HoTo01]).

Table 6.3: Target DL E_b/N_0 Values Adopted for the UMTS ATTPM.

Application		DL Target E_b/N_0 [dB]
Voice Call		7.5
Video Call (Video Component)		5.7
Video-on-Demand (Video Component)		5.6
Data Applications (Web Browsing, Email and FTP)	**8 kb/s**	5.7
	32 kb/s	5.7
	64 kb/s	5.6
	144 kb/s	5.3
	384 kb/s	3.8

For HIPERLAN/2, PHY Mode 3 was selected. A total of 47 LCHs for the baseline SISO case were considered available per MAC frame (2 ms) for user traffic, providing an overall throughput (DL + UL) of approximately 9 Mb/s at the AP. These values are based on the throughput calculations and simulation results presented in [KrSa01].

The traffic characteristics are gathered into three types of traffic scenarios:
- the access technology scenario, which defines the set of radio access techniques available to users, and their specific parameterisation,
- the user scenario, which defines the number of active users, and their user type penetration (market segmentation),
- the application scenario, which defines the active applications for all users, and their traffic characteristics per user type.

Seven different access technology scenarios were considered in the present chapter for simulation purposes. These scenarios correspond to all possible combinations of available access technologies, as listed in Table 6.4.

Table 6.4: Radio Access Technology Scenarios.

Access Technology Scenario	Available Access Technologies		
	GSM/GPRS	**UMTS**	**HIPERLAN/2**
G	✓		
U		✓	
H			✓
G+U	✓	✓	
G+H	✓		✓
U+H		✓	✓
G+U+H	✓	✓	✓

Ten different user scenarios are considered, corresponding to different number of users/MTs, ranging from 500 to 1 400 users in steps of 100 users, Table 6.5. These user scenarios will enable to evaluate the impact of the variation of the number of users for different access technology and applications scenarios. For a lower number of users (*e.g.*, from 100 to 500) the access technologies provided with SISO already achieve the highest performances (negligible number of blocked calls, discarded packets, etc.), not profiting from the use of MIMO.

Table 6.5: User Scenarios.

User Scenario	1	2	3	4	5	6	7	8	9	10
No. of Users	500	600	700	800	900	1 000	1 100	1 200	1 300	1 400

For all considered user scenarios, fixed user type penetration values were adopted, as presented in Table 6.6. These user types allow for a more realistic representation of different market segments with different applications requirements and usage profiles.

Table 6.6: User Type Penetration Values.

	User Type 1	**User Type 2**	**User Type 3**
Penetration [%]	25	40	35

A fixed application scenario, with all six implemented applications activated, was considered throughout all the simulations, Table 6.7. Although the IST-FLOWS [FLOW03] and IST-MOMENTUM [MOME04] projects address the issue, the precise values that were adopted for the BHCAs and average call/session durations, were arbitrated (with reasonable values),

since rather scarce literature exists on user traffic profiles for next generation networks and applications.

Different BHCA values (providing the average number of CS call attempts/PS sessions per application during the BH) were considered for each user type. Users of type 1 are the most traffic demanding, representing a market segment such as business users, while users of type 3 are the least traffic demanding, representing, *e.g.*, a mass market segment. The user type 2 traffic demands represent an intermediate market segment, in which users, for example, use their MTs for both personal and professional communications, but with lower overall demand than users of type 1.

Table 6.7: Applications Scenario Characterisation.

Application	BHCA [Calls or Sessions/h]			Average Call/Session Duration [s]
	User Type 1	User Type 2	User Type 3	
Voice Call	0.5	0.3	0.1	120
Video Call	0.4	0.2	0.1	120
Video-on-Demand	0.3	0.3	0.3	120
Web Browsing	0.4	0.3	0.2	Given by Traffic Source Models
Email	0.3	0.2	0.1	
FTP	0.2	0.1	0.05	

For the Voice Call, Video Call and Video-on-Demand applications, average session durations of 120 s were considered for all three user types. For the remaining applications, the session duration is provided by the TSMs in function of the session volumes (randomly generated according to the respective TSMs [AgCo04]).

As mentioned in the previous chapter, the overall convergence strategy is defined by means of a PT implemented in the CMM. A fixed PT was considered in the current simulation platform, Table 5.3. For each application, the PT defines the priorities to select an access technology and an application bitrate/quality (given by the TSM column). If the system's load is such that there is no capacity for a new incoming session in all technology priorities defined in the PT, the session is routed to the highest priority technology (that is available) and selects the lowest application quality/bitrate. One may think that this default choice always leads to blocked calls or discarded packets, because it has been previously verified that all the alternatives were unable to accommodate the new session. However, this may not be true, because the loads of the ATTPMs are calculated as the sum of mean capacity occupations of the active sessions and not based on real instantaneous ones. Therefore, even if the *mean*

capacity occupation of the incoming session is larger than the difference between the maximum load the ATTPM can support and the sum of the *mean* capacity occupations of the active sessions, there might still be *real* available capacity in the ATTPM to accept the *real* capacity occupation of the new session.

6.2 User Scenarios Variation

6.2.1 General Considerations

In this section, the impact of the use of MIMO on a context of traffic convergence is analysed for each user scenario of Table 6.5, under the access technology scenario G+U+H. Although all performance indicators are completely interrelated in a converged system, this analysis considers the CS applications performance indicator (call blocking rate) and the PS applications performance indicators (discarded packet/frame rate and mean bitrate) separately. It has been observed that for a number of users below 500, the gain of MIMO was negligible as the SISO version of the convergent system already achieved nearly optimum performances. In fact, even for more than 500 users, some applications still have optimum performances in the SISO case, in which cases the relative gains are null (bars not visible in the plots). For each user scenario, the UTVs are all regenerated. This type of analysis is useful to obtain the number of users supported with a given QoS under a specific technology scenario.

This section comprises two more subsections to show the impact of Configurations 1 and 2 of Table 6.1. In Subsection 6.2.2, the MIMO Configuration 1 relatively to SISO will be studied; in Subsection 6.2.3, the focus is shifted to the gain of MIMO Configuration 2 relatively to Configuration 1. In this way, one cannot only clearly see the performance increase of MIMO over SISO, but also of Configuration 2 over 1. Symbolically, the relative gains defined in (5.4) − (5.7) have, in Subsection 6.2.2, $M{\times}N{=}2{\times}2$, and $M'{\times}N'{=}1{\times}1$; in Subsection 6.2.3, $M{\times}N{=}\{2{\times}8,\ 4{\times}16\}$, and $M'{\times}N'{=}2{\times}2$.

The graphical plots begin by the PS applications performances, followed by the CS ones, and finish with the 1st priority decisions indicator, which concerns both PS and CS applications. The values obtained for some indicators, namely the mean bitrate and the number of sessions routed through their most prioritised option, follow monotonic trends that were mathematically characterised by second-order polynomial functions.

In order to fully characterise the impact of MIMO, the performances of the SISO, MIMO Configuration 1, and MIMO Configuration 2 versions of the simulator are shown on top of the relative gains. The aim is to provide approximate values of the absolute performances,

since the relative ones can easily lead to misconceptions. For example, $G_{M/S}$ =100% indicates that MIMO performs optimally while SISO did not, but the real gain of MIMO depends on how close to the optimum values the SISO performance was. The absolute values are shown as continuous functions when there is a numerical scale in the X-axis (user scenarios variation), and as discontinuous ones when each value of the X-axis represents a different system (access technology scenarios variation).

6.2.2 Performance Enhancement with Configuration 1

Figure 6.1 illustrates the MIMO relative gains of the mean bitrate G_{Rb} per user scenario and per PS application. Even though the MIMO gain does not depend on the number of users, an increase of G_{Rb} is observed due the fact that the SISO version of the traffic simulator almost reached the maximum bitrates of the traffic models in the scenarios with lower number of users. Consequently, as the number of users increases and the SISO bitrates decrease relatively to their maxima, MIMO progressively enlarges its contribution. The envelopes of the WWW and video-on-demand mean bitrates for MIMO and SISO confirm the increasing gain of MIMO over SISO as they become more and more separated.

A clear difference between the video-on-demand and WWW relatively to the other applications is observed due to way the PT is defined. The video-on-demand (the one with the largest gain) is never routed through GSM/GPRS and therefore always benefits from a MIMO capacity enhancement. Similarly, the WWW application is rarely supported by the GSM/GPRS as this ATTPM occupies the 9th, 10th, and 11th positions in the ranking of the possible options in the PT. The bars depict a stabilisation of the bitrate for the largest numbers of users (roughly around 1 400 for WWW and video-on-demand and 1 100 for the other applications). This indicates that, for this cell-crowd levels onwards, MIMO can be fully exploited, presenting a bitrate relative gain of about 25-30 % for video-on-demand and WWW and around 5 % for the other applications. Some negative values are found when MIMO contribution is likely to be small (500-800 users) due to the statistical nature of the simulator. However, it has been observed that, as more and more BHCAs were average out, the negative values tend to vanish.

The monotonic trend of WWW and video-on-demand are *well approximated*[8] by the following second-order polynomial function:

$$G_{R_b} = 0.18p^2 + 1.46p - 2.1 \tag{6.1}$$

---

[8] By *well approximated*, it is meant that higher order polynomial functions do not reduce the mean square error of the estimated trend relatively to the actual data, but lower order polynomials do.

where $p \in [1,10]$, $p=1$ is the user scenario with 500 users, $p=2$ is the one with 600, $p=3$ the one with 700, and so on.

The scale of the envelopes is shown in the Y-axis along the right edge of the figure, while the scale of the bars is shown in the Y-axis along the left edge one. To avoid over-crowded figures, this was explicit with arrows only in Figure 6.1.

Figure 6.2 illustrates the relative gains of the discarded packets/frames rate $G_{\eta D}$ per user scenario and PS application. The envelopes show that the MIMO gain can be well exploited for the majority of user scenarios, *i.e.*, that SISO has sufficient discarded packets/frames that allows achieving almost full profit from MIMO. One can see that MIMO discards packets for practically all scenarios, therefore not being specially limited by the superior performance of SISO. However, a shy decreasing trend is observed because MIMO discards few packets in the scenario with lower number of users (500 and 600), boosting the relative gains to 100 %. The statistical nature of the simulator is well expressed by random fluctuations of the gains. This was already expressed in Table 5.5, as this parameter presented the larger standard deviations among the four parameters. This means that, to achieve a smooth behaviour, more BHCAs should be simulated and averaged out. The use of multiple antennas can in general reduce the number of the discarded packets/frames in more than 50 % and can be up to 100 % for some applications and user scenarios. The voice and video calls are only blocked in SISO for 1 300 users onwards.
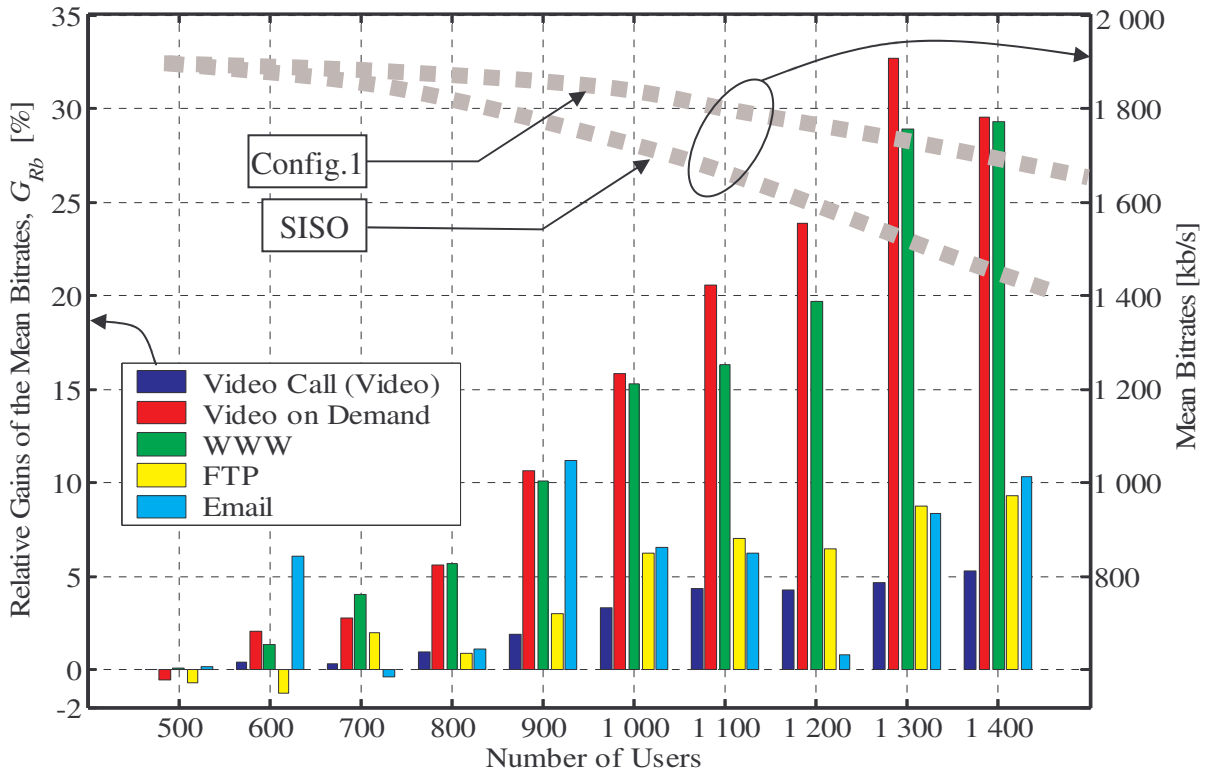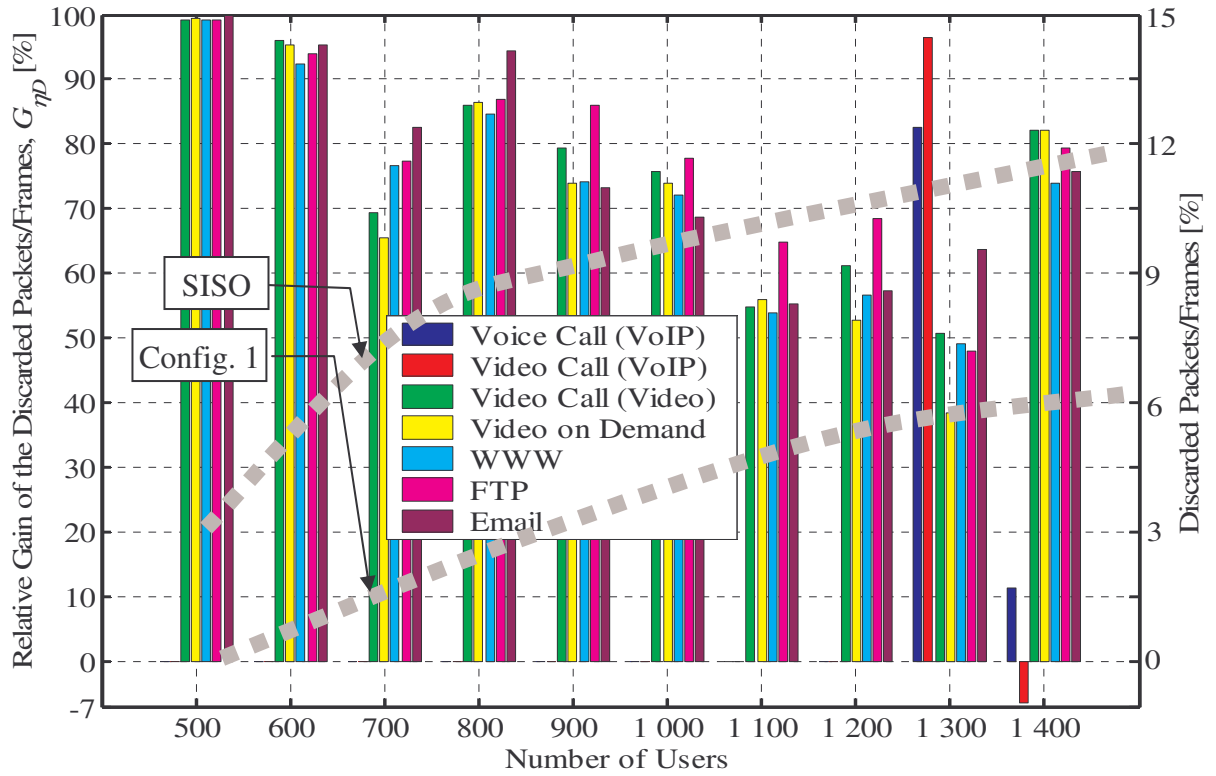

Figure 6.1: Relative Gain of the Mean Bitrate versus User Scenario with Configuration 1 (G+U+H).

Figure 6.2: Relative Gains of the Discarded Packets/Frames versus User Scenario with Configuration 1 (G+U+H).

Figure 6.3 illustrates the relative gains of the call blocking rate G_{RCB} per user scenario and CS application. The figure shows that, in the SISO case, there are blocked voice and video calls only for a number of users equal and larger than 1 100 and 1 300, respectively (until then, G_{RCB}=0 %). It also shows that, when MIMO is used, blocked calls are only found when 1 300 or more users are active in the system (for 1 100 and 1 200 users, G_{RCB}=100 %). Even though the bars do not point to a stabilisation of the gain, the fact that the envelopes are approximately parallel when many users are active is an evidence of its stabilisation for large cell-crowd levels.

Figure 6.4 illustrates the relative gains of the number of sessions routed to the 1st priority of access technology $G_{\eta lPD\text{-}T}$ and bitrate/quality $G_{\eta lPD\text{-}B}$ per user scenario (for all applications). The priorities are defined in the PT concerning both the access technologies and bitrates/ qualities. The first observation is the monotonic increase of $G_{\eta lPD\text{-}B}$: as the number of users increases, the number of sessions routed through the more prioritised bitrate/quality option of the original SISO version of the simulator decreases. This is obvious since the access technologies become more loaded and can support less capacity demanding services. Therefore, MIMO can contribute more as the system with SISO progressively moves away from the optimum performance.

Similarly to the mean bitrate indicator, the monotonic behaviour of the $G_{\eta IPD\text{-}B}$ is accurately approximated by a second-order polynomial function with large aperture, *i.e.*, with a low second-order variable coefficient:

$$G_{\eta IPD\text{-}B} = 0.14p^2 + 1.95p - 2.98 \tag{6.2}$$

where *p* is mapped to the user scenarios as in (6.1).

It is expected that, for a certain number of users (larger than 1 400), the $G_{\eta IPD\text{-}B}$ stabilises in a value that would represent the full MIMO gain (probably above 30 % as shown in the plot). In fact, a shy stabilisation can already be depicted by the envelopes, as they seem to maintain their separation for 1 400 users and onwards.

A similar behaviour is observed for $G_{\eta IPD-T}$ until 1 100 users, but with lower values (up to nearly 4 %). In the SISO case, the probability of one session to be routed through its 1st priority in terms of access technology is higher that the one in terms of bitrate/quality because, for the majority of the applications, more than one bitrate/quality is defined for each technology. Therefore, a small gap between the simulated $G_{\eta IPD-T}$ and the optimum performance is left by SISO. As it has become clear, larger relative gains are generally obtained when SISO performs worse, which in these case leads to higher values of $G_{\eta IPD-B}$ than the ones of $G_{\eta IPD-T}$.

From 1 100 users onwards, the effect of the default option of the PT is unburied. For such crowd levels, the increasing probability of one session not be allocated in any option of Table **5.3** triggers the default option of routing it to its 1st technology priority with the lowest bitrate/quality. The consequence, for both SISO and MIMO, is a coarse stabilisation of the number of sessions routed through their 1st priority of technologies, instead of a constant negative slope. The difference between MIMO and SISO is that this stabilisation occurs for different number of users (obviously larger for MIMO) as the envelopes denounce. Hence, the behaviour of the MIMO gain depends on the user scenarios. For a number of users below 500, $G_{\eta IPD-T} = 0$ (SISO performance is optimum), for a number of users between 500 and 1 100, $G_{\eta IPD-T}$ increases up to 4 % (SISO performance is decreasing while the MIMO one is still optimum), and for a number of users above 1 100, $G_{\eta IPD-T}$ decreases (SISO performance has stabilised while the MIMO one begins to decrease). This explains the bell-shaped curve of $G_{\eta IPD-T}$ in Figure 6.4.

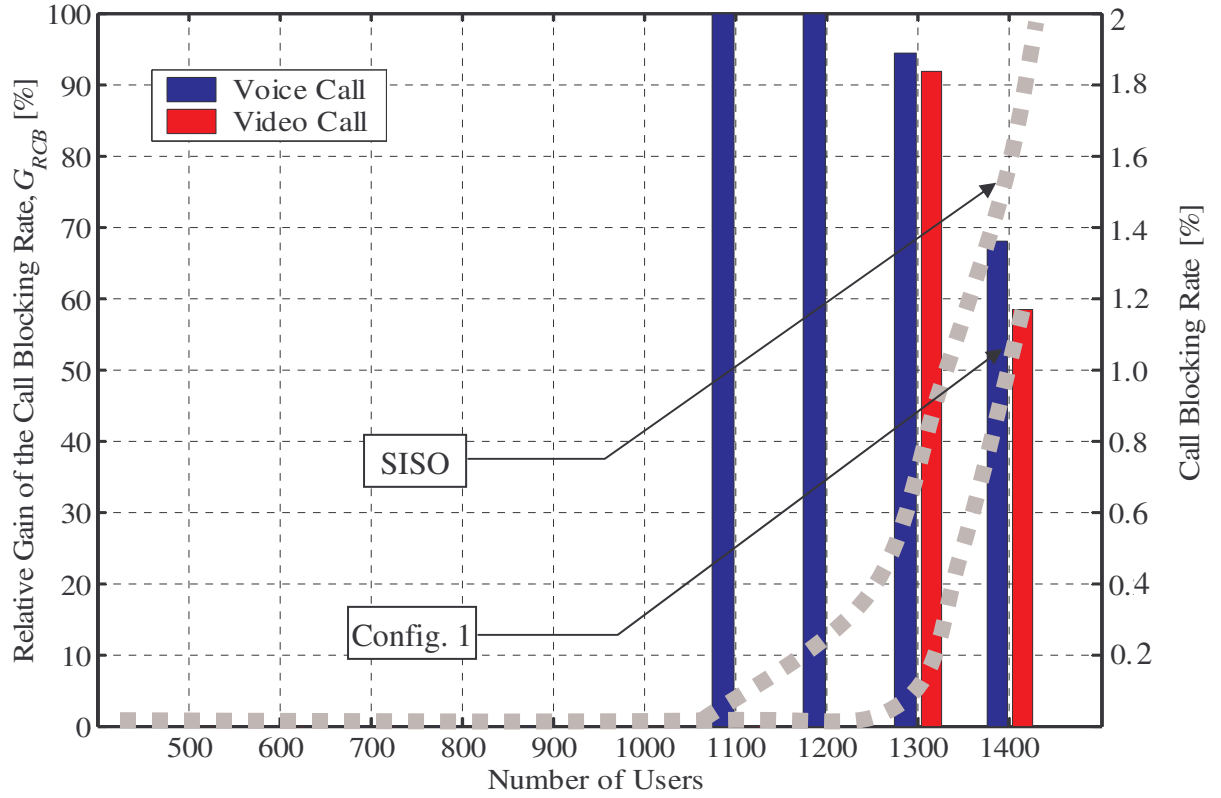For larger number of users than 1 400, however, the MIMO curve is likely to stabilise, naturally above the SISO one.

Figure 6.3: Relative Gains of the Call Blocking Rate versus User Scenario with Configuration 1 (G+U+H).
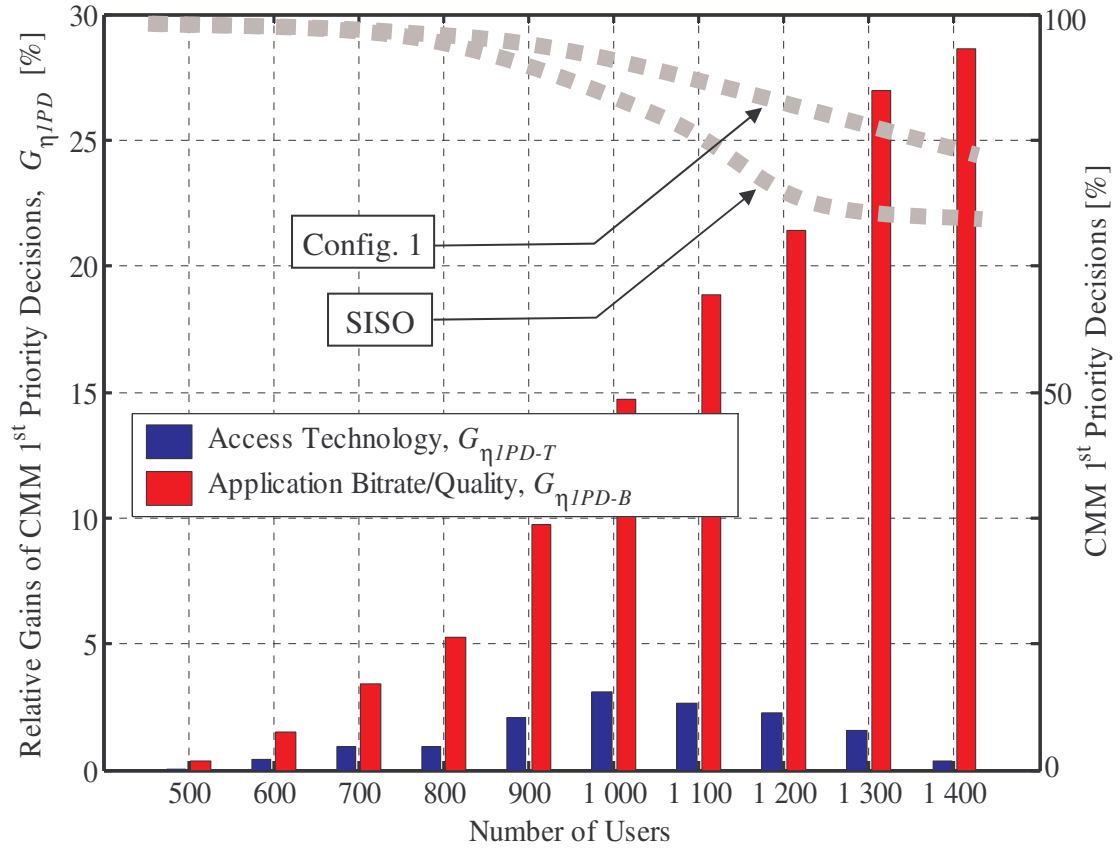

Figure 6.4: Relative Gains of the CMM 1st Priority Decisions versus User Scenario with Configuration 1 (G+U+H).

6.2.3 Performance Enhancement with Configuration 2

The more optimistic situation of Configuration 2 has a greater impact on the QoS of the convergent system. The transitory effects of MIMO before reaching its total gain are now longer, *i.e.*, more users would have to be put in the system for the gain to stabilise than in Configuration 1. This happens because MIMO capacity is now larger so SISO performance has to decrease more to realise the full MIMO gain. As mentioned before, this subsection shows the gain of going from Configuration 1 to 2. This analysis is useful to realise that, even though both configurations are limited by the superior SISO performance, the number of antennas dictates how well this limitation is exploited.

Figure 6.5 shows how much the mean bitrates, achieved with Configuration 2, go beyond those of Configuration 1. The increasing gap between the SISO and the optimum performances (caused by the increasing number of users) is exploited by Configuration 2 up to 15 % better than by Configuration 1 (WWW with 1 400 users). Its constant increase indicates that, unlike Configuration 1, user scenario no. 10 (1 400 users) does not represent the approximate maximum MIMO gain anymore, as it is not visible a stabilisation of the curve. In fact, the envelope of the two applications with higher gains can be approximated by:

$$G_{R_b} = 0.21p^2 - 0.79p + 0.75$$

(6.3)

The fact that the video call and WWW perform better than the other applications is due to the same reasons as in Configuration 1, and amplifies their difference seen in Figure 6.1.

The relative gains of the discarded packets/frames for Configuration 2 is always nearly 100 % relatively to Configuration 1, so the corresponding figure is not shown. This means that even for the maximum number of users considered, Configuration 2 hardly discards any packets/frames. Regarding the blocking rate of the CS sessions, the comparison of Figure 6.6 with Figure 6.3, tells that Configuration 2 increases its gain as the one of Configuration 1 decreases. The high gains obtained in Figure 6.6, indicate that practically no sessions are blocked with Configuration 2.

Finally, the percentage of sessions routed to the most prioritised option of the PT with Configuration 2 that were routed to other options with Configuration 1 is shown in Figure 6.7. The monotonic increase indicates a phenomenon similar to the ones of the bitrates of Figure 6.5: as SISO leaves "space" for MIMO to provide gain, Configuration 2 exploits it better. Again, this proves that even if the MIMO gain is limited to some extent by the good performance of SISO, the number of antennas has an important role in the system capacity.

It can be generally concluded that, for the user scenarios considered, the greatest gain comes from the use of a simple 2×2 rather than larger configurations. This is because the SISO

version of the system had good performances, and therefore nearly optimum performances are obtained with a 2×2 array size.
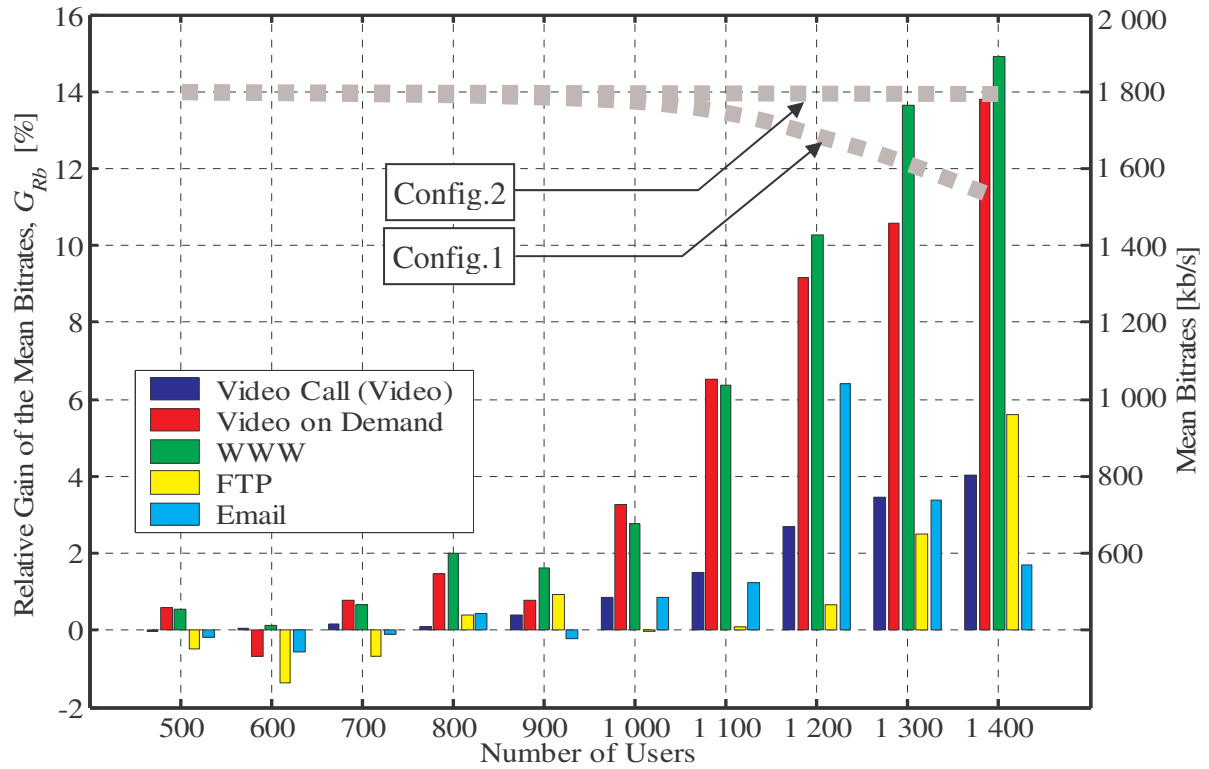

Figure 6.5: Gain of the Mean Bitrates with Configuration 2 Relatively to 1 versus User Scenario (G+U+H).
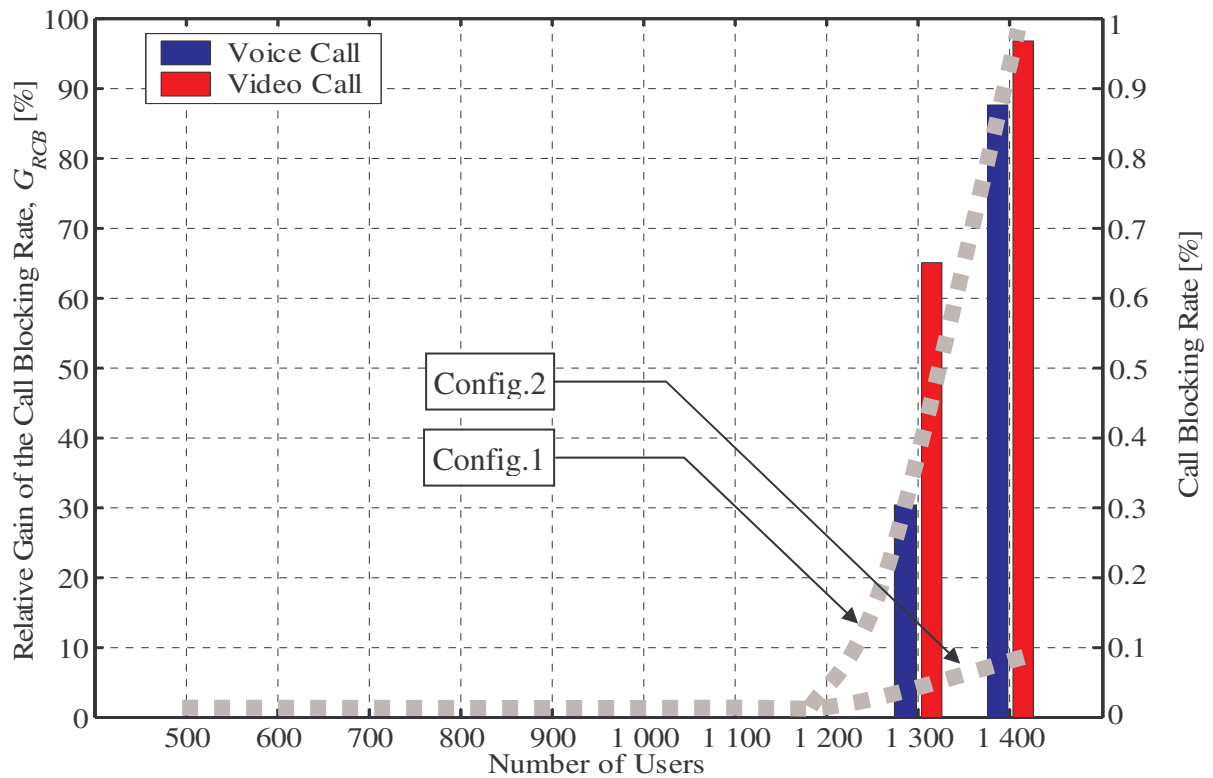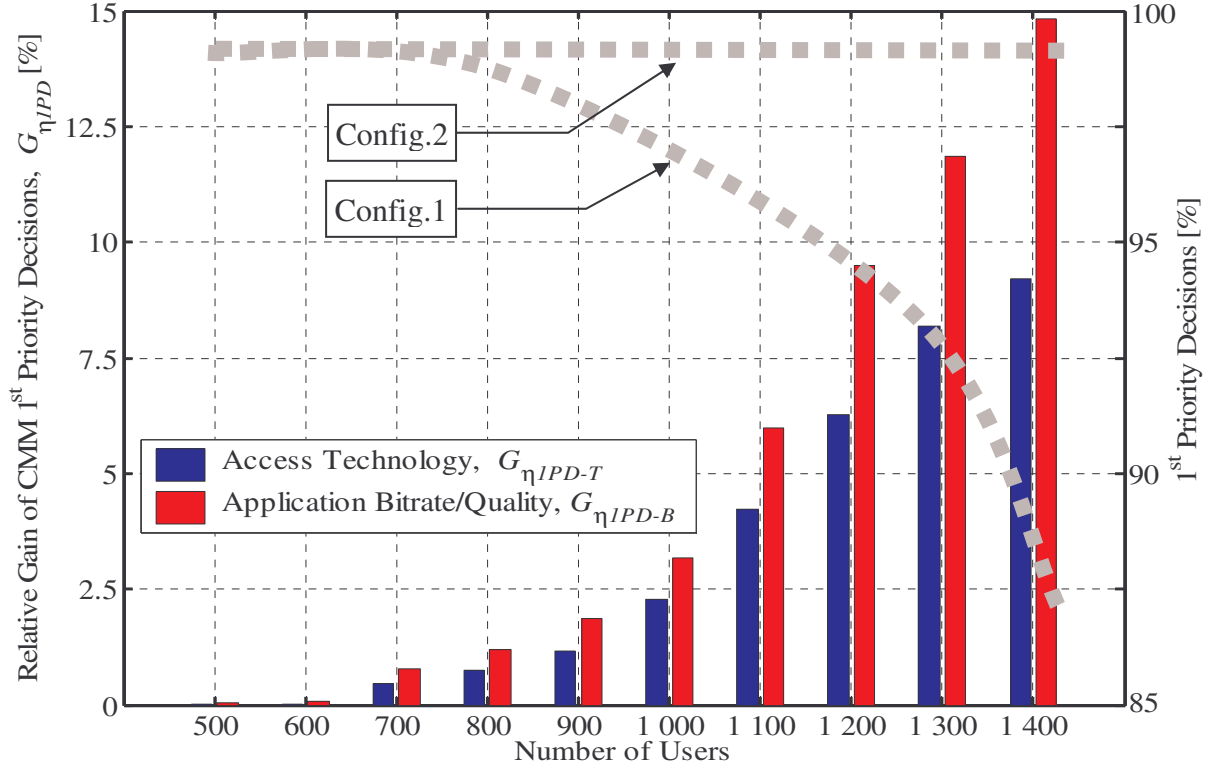

Figure 6.6: Gain of the Call Blocking Rate with Configuration 2 Relatively to 1 versus User Scenario (G+U+H).

Figure 6.7: Gain of the CMM 1st Priority Decisions with Configuration 2 Relatively 1 versus User Scenario (G+U+H).

This later figure shows an ever-increasing trend given by:

$$G_{\eta_{IPD}} = 0.23p^2 - 0.89p + 0.91$$

(6.4)

Some remarks should now be done to relate the MIMO capacity increase at propagation level seen in Figure 4.10 with the one at system level, seen in the previous figures. Figure 4.10 tells that in 50 % of the time, a 2×2 MIMO configuration provides a channel capacity gain relatively to SISO of about 54 %. However, Figures 6.1 and 6.4 depict maximum gains of about 30 % for 1 400 users. Considering that the stabilisation tendencies perceived for that number of users prevent the gains to increase much more, there is a loss of about 20 % of the MIMO gain at propagation level. The variety of applications with different time constraints and bandwidth demands, the random generation of CS and PS sessions (in number of packets/frames, their length, volume, etc.) along with the mismatching randomness of the traffic generation and capacity of the channel, makes it impossible to fully exploit the channel. One should note that this is true even with the assumption of the ATTPMs adapting their capacity models perfectly and dynamically to the channel, Figure 5.9.

The difference between the potential of the MIMO channel and its realisation on the traffic is however much more significant for larger antenna configurations. Going from Configuration 1 to 2 increases the channel capacity in approximately 700 % during 50 % of the time, Figure 4.10. Nevertheless, no more than 15 % of gain can be obtained in the mean

bitrate and sessions that are routed to their 1st option in the PT. Besides the effects mentioned for the 2×2 case, the impact of MIMO in the traffic for larger antenna array sizes is clearly limited by the inherent qualities of a convergent system: the standard diversity.

6.3   Access Technology Scenarios Variation

6.3.1 General Considerations

The second approach adopted for the analysis of the impact of MIMO is presented in this section. The focus is now shifted to the analysis of different access technology scenarios for a specific user scenario, the one with 1 000 users. This number of users represents a reasonable balance between the realisation of the MIMO gain (MIMO would bring little benefit for fewer users) and simulation times. In order to allow a more precise comparison between the technology scenarios, the same UTVs were used in all scenarios. This type of analysis is useful to know which access technologies should be present to provide a certain number of users with a given QoS.

A structure parallel to the one of Section 6.2 is taken here: two subsections, the first characterising the performance of Configuration 1 over SISO, and the second characterising the performance of Configuration 2 over 1. Graphical plots of the performance indicators defined in (5.4)−(5.7) are shown in the same order as in the previous section.

A common consideration for all following figures can be made *a priori*: The G Scenario is only shown here to assess the statistical averaging of the other scenarios; for a sufficiently high number of samples (BHCAs) taken for each scenario, the G scenario should have arbitrarily low relative gains (as it is not provided with MIMO). When the relative gains are not negligible they can be used as a measure of the error margins for the other scenarios.

6.3.2 Performance Enhancement with Configuration 1

The first remark about Figure 6.8 is that the statistical averaging is appropriate as the G scenario presents an average gain lower than 1 %. The scenarios that do not include HIPERLAN/2 profit more from the use of MIMO because this ATTPM boosts the bitrates in the single antenna case, as depicted from the absolute values. This profit more than duplicates the SISO performance of the FTP and Email applications in the U and G+U scenarios (G_{Rb}>100 %). There is a general decrease trend, evident for the mentioned applications, and slight for the others: as the technology scenarios include more and more access techniques, the bitrates approach their maxima, and MIMO's potential is progressively less exploited.

Figure 6.9 depicts the relative gains of the discarded packet rate G_{η_D} per user scenario and PS application. Error margins, depicted from the G scenario, are around and below 10 %. The achieved gains are very significant, which means that in the SISO case there were not many discarded packets and Configuration 1 can recover them all.

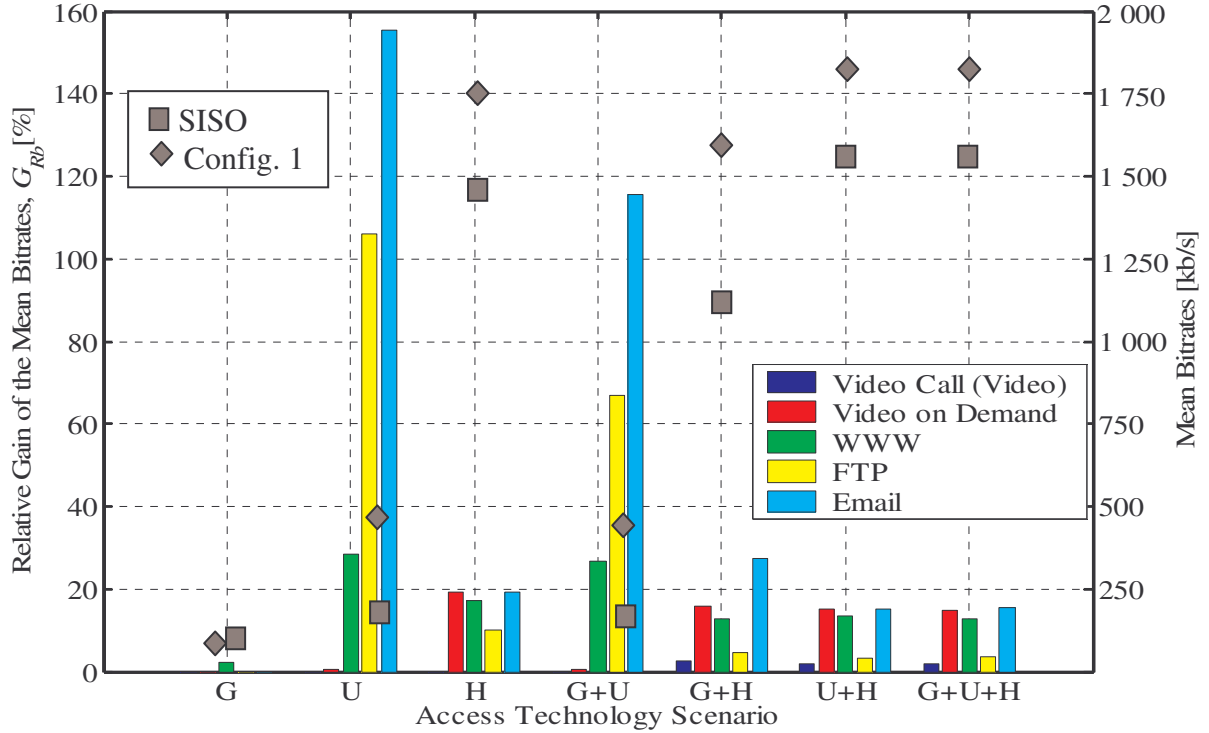**Figure 6.8: Relative Gains of the Mean Bitrate versus Access Technology Scenario with Configuration 1 (1 000 Users).**
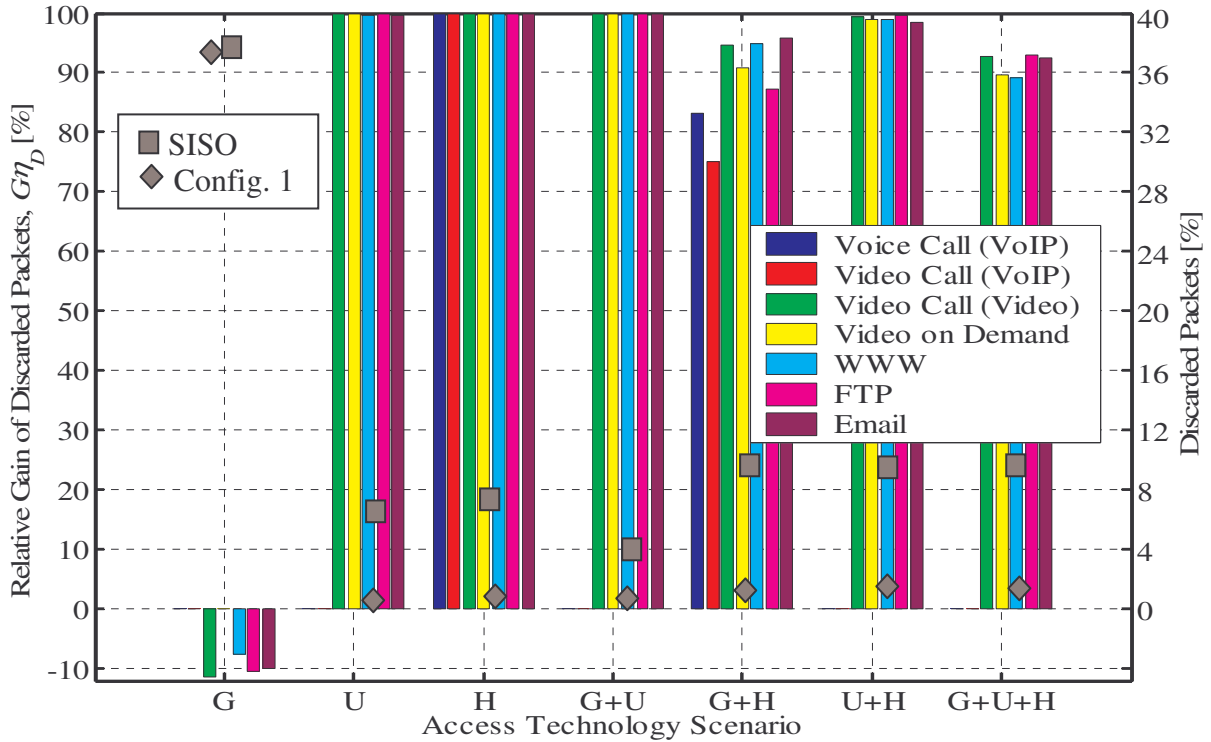

Figure 6.9: Relative Gains of the Discarded Packets versus Access technology Scenario with Configuration 1 (1 000 Users).

For the CS applications, the G scenario of Figure 6.10 again shows that the generated statistics provide quite low error margins (below 8 %). The envelopes show that, for 1 000 users, the scenarios H, U+H, and G+U+H do not block calls when SISO is used (G_{RCB}=0 %). With multiple antennas, the MIMO version of the UMTS ATTPM accepts and transmits the majority of the calls routed to it (G_{Rcs}>75 %), while the other scenarios have also fair performances ($G_{RCB} \in$]30,70[%). Although the bars denounce high relative gains, the absolute values show that the MIMO contribution is poor, as the SISO system blocks very few calls.

The impact of MIMO in terms of the number of sessions routed through their most prioritised technology ($G_{\eta IPD-T}$) and bitrate/quality ($G_{\eta IPD-B}$) for all applications is represented in Figure 6.11. The gains for the G scenario are once again insignificant. In the SISO case, as more technologies are available, the traffic convergent system approached the highest percentages of sessions routed through their first priority. Therefore, MIMO's profit decreases as more complete scenarios are considered. Besides, the scenarios that do not include HIPERLAN/2 correspond to those where MIMO performance is greater, because this ATTPM improves the SISO system performance significantly. It is important to note that in the U scenario no gain is obtained for $G_{\eta IPD-T}$, because the UMTS is not the 1st priority for any application. Similarly, in the G+U scenario almost no gain is perceived for the same parameter, because GSM/GPRS is the most prioritised technology only for the CS applications.
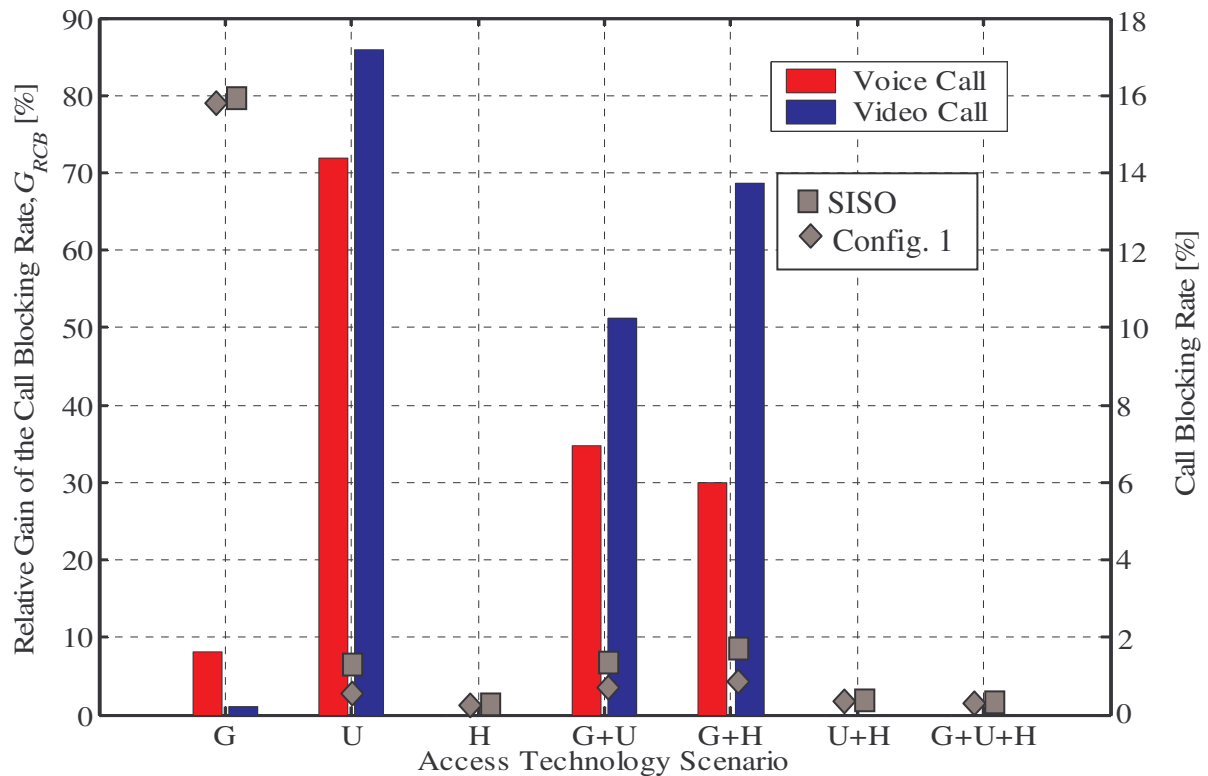

Figure 6.10: Relative Gains of the Call Blocking Rate versus Access Technology Scenario with Configuration 1 (1 000 Users).
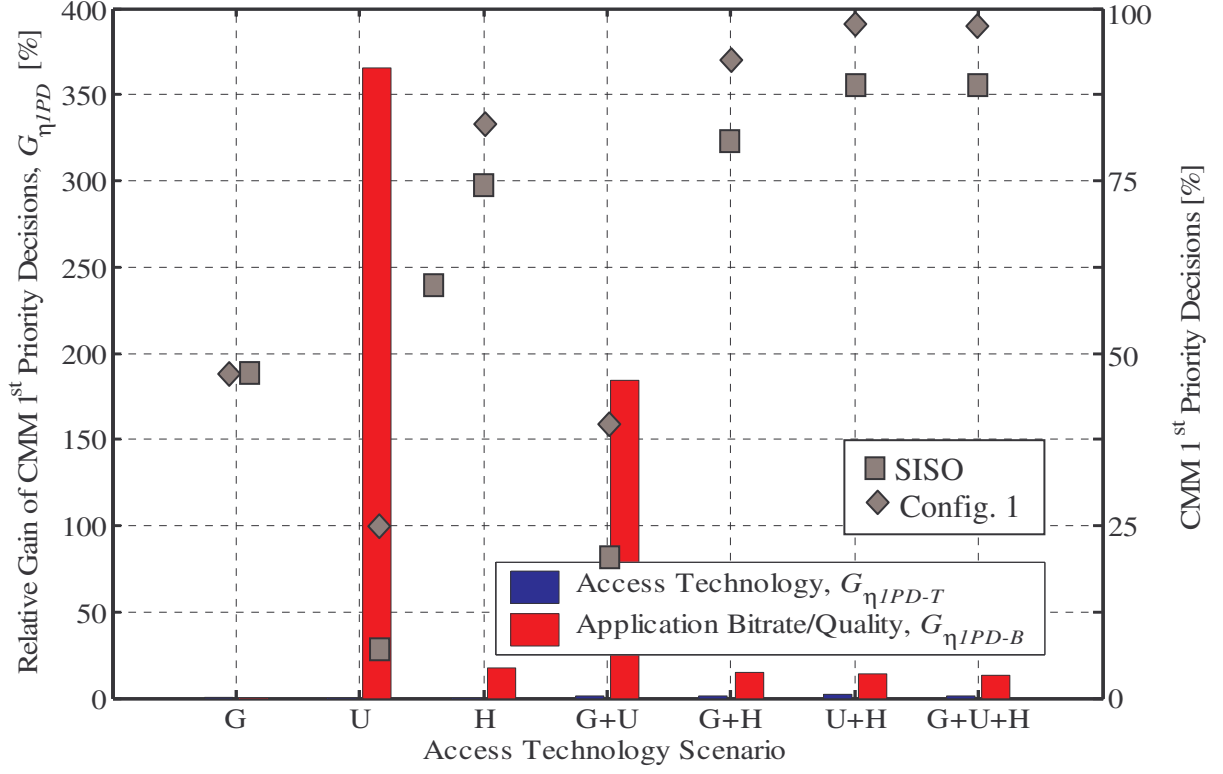
Figure 6.11: Relative Gains of the CMM 1st Priority Decisions versus Access Technology Scenarios with Configuration 1 (1 000 Users).

6.3.3 Performance Enhancement with Configuration 2

Similarly to Subsection 6.2.3, Figure 6.12 to Figure 6.14 are evidence for the gain of MIMO with Configuration 2 relatively to 1. The general shape of the bars in Figure 6.12 resembles the one in Figure 6.8, meaning that the already significant differences in the performances of the applications depicted in the later figure enlarge with Configuration 2. The same remarks done for the gain of Configuration 1 over SISO, Figure 6.8, can be applied to explain the gain of Configuration 2 over 1, Figure 6.12. One can conclude from the G scenario that Configuration 2 presents higher error margins than its corresponding Figure 6.8, but still below 10 %.

The percentage of packets that Configuration 2 discards less than Configuration 1 is not shown because the values are negligible. Configuration 1, Figure 6.9, already achieved gains of nearly 100 % for the majority of the access technology scenarios.

Regarding the CS applications, Configuration 2 reduces the call blocking rate of the same scenarios in which Configuration 1 did: U, G+U, and G+H, Figure 6.13. This happens because these scenarios were the ones in which SISO did not perform optimally. The gains of Figure 6.13 are such that Configuration 2 eliminates almost all blocked calls (only the voice application presents some blocked calls in the G+H scenario).
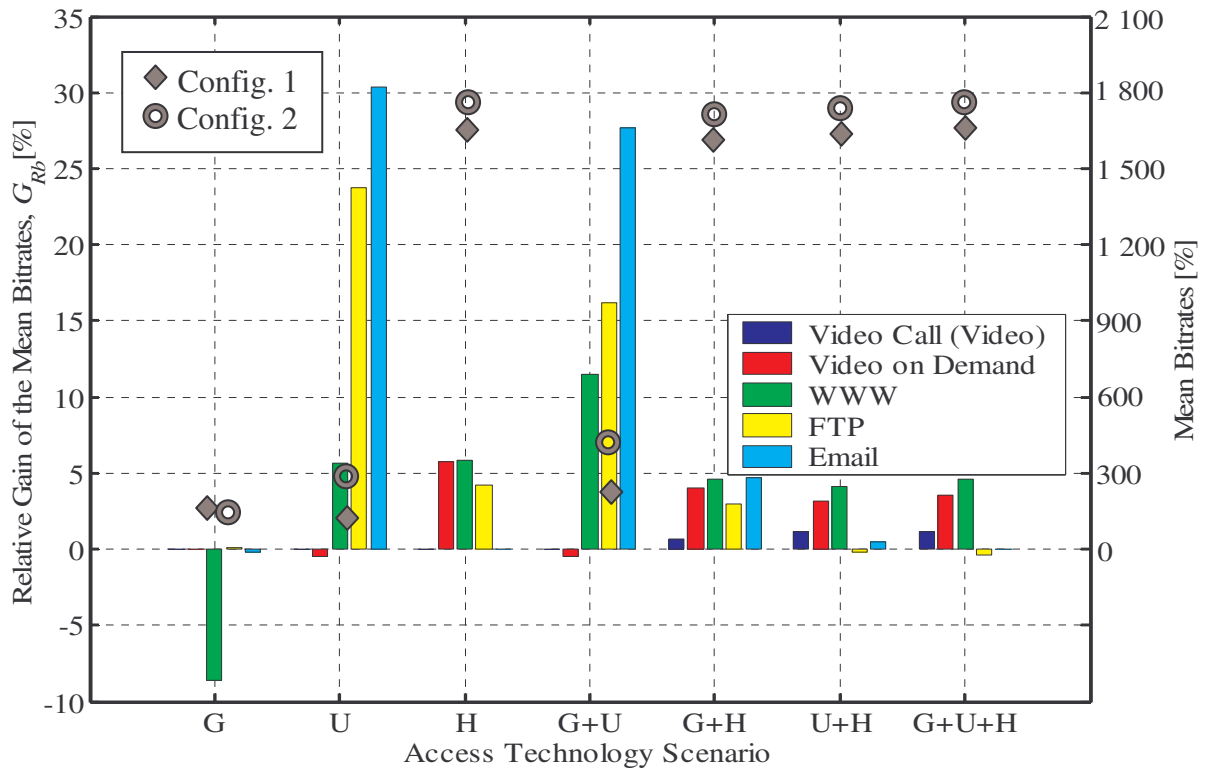
Figure 6.12: Gain of the Mean Bitrates with Configuration 2 Relatively to 1 versus Access Technology Scenario (1 000 users).

Figure 6.13: Relative Gains of the Call Blocking Rate with Configuration 2 Relatively to 1 versus Access Technology Scenario (1 000 users).

Finally, the percentage of sessions that are routed to the 1st option of the PT with Configuration 2, and that were not with Configuration 1, is shown in Figure 6.14. Expectably,

this figure resembles the one with the gains of Configuration 1 over SISO, Figure 6.11, since both represent relative gains over smaller configurations. However, the values are much lower now due to the same reason: there is not much more to gain from since Configuration 1 delivered almost optimum performances.
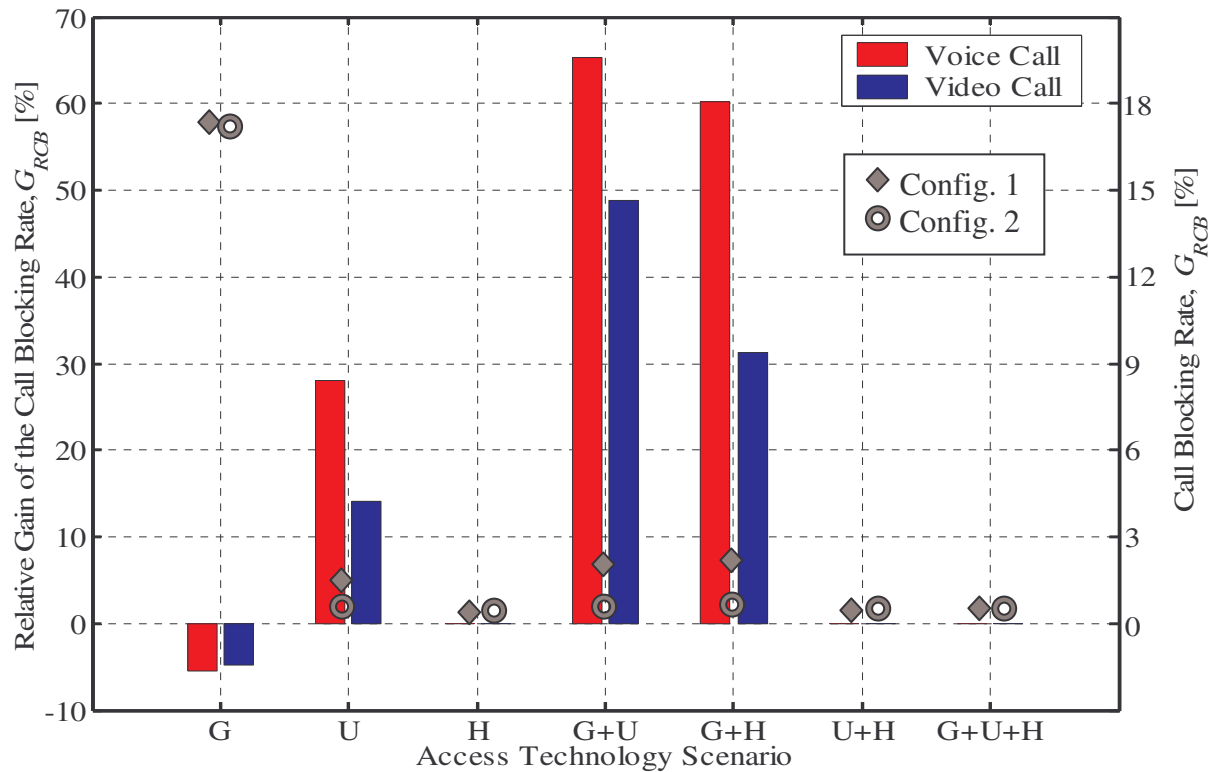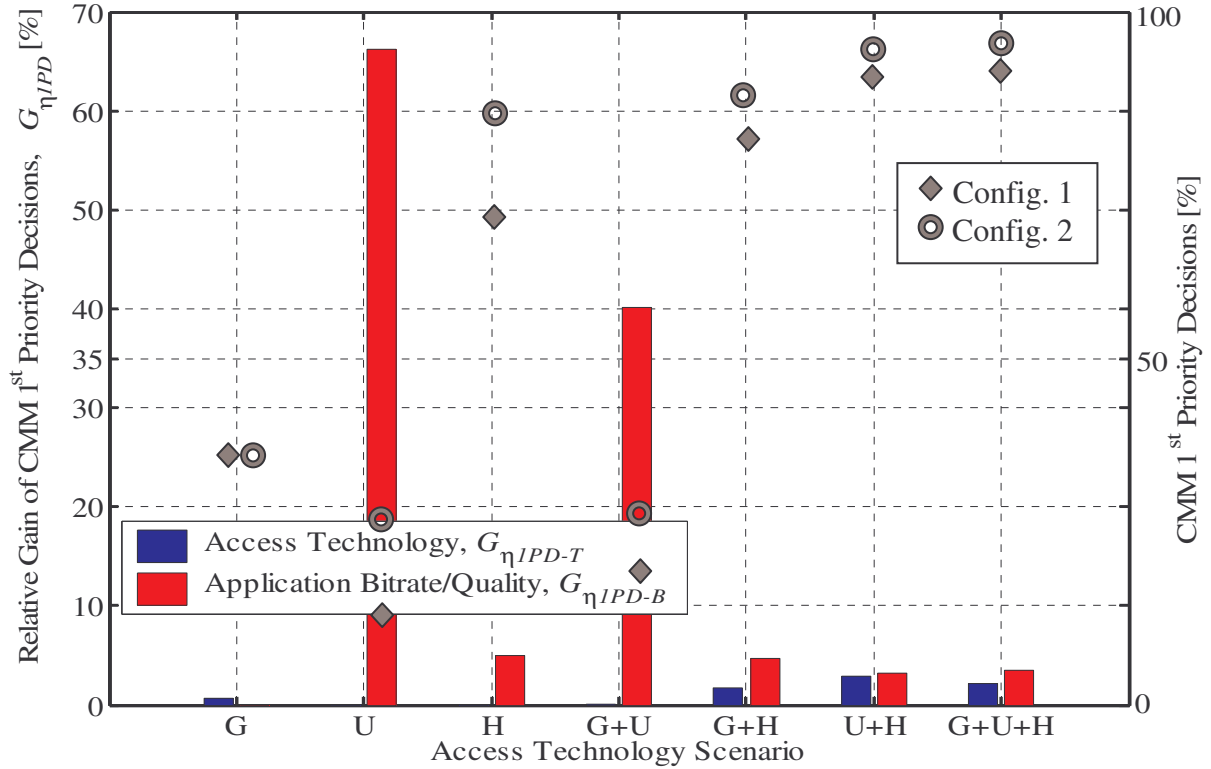

Figure 6.14: Gain of the CMM First Priority Decisions with Configuration 2 Relatively to 1 versus Access Technology Scenario (1 000 users).

Again, it can be concluded that the main benefit comes from the use of a dual antenna array at both ends of the connection. The use of more antennas cannot significantly improve the performance for the scenarios considered relatively to the 2×2 case. Obviously, this is more evident in scenarios with more available technologies.

Similarly to the previous section, the bridge between capacity at propagation and traffic levels is based on two pillars: impossibility to take full advantage of the channel capacity, and the fact that the SISO (and MIMO Configuration 1) convergent system does not leave much space for further increases in its capacity. Both were explained in Subsection 6.2.3, and the same remarks apply to this subsection. Furthermore, this section has made clear that MIMO is not worthwhile for all scenarios: in general, if users have access to HIPERLAN/2, the presence of MIMO is almost irrelevant.

7

Conclusions

The main conclusions from the channel modelling to the traffic convergence are drawn in this last chapter. Some guidelines for future work in this area are also pointed out.

The purpose of this thesis was to assess the impact that a promising technique such as MIMO has on the traffic of a converged multi-technological mobile wireless network. Three standards were considered: GSM/GPRS, UMTS, and HIPERLAN/2, even though only the latter two were supplied with MIMO, as the GSM/GPRS may no be part of the future of mobile communications. To carry out this study, it was essential to determine the interaction between the physical layer of each standard and the layer that links the standards among themselves (*e.g.*, convergence layer in HIPERLAN/2). More generally, it was explained how MIMO and standards convergence can be seen as two ways of diversity in its wider sense, and how they inter-depend and need to be considered together to enable obtaining full advantage from both.

The software tool used to quantify the mentioned impact is based on an already implemented traffic convergent simulator that did not consider propagation aspects. A physical layer was then developed to link the channel capacity to the way that traffic was routed in the system. It consisted of three main modules: a MIMO channel simulator, a channel capacity calculation module, and an implementation of a particular link between channel capacity and the capacity of the standards.

The results from simulations were then presented in the form of four parameters, under environments with varying number of users and available technologies.

As a first step towards the goal of the thesis, the wideband GBSBEM, described in Chapter 4, was extended to support MIMO, following the narrowband array assumption. The resulting model was assessed in terms of capacity with good compliance with theoretical results, and other published work. Expected behaviours were also obtained when the parameters were varied. The general conclusions drawn for the considered micro-cell environments are:

- For inter-antenna distances below 0.6λ, the narrowband array assumption is valid, providing realistic capacities in environments with varying number of antennas, scattering richness, and inter-antenna spacing (as long as these are below 0.6λ).
- For inter-antenna distances above 0.6λ, the AoAs, AoDs can no longer be seen as invariant from one antenna to another and the obtained capacities are in general pessimistic, since sources of spatial decorrelation are being ignored.
- In order to simulate sources of spatial decorrelation that are not directly accounted for in the model, a randomness can be added to the phases of the scatterers' reflection coefficients. This randomness plays a critical role, because it can boost the channel's capacity up to the one of a totally uncorrelated channel, independently of the scattering richness of the considered environment.
- The larger bandwidth of HIPERLAN/2 comparatively to the UMTS one does not seem to have great impact on the capacity relative gains of MIMO over SISO. This is

mainly due to the fact that even the 20 MHz of HIPERLAN/2 does not greatly improve the accuracy of the propagation paths resolvability.

Afterwards, the link between channel capacity and traffic convergence was implemented. The followed approach is designated as "MIMO system as enhanced single link", where the spatial modes of MIMO are selected within each standard, and not jointly with the standards in the CMM. The main assumption is that the channel capacity gain of MIMO over SISO is directly included in the capacity models of the ATTPMs, as if, for example, the extra signalling needed with MIMO did not reduce it.

Finally, the results showing the impact of MIMO in the traffic convergence were put on the form of four relative gains. They characterise the increase of the bitrate and of the number of sessions routed through their 1st option of access technologies and quality/bitrate, and the decrease of the call blocking rate of the CS applications and of the discarded packets/frames of the PS ones. Regarding the number of users and available technologies, the results are shown for:
- the G+U+H scenario, with users ranging from 500 to 1 400,
- the 1 000 users scenario, with all seven possible combinations of the three access technologies.

Some common remarks can be made a priori. In convergent networks, the standard diversity significantly increases the system capacity in relation to single standard networks, and the provided performance may not be acceptable only for a high number of users. Therefore, an increase of capacity is only useful if there is an increase of the number of users or an increase of the capacity demanded from the applications. The former approach was taken by shifting the range of the number of users from [100, 1 000] [Agui03] to [500, 1 400], when varying the number of users, and by considering 1 000 users instead of 700 [Agui03], when varying the available set of access technologies. The TSMs were left unaltered. Still, practically all the performance parameters indicate that the MIMO performance is limited by the small gap left by SISO to accommodate more gain. However, this does not mean that enlarging the number of antennas is useless: due to the statistical nature of the generated traffic and of the channel capacity, larger configurations exploit better the (small) gap left by SISO.

The duration of the simulations took a good part of the thesis timeframe, preventing the inclusion of more users, which would allow the full development of the MIMO potential. This was specially limiting in Configuration 2 where, even for 1 400 users, the gain was still increasing, indicating that, for more users, the gain would be larger.

The impact of MIMO was shown to be highly PT-dependent. Because the three standards do not benefit from the same capacity enhancements (GSM/GPRS does not benefit it at all),

except for the UMTS and HIPERLAN/2 in Configuration 1, the routing priorities of the sessions influence the overall MIMO gain.

Some specific conclusions follow. The gains of Configuration 1 relatively to SISO are:

- For the mean bitrates, a maximum of 30 % is verified for the WWW and video-on-demand applications, and of about 5-10 % for all the others, when varying the number of users. The difference is due to the way the PT is defined. When the available standards vary, the largest gains are obtained in the U scenario (up to almost 160 %) as it is the one with the worse performance in SISO.
- For the discarded packets/frames, the gains vary significantly, but are generally above 50 %, for both variations of number of users and available standards.
- For the call blocking rate, the gains are only visible for more than 1 000 users if the three standards are available because, for fewer users, SISO presented optimum performances. With 1 000 users, SISO only blocks calls in the H, U+H, and G+U+H scenarios. In the U scenario, MIMO can recover more than 75 % of both video and voice calls, while in the G+U and G+H ones, MIMO recovers between 40 and 70 % of both types of calls.
- For the number of sessions routed through their 1st priority option of access technology, a maximum below 4 % is depicted with the curve along the users scenarios having a bell shape; regarding the quality/bitrate, a maximum gain of almost 30 % is obtained for 1 400 users when G+U+H is present. The variation along the available standards scenarios shows an expectable decrease as more complete scenarios were used and less "space" is left for MIMO. Therefore, the maximum gain (more than 350 %) occurs for the only single standard scenario that does not include HIPERLAN/2: the U scenario.

The gains of Configuration 2 over Configuration 1 are:

- For the mean bitrates, a maximum gain of 15 % for the scenario with the largest number of users is obtained in the G+U+H scenario. With this configuration a stabilisation of the gains is not seen. When the available standards vary, once again the scenarios with fewer standards are the ones that allow Configuration 2 to improve the bitrate. The maximum (33 %) is observed in the U scenario.
- For the discarded packets/frames, the gains allow almost no discarded packets or frames in any user scenario.
- For the call blocking rate, SISO performs optimally until 1 300 users, and for 1 400, MIMO Configuration 2 recovers the totality of the calls blocked with Configuration 1. The access technology scenarios that present blocked calls are the same as in Configuration 1, gaining up to 50 % in relation to it.

- For the number of sessions routed through their 1st priority option of the PT, there is a constant increase up to almost 10 % for the access technologies and up to almost 20 % for the bitrate/quality. With 1 000 users, and like in Configuration 1, the U and G+U scenarios dominate the gains with almost 90 and almost 50 %, respectively.

Establishing a relation between the MIMO capacity increase at propagation level with the one at system level was done both qualitative and quantitative for a specific convergent system. It was known for many years that the Shannon limits were never achieved. However, this thesis has shown preliminary results that indicate that the differential between the MIMO and SISO capacities cannot also be fully exploited. The unmatching randomness of the channel capacity and of the generation of the traffic is one reason that explains the fact. Another general conclusion is that the standard diversity of the considered system is efficient enough to reach optimum performances for exigent scenarios, *e.g.*, high number of users.

As mentioned in the introduction, this thesis aims at opening the discussion of how can MIMO and convergence of wireless standards be considered together, and which is the impact of the former technique on the latter. Some guidelines for continuing this research path are:

Regarding the channel modelling, the single user simulations should be replaced by a multi-user scenario, where at least interference from other users of the same cell are considered.

- Regarding the MIMO modelling, an interesting issue would be to abandon the narrowband array assumption, and study the channel capacity for large inter-antenna spacings. On a laptop, for example, there might be physical space to accommodate multi-band antennas inter-spaced by more than 0.5λ.
- Regarding the scenarios, macro- and pico-cells should also be considered instead of only micro-cells.
- Regarding the traffic convergent system, the study of the accommodation (and its necessary deterioration) of the MIMO gain at propagation level in the higher layers is still an open issue for research.
- Regarding the philosophy that considers the MIMO spatial modes and the available standards as two forms of diversity, the approach "MIMO system for diverse spatial modes" is necessarily more profitable as optimises both diversities jointly, exploiting their inter-dependences.
- The approach of having more sophisticated applications (and respective TSMs) that are more capacity demanding and would profit from all MIMO capacity enhancement (especially the one of Configuration 2) might be more useful than enlarging the number of users indefinitely.
- The variation of the number of users with other combinations of standards besides the G+U+H one, and the variation of the available standards with other number of users

besides 1 000, is a straightforward improvement of this thesis that would only require more simulations.

In conclusion, more issues were opened than the ones that were closed.

References

[3GPP04]   3GPP (http://www.3gpp.org)

[4GMF04]   4th Generation Mobile Forum (http://www.4gmf.org)

[ACGN02]   Aguiar,J., Correia,L.M., Gil,J., Noll,J., Karlsen,M., Syaet,S., Mously,T., Hunt,B., Raynes,D., Lehmann,G., Müller,R., Hofstetter,H., Tröger,H. and Burr,A., *Definition of Scenarios*, IST-FLOWS Project, Deliverable 1, IST-TUL, Lisbon, Portugal, Mar. 2002.

[AgCo04]   Aguiar,J. and Correia,L.M., "Traffic source models for the simulation of next generation mobile networks", in *Proc. of WPMC'04–7th International Symposium on Wireless Personal Multimedia Communications,* Venice, Italy, Sep. 2004.

[Agud89]   Agudo,F.D., *Introduction to Linear Algebra and Analytic Geometry* (in Portuguese), Escolar Editora, Lisbon, Portugal, 1989.

[Agui03]   Aguiar,J., Traffic Analysis at the Radio Interface in Converging Mobile and Wireless Communication Systems, Master Thesis, Instituto Superior Técnico, Lisbon, Portugal, 2003.

[AMSH01]   Artés,H., Matz,G., Schafhuber,D. and Hlawatsch,F., "Space-time multicarrier matrix modulation for unknown dispersive MIMO channels", in *Proc. of 39th Allerton Conference on Communication, Control and Computing*, Urbana, Illinois, USA, Oct. 2001.

[ATEM02]   Almers,P., Tufvesson,F., Edfors,O., and Molisch,A., "Measured Capacity gain using waterfilling in frequency selective MIMO channels", in *Proc. of PIMRC'02 – 13th IEEE International Symposium on Personal, Indoor and Mobile Radio Communications*, Lisbon, Portugal, Sep. 2002.

[Burr02]   Burr,A., "Evaluation of Capacity of Indoor Wireless MIMO Channel Using Ray Tracing", in *Proc. of IZS'02 − International Zürich Seminar*, Zürich, Switzerland, Feb. 2002.

[Burr04]   Burr,A., *MIMO and Convergence,* IST-FLOWS Project, Internal Document WP5_UoY_TN_INT_023_01, University of York, York, UK, Feb. 2004.

[CELL04]   Cellular Online (http://www.cellular.co.za)

[Chan04]   Chandran,S. (ed.), *Adaptive Antenna Arrays: Trends and Applications*, Springer-Verlag, Berlin, Germany, 2004.

[CoPa03]   Conrat,J-M. and Pajusco,P., "A Versatile Propagation Channel Simulator for MIMO Link Level Simulation", *COST 273*, Internal Document TD(03)120, Paris, France, May 2003.

[Corr01]   Correia,L.M. (ed.), Wireless Flexible Personalised Communications – COST 259 Final Report, John Wiley & Sons, Chichester, UK, 2001.

[Fail89]   Failli,M., *Digital Land Mobile Radio Communications - COST 207 Final Report*, COST Office, European Commission, Brussels, Belgium, 1989.

[CRLL00]   Chizhik,D., Rashid-Farrokhi,F., Ling,J. and Lozano,A., "Effect of Antenna Separation on the Capacity of BLAST in Correlated Channel*s*", *IEEE Communication Letters*, Vol. 4, No. 11, Nov. 2000, pp. 337-339.

[Debb03]   Debbah,M., *An Information Theoretic point of view to MIMO channel modelling,* IST-FLOWS Project, Deliverable 13, Forschungszentrum Telekommunikation Wien (FTW), Vienna, Austria, Sep. 2003.

[ECSR98]   Ertel,R., Cardieri,P., Sowerby,K., Rappaport,T. and Reed,J., "Overview of Spatial Channel Models for Antenna Array Communication Systems", *IEEE Personal Communications*, Vol. 5, No. 1, Feb. 1998, pp.10-22.

[ETSI00a]   ETSI, *HIPERLAN type 2: System Overview*, Broadband Radio Access Networks (BRAN) Technical Report, No. TR 101.683, Ver. 1.1.1., Sophia-Antipolis, France, Feb. 2000.

[ETSI00b]   ETSI, *HIPERLAN type 2: Data Link Control (DLC) Layer part 1: Basic Data Transport Functions*, Broadband Radio Access Networks (BRAN) Technical Standard, No. TS 101.761-1, Ver. 1.1.1., Sophia-Antipolis, France, Apr. 2000.

[ETSI00c]   ETSI, *HIPERLAN Type 2: Physical (PHY) layer*, Broadband Radio Access Networks (BRAN) Technical Standard, No. TS 101.475, Ver. 1.3.1., France, Dec. 2000.

[FCSC02]   Ferreira,L.,   Correia,L.M.,   Serrador,A.,   Carvalho,G.,   Fledderus,E.   and Pereira,R., *UMTS Deployment and Mobility Scenarios*, IST-MOMENTUM Project, Deliverable D1.3, IST-TUL, Lisbon, Portugal, Oct. 2002.

[FCXV03]   Ferreira,L., Correia,L., Xavier,D., Vasconcelos,A. and Fledderus,E., *Final report on traffic estimation and services characterisation*, IST-MOMENTUM Project, Deliverable D1.4, IST-TUL, Lisbon, Portugal, May 2003.

[FeMa03]   Fernandes,P. and Mártires,J., *MIMO Scheduling and Cooperative Detection for Systems Beyond 3G*, Master Thesis, University of Aalborg, Aalborg, Denmark, June 2003.

[Fleu02]   Fleury,B., "First- and Second-order characterisation of the direction dispersion and space selectivity in the radio channel", *IEEE Transactions on Information Theory*, Vol. IT-46, No. 6, Sep. 2002, pp. 2027-2044.

[FLOW03]   IST-FLOWS Project (http://www.flows-ist.org).

[FiGC03]   Cardoso,F., Gil,J. and Correia,L., *IST/TUL Wideband Double Directional Channel Model–Description of Simulation Software*, IST-FLOWS Project, Internal Document WP2_IST-TUL_TN_INT_073_01, IST-TUL, Lisbon, Portugal, Nov. 2003.

[FoGa98]   Foschini,G.J. and Gans,M.J., "On limits of wireless communications in a fading environment when using multiple antennas", *Wireless Personal Communications*, Vol. 6, No. 3, Mar. 1998, pp. 311–335.

[Fosc96]   Foschini,J., "Layered space-time architecture for wireless communication in a fading environment when using multiple antennas", *Bell Labs Technical Journal*, Vol. 1, No. 2, Autumn 1996, pp.41-59.

[FSCS04]   Ferreira,L., Serrador,A., Correia,L. and Svaet,S., "Concepts of Simultaneous Use in the Convergence of Wireless Systems", in *Proc. of 13th IST Mobile and Wireless Communications Summit*, Lyon, France, June 2004.

[GBGP00]   Gesbert,D., Bölskei,H., Gore,D. and Paulraj,A., "MIMO wireless channels: capacity and performance prediction", in *Proc. of Globecom2000− IEEE Global Communications Conference*, San Franscisco, California, USA, Nov. 2000.

[GeAk02]   Gesbert,D. and Akhtar,J., "Breaking the barriers of Shannon Capacity: An Overview of MIMO wireless systems", *Telektronikk Telenor Journal*, Vol. 98, Jan. 2002, pp. 53–64.

[GSLV01]   German,G., Spencer,Q., Lee,A. and Valenzuela,R., "Wireless indoor channel modelling: statistical agreement of ray tracing simulations and channel sounding measurements", in *Proc. of ICASSP'01 − 26th IEEE International Conference on Acoustics, Speech and Signal Processing*, Salt Lake City, Utah, USA, May 2001.

[GVCM03]   Gil,J., Venes,J., Cardoso, F., Marques,M.G. and Correia,L.M., *IST/TUL Contribution for D13,* IST-FLOWS Project, Internal Document WP2_IST-TUL_TN_INT_066_01, IST-TUL, Lisbon, Portugal, June 2003.

[HIPE04]   HiperLAN2 Global forum (http://www.hiperlan2.com)

[HoTo01]   Holma,H. and Toskala,A. (eds.), *WCDMA for UMTS*, John Wiley & Sons, Chichester, UK, 2001.

[HoTW03]   Hottinen,A., Tirkkonen,O. and Wichman,R., *Multi-antenna transceiver techniques for 3G and beyond*, John Wiley & Sons, Chichester, UK, 2003.

[JeBF00]   Jelitto,J., Bronzel,M. and Fettweis,G., "Reduced Complexity Space-Time Optimum Processing", in *Proc. of 2000 Virginia Tech Symposium on Wireless Personal Communications*, Blacksburg, Virginia, USA, June 2000.

[JiIn03]   Jiang,J.S. and Ingram, M.A., "Distributed source model for short-range MIMO", in *Proc. of VTC'03 Fall − 57th IEEE Vehicular Technology Conference*, Orlando, Florida, USA, Oct. 2003.

[KCVW03]   Kyritsi,P., Cox,D., Valenzuela,R. and Wolniansky,W., "Correlation Analysis Based on MIMO Channel Measurements in an Indoor Environment", *IEEE Journal on Selected Areas in Communications*, Vol. 21, No. 5, June 2003, pp.713-720.

[KlMo96]   Klein,A. and Mohr,W., "A Statistical Wideband Mobile Radio Channel Model Including the Directions-of-Arrival", in *Proc. of ISSSTA'96 − IEEE 4th International Symposium on Spread Spectrum Techniques and Applications*, Mainz, Germany, Sep. 1996.

[KMST00]   Khun-Jush,J., Malmgren,G., Schramm,P. and Torsner,J., "HIPERLAN type 2 for broadband wireless communication", *Ericsson Review*, No. 2, Nov. 2000, pp. 108-119.

[KrSa01]   Kristensen,F. and Sandgren,M., *A System Simulation of Wireless Local Area Networks Operating in the 5 GHz Band*, Master Thesis, Telia Research, Malmo, Sweden, Aug. 2001.

[KSPM02]   Kermoal,J.P, Schumacher,L., Pedersen,.K. and Mogensen,P., "A Stochastic MIMO Radio Channel Model with Experimental Validation", *IEEE Journal on Selected Areas in Communications*, Vol. 20, No. 6, August, 2002, pp.1211-1226.

[Kyri01]   Kyritsi,P., *Multiple element antenna systems in an indoor environment*, Ph. D Thesis, Stanford University, Stanford, California, USA, 2001.

[LiRa99]   Liberti,J. and Rapapport,T., *Smart Antennas for Wireless Communications: IS-95 and Third Generation CDMA Applications*, Prentice Hall, Upper Saddle River, New Jersey, USA, 1999.

[LUCE01]   Lucent Technologies, Nokia, Siemens, Ericsson, *A Standardized Set of MIMO Radio Propagation Channel*, 3GPP, TSG R1-01-1179, Nov. 2001. (http://www.3gpp.org).

[LuLL97]   Lu,M., Lo,T. and Litva,J., "A Physical Spatio-temporal Model of Multipath Propagation Model", in *Proc. of VTC'97 – 47th IEEE Vehicular Technology Conference*, Phoenix, Arizona, USA, May 1997.

[MaCo01]   Marques,M.G. and Correia,L.M., "A Wideband Directional Channel Model for UMTS Micro-cells", in *Proc. of PIMRC'01 – 12th IEEE International Symposium on Personal, Indoor and Mobile Radio Communications*, San Diego, California, USA, Sep. 2001.

[Marq01]   Marques,M.G., *A wideband Directional Model for Micro-cells in UMTS*, Master Thesis, IST/TUL, Lisbon, Portugal, 2001.

[KSBO01]   Kermoal,J.P., Schumacher,L., Beach,M., Ottersten,B., Bengtsson,M. Laspougeas,P., Pajusco,P., Mayrargue,S. and Herault,L., "Smart Antennas IST Cluster", in *Proc. of 1st cluster meeting with SATURN, METRA and ASILUM*, Galway, Ireland, Oct. 2001.

[MFGH99]   Martin,U., Fuhl,J., Gaspard,I., Haardt,M., Kuchar,A., Math,C., Molisch,A. and Bonek,E., "Model Scenarios for Direction-Selective Adaptive Antennas in Cellular Mobile Communication Systems - Scanning the Literature", *Wireless Personal Communications*, Vol.11, No.1, Oct. 1999, pp. 109-129.

[MGFC01]   Marques,M.G., Gil,J., Ferreira,L. and Correia,L.M., *The COSSAP radio channel modules: models, implementation and interface description*, IST-ASILUM Project, Internal Report IST/TUL/IN/Int./029/0.4,   IST-TUL, Lisbon, Portugal, June 2001.

[MOME04]   IST-MOMENTUM Project (http://momentum.zib.de).

[ÖHWW03]   Özcelik,H., Herdin,M., Weichselberger,W., Wallace,J. and Bonek,E., "Deficiencies of the 'Kronecker' MIMO Radio Channel Model", *IEE Electronics Letters*, Vol. 39, No. 16, July 2003, pp. 1209-1210.

[PAKM00]   Pedersen,K., Andersen,J.B., Kermoal,J.P. and Mogensen,P., "A Stochastic Multiple-Input-Multiple-Output Radio Channel Model for Evaluation of Space-Time Coding Algorithms", in *Proc. of VTC'00 Fall − 52th IEEE Vehicular Technology Conference*, Boston, Massachusetts, USA, Sep. 2000.

[PFMC02]   Peixeiro,C., Fernandes,C., Moreira,A., Capstick,M., Kemp,B., Brissos,J., Guerra,F. and Teixeira,B., *Antenna Feasibility Study*, IST-FLOWS Project, Deliverable 7, IST-TUL, Lisbon, Portugal, Nov. 2002.

[PiTs99]   Piechocki,R. and Toulos,G., "Combined GWSSUS and GBSR Channel Model with temporal Variations", in *Proc. of COST259/260 Joint Workshop Spatial Channel Models and Adaptive Antennas*, Vienna, Austria, Apr.1999.

[Proa01]   Proakis, J.,G., *Digital Communications*, Mac Graw Hill, New York City, New York, USA, 2001.

[Rapp01]   Rappaport, T.,S., *Wireless Communications − Principles and Practice*, Prentice Hall, New Jersey, USA, 2001.

[Reis04]   Reis,C., *An analytical traffic model for the UMTS radio interface*, Master Thesis, IST-TUL, Lisbon, Portugal, Mar. 2004.

[SaVa87]   Saleh,A. and Valenzuela,R., "A Statistical Model for Indoor Multipath Propagation", *IEEE Journal on Selected Areas in Communications*, Vol. 5, No. 2, Feb. 1987, pp.128-137.

[Saye02]   Sayeed,A., "Deconstructing Multiantenna Fading Channels", *IEEE Transactions on Signal Processing*, Vol. 50, No. 10, Oct. 2002, pp. 2563-2579.

[SFGK00]   Shiu,D-S., Foschini,G., Gans,M. and Kahn,J., "Fading Correlation and its Effect on the Capacity of Multielement Antenna Systems", *IEEE Transactions on Communications*, Vol. 48, No. 3, Mar. 2000, pp. 502-513.

[Sibi01]   Sibille,A., *Keyholes and MIMO Channel Modelling*, COST 273 Technical Report TD (01) 017, Bologna, Italy, Oct. 2001.

[SJBF00]   Stege,M., Jelitto,J., Bronzel,M. and Fettweis,G., "A Multiple-Input Multiple-Output Channel Model for Simulation of TX- and RX-Diversity Wireless Systems", in *Proc. of VTC'00 Fall – 52th IEEE Vehicular Technology Conference*, Boston, Massachusetts, USA, Sep. 2000.

[SJJS00]   Spencer,Q., Jeffs,B., Jensen,M. and Swindelhurst,L.A., "Modelling the Statistical Time and Angle of Arrival Characteristics of an Indoor Multipath Channel", *IEEE Journal on Selected Areas in Communications*, Vol. 18, No. 3, Mar. 2002, pp. 347-360.

[StMB01]   Steinbauer,M., Molisch,A. and Bonek,E., "The Double-Directional Channel Model", *IEEE Antennas and Propagation Magazine*, Vol. 43, No. 4, 2001, pp. 51-63.

[Tela95]   Telatar,I.E., *Capacity of Multi-Antenna Gaussian Channels,* Technical memorandum BL011217-950615-07TM, AT&T Bell Labs, Newark, New Jersey, USA, June 1995.

[THRS01]   Thomä,R., Hampicke,D., Richter,A. and Sommerkorn,G., "Measurement and identification of mobile radio propagation channels", in *Proc. of IMTC'01 – IEEE Instrumentation and Measurement Technology Conference*, Budapest, Hungary, May 2001.

[ToMa99]   Torsner,J. and Malmgren,G., "Radio Network Solutions for HIPERLAN/2", in *Proc. of VTC'99 – 49th IEEE Vehicular Technology Conference*, Houston, Texas, USA, May 1999.

[VGCC03]   Venes,J., Gil,J., Cardoso,F. and Correia,L.M., *Antenna Arrays for Wideband Directional Channel Models*, IST-FLOWS Project, Internal Document WP2_IST-TUL_TN_INT_048_02, IST-TUL, Lisbon, Portugal, May 2003.

[VLLX02]   Vriendt,J., Lainé,P., Lerouge,C. and Xu,X., "Mobile Network Evolution: A Revolution on the Move", *IEEE Communications Magazine*, Vol. 40, No. 4, Apr. 2002, pp. 104-111.

[WeÖz03]   Weichselberger,W. and Özcelik,H., "A novel stochastic MIMO channel model and its physical interpretation", in *Proc. of WPMC'03 – Wireless Personal Multimedia Communication*, Yokosuka, Japan, Oct. 2003.

[WSI04]   IST-WSI Project (http://www.ist-wsi.org).

[XCHV04]   Xu,H., Chizhik,D., Huang,H., Valenzuela,R., "A generalized space-time Multiple-Input Multiple-Output (MIMO) channel model", *IEEE Transactions on Wireless Communications*, Vol. 3, No. 3, May 2004, pp. 966-975.

[YBOM01]   Yu,K., Bengtsson,M., Ottersten,B., McNamara,D., Karlsson,P. and Beach,M., "Second order statistics of NLoS indoor MIMO channels based on 5.2 GHz measurements", in *Proc. of GLOBECOM '01 – IEEE Global Telecommunications Conference*, San Antonio, Texas, USA, Nov. 2001.

[YBOM02]   Yu,K., Bengtsson,M., Ottersten,B., McNamara,D., Karlsson,P. and Beach,M., "A wideband statistical model for NLoS indoor MIMO channels", in *Proc. of VTC'02 Spring – 54th IEEE Vehicular Technology Conference*, Birmingham, Alabama, USA, May 2002.